ENGINEERING SCIENCES IN A GLOBALIZING WORLD

Editors

Asst. Prof. Dr. Umut ÖZKAYA

Dr. Fatma GÜNDÜZ BALPETEK

DUVAR

ENGINEERING SCIENCES IN A GLOBALIZING WORLD

Editors

Asst. Prof. Dr. Umut ÖZKAYA

Dr. Fatma GÜNDÜZ BALPETEK

Engineering Sciences in A Globalizing World
Editor: Asst. Prof. Dr. Umut ÖZKAYA, Dr. Fatma GÜNDÜZ BALPETEK

Editor in chief: Berkan Balpetek
Cover and Page Design: Duvar Design
Printing : First Edition-MARCH 2023
Publisher Certificate No: 49837
ISBN: 978-625-6945-45-6

853 Sokak No:13 P.10 Kemeraltı-Konak/Izmir/ Turkey
Phone: 0 232 484 88 68
www.duvaryayinlari.com
duvarkitabevi@gmail.com

Printing and Binding: REPRO BİR
Repro Bir Mat Kağ. Rek. Tas. Tic. Ltd. Şti.
İvogsan 1518. Sokak 2/30 Mat-Sit iş Merkezi Ostim
Yenimahalle/Ankara
Certificate No: 47381

TABLE OF CONTENTS

Chapter 1

State of the Art of Electrical Motors, Control Management System and Trends for Modern Electric Vehicles

Mohamed Fadi KETHIRI[1]

Omar CHARROUF[2]

[1] Laboratoire Génie Electrique Biskra (LGEB), University of Biskra, Biskra-Algeria
fadi.kethiri@univ-biskra.dz

[2] Laboratoire Génie Electrique Biskra (LGEB), University of Biskra , Biskra-Algeria
omar.charrouf@univ-biskra.dz

I. INTRODUCTION

The electric force is the primary source of energy for electric vehicle technology. It is stored in a storage system, often hybrid, and is converted by the motor into mechanical energy and then transformed on the vehicle wheels using the best possible transmission device, which must be characterized by high efficiency, provide the required torque andspeed for the wheels, and be reversible [1] The present paper proposes a macroscopic study of the main electrical machines used in the traction part of electrical vehicles. This study is important in order to gain an understanding of the various skills of these motors, including their design and control strategies. The most common types of electrical machines used in the traction part of electrical vehicles are permanent magnet and variable reluctance machines. These machines are preferred due to their high power density and relatively simple control strategies. Permanent magnet machines are characterized by their high efficiency and power density, as well as their low cost and low maintenance requirements. Variable reluctance machines, on the other hand, are characterized by their high torque density and low cost. In addition to these two types of machines, there are also other types of electrical machines that can be used in the traction part of electrical vehicles. These include brushless DC motors, induction motors, and switched reluctance motors. Each of these machines has its own advantages and disadvantages, and the choice of which type of machine to use depends on the specific application. In terms of design, the permanent magnet and variable reluctance machines are the most commonly used in the traction part of electrical vehicles. These machines are designed to be compact and lightweight, which makes them ideal for use in vehicles. They also have a high power density, which allows them to generate more power than other types of machines. Furthermore, these machines are relatively easy to control, which makes them suitable for use in vehicles. In terms of control strategies, the permanent magnet and variable reluctance machines are the most commonly used in the traction part of electrical vehicles. These machines are typically controlled using a combination of current and voltage control strategies. Current control strategies are used to regulate the speed of the motor, while voltage control strategies are used to regulate the torque. This allows the motor to be operated at different speeds and torques, depending on the application. Overall, the permanent magnet and variable reluctance machines are the most prometheus in the traction part of electrical vehicles due to their high power density and relatively simple control strategies. These machines are also relatively easy to design and control, which makes them ideal for use in vehicles.

II.TYPES OF ELECTRIC VEHICLES

In the current market, the most popular vehicles are the Hybrid electric vehicles (HEVs), which combine mechanical and electrical based motors. The most popular EV in the research world, which are the pure electric vehicles use either a source of electricity or a renewable source to supply an electrical traction motor. For instance, the fuel-cell Vehicles require a DC - DC converter while the other types do not [2]. Hybrid electric vehicles (HEVs) have become increasingly popular in the current market due to their ability to combine mechanical and electrical based motors. This combination allows for a more efficient and cost-effective way to power a vehicle. HEVs are able to use both gasoline and electricity to power the vehicle, which allows for a more efficient use of fuel and a reduction in emissions. Additionally, HEVs are able to use regenerative braking, which captures energy from the brakes and stores it in the battery for later use. This helps to reduce the amount of energy that is wasted when braking. Pure electric vehicles (EVs) are the most popular type of EV in the research world. EVs use either a source of electricity or a renewable source to supply an electrical traction motor. This type of vehicle is becoming increasingly popular due to its ability to reduce emissions and its cost-effectiveness. EVs are able to use regenerative braking, which helps to reduce the amount of energy that is wasted when braking. Additionally, EVs are able to use renewable sources of energy, such as solar or wind, to power the vehicle. This helps to reduce the amount of emissions that are released into the atmosphere. Fuel-cell vehicles are another type of EV that require a DC-DC converter. Fuel-cell vehicles use a combination of hydrogen and oxygen to create electricity, which is then used to power the vehicle. This type of vehicle is becoming increasingly popular due to its ability to reduce emissions and its cost-effectiveness. Additionally, fuel-cell vehicles are able to use renewable sources of energy, such as solar or wind, to power the vehicle. This helps to reduce the amount of emissions that are released into the atmosphere. Overall, hybrid electric vehicles, pure electric vehicles, and fuel-cell vehicles are all becoming increasingly popular in the current market due to their ability to reduce emissions and their cost-effectiveness. Each type of vehicle has its own unique advantages and disadvantages, so it is important to research each type of vehicle before making a decision.

III. CHALLENGES FACE THE DESIGN OF EVS

Electric vehicles (EVs) have become increasingly popular in recent years due to their environmental benefits and cost savings. [3] However, there are still several challenges that need to be addressed before EVs can become a viable alternative to traditional gasoline-powered vehicles. The first challenge is the battery size and capability. Currently, the batteries used in EVs are large and heavy, which limits the range of the vehicle and increases the cost. Additionally, the batteries are not able to store enough energy to power the vehicle for long distances. This means that EVs are not suitable for long-distance travel and are limited to short trips. The second challenge is the performance of the electric motor used to drive the vehicle. Electric motors are not as powerful as gasoline engines, which means that EVs are not able to accelerate as quickly or reach the same top speeds as gasoline-powered vehicles. This can be a major issue for drivers who need to travel at high speeds or who need to accelerate quickly. The third challenge is the control system used. EVs use complex control systems to manage the power output of the electric motor and the battery. These systems are not as reliable as the systems used in gasoline-powered vehicles, which can lead to problems with the performance of the vehicle. Additionally, the control systems are expensive to maintain and repair, which can add to the cost of owning an EV. Overall, the main challenges that face electric vehicles are the battery size and capability, the performance of the electric motor, and the control system used. These challenges need to be addressed before EVs can become a viable alternative to traditional gasoline-powered vehicles.

IV. TYPES OF MOTORS USED IN EVS

Main challenges that face electric vehicles are the battery size and capability, the performance of the electric motor, and the control system used. These challenges need to be addressed before EVs can become a viable alternative to traditional gasoline-powered vehicles.

1. DC Motors: DC motors are the oldest type of electric motor and are still used in many applications. They are simple and reliable, and can be used in a wide range of applications. DC motors are typically used in applications where high torque is required, such as in electric vehicles. The main advantage of DC motors is that they are relatively inexpensive and easy to maintain. However, they are not as efficient as other types of motors and require more power to operate.

2. Induction Motors (IM): Induction motors are the most common type of motor used in electric vehicles. They are relatively efficient and reliable, and can be used in a wide range of applications. The main advantage of induction motors is that they are relatively inexpensive and easy to maintain. However, they are not as efficient as other types of motors and require more power to operate.

3. Permanent Magnet (PM) Motors: Permanent magnet motors are the most efficient type of motor used in electric vehicles. They are relatively expensive and require more power to operate, but they are also the most efficient type of

motor. The main advantage of permanent magnet motors is that they are very efficient and require less power to operate.

4. Switched Reluctance (SRM) and Synchronous Reluctance (SynRM) Motors: Switched reluctance and synchronous reluctance motors are relatively new types of motors that are becoming increasingly popular in electric vehicles. They are relatively efficient and reliable, and can be used in a wide range of applications. The main advantage of these motors is that they are relatively inexpensive and easy to maintain. However, they are not as efficient as other types of motors and require more power to operate.

Overall, the four major types of motors used in electric vehicles are DC motors, induction motors, permanent magnet motors, and switched reluctance and synchronous reluctance motors. Each type of motor has its own advantages and disadvantages, and the type of motor that is best suited for a particular application will depend on the specific requirements of the application. [4]; and each of these machines has different topologies, advantages and disadvantages, as shown in Fig 1.

In most recent vehicles, three classes of machines have been applied including induction machines, synchronous machines, permanent magnet machines and reluctance machines, as depicted in the flowchart of Fig.2. [5]

V. DC MOTORS

DC drives can be accepted for EVs because of their simple control; which is a very important factor when considering an EV application, due to their orthogonal disposition of field and armature MMFs; but they are less reliable because of their brushes and commutators which, make the maintenance-free that is needed not available in such motors, as well as the limited operation of this type. This kind of machines was only used in electric vehicle’s applications in their early stage while it’s not favoured in the current century electric vehicle’s applications.[3]

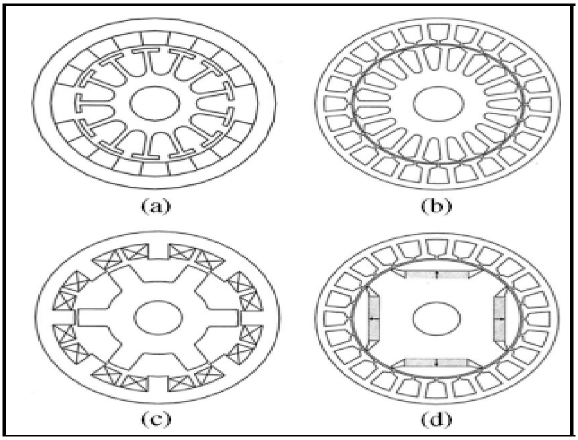

Fig. 1. (a) DC, (b) Induction, (c) SR and (d) PM [4].

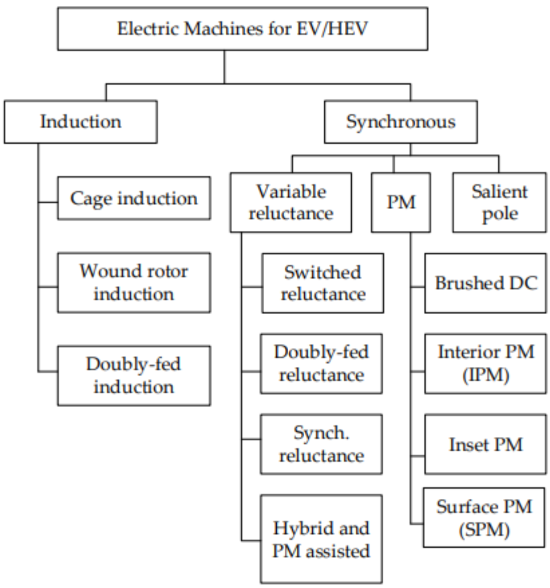

Fig. 2. Motor types available for electric /hybrid electric vehicles (EV/HEVs). [6]

VI. INDUCTION MOTORS

On the other hand, the induction motor is more popular in EVs and HEVs due to its several advantages such as its low cost, reliability, free maintenance and high efficiency in the constant power region, where the magnetized current required is low [7][8].

They are safer for vehicle applications due to their natural zero short-circuit current. They also use power electronic converters for power transfer. [9-12]. Beside these advantages IMs have some disadvantages as pointed in the followings:

IMs have low efficiency at the low speed region. IMs have low torque density; hence it is more preferable in high speed and low torque applications. A vector control is needed to be implemented to IMs in order to reach their desired performance due to their variable frequency and voltage; those rise from the nonlinearities of the IM dynamic model. [4]. Complex inverter control is needed [12].

VII. CONTROL AND MANAGEMENT SYSTEM OF INDUCTION MOTOR

As seen in Fig. 3, VFD can be divided into two types of control techniques: scalar and vector based control. [13]

Scalar control one of the control techniques used in VFDs for induction motors is scalar control. Scalar control philosophy, unlike vector control, is drawn from the IM steady-state model [14]. But scalar control has better control technique for three- phase induction motors [15].

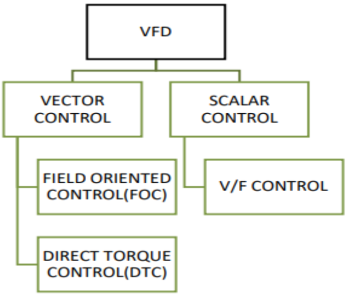

Fig. 3. Hierarchy of VFD control technique [13]

(Voltage/Frequency) V/F Control is built on the IM speed's open loop and closed loop control systems. This control method, known as scalar control, was first used in 1960 for IM control [16]

Vector control is the most often utilised technique in many IM implementations due to its high performance for IM communication. The magnitude and phase of the voltages or currents used to power the IMs were determined using vector control theory. Controlling the direction of the IM flux, voltage, and current vectors is the base for vector power [17]

Field Oriented Control (FOC) the torque and speed control are directly dependent on the motor's electrical state, which is like that of a DC motor, according to Field Oriented Control. The first technology to command the torque and flux variables in real- time is FOC [18]. The two forms of FOC systems are rotor field-oriented control (RFOC) and stator field oriented control (SFOC) [13].

Direct Control Torque (DTC) this control method known as Direct Control Torque (DTC) was introduced in the mid-1980 by Takahashi [19] and Depenbrock [20]. Due to its instant dynamic control and ability to produce comparable output in DC machines, the DTC induction motor drive system has recently become prominent. Because of its high torque response and fast control algorithm, the DTC method can be utilized to replace the well-known FOC technique [21]

	V/F	DTC	FOC
Dynamics	LOW	HIGH	HIGH
Current	HIGH	LOW	LOW
Torque Ripples	HIGH	HIGH	LOW
Complexity	MEDIUM	LOW	HIGH

Table 1. Summary table of comparison V/F, DTC and FOC [13]

VIII. PERMANENT MAGNET MOTORS

The majority of the machines currently used in vehicles are permanent magnet machines. The increasing requirements of high efficiency, high specific power, and high power density caused a shift toward permanent magnet machines [5]. Permanent magnet (PM) drives are more attractive in all types of EVs because of their advantages when compared to other types of machines. Although PM drives have some disadvantage such that their cost is relatively high due to the PM materials cost. PM brushless drives have two types according to the operating current and no load electromotive force (EMF) waveforms [22].

The first PM sine wave machine has a sinusoidal back EMFs and armature current, named: PM synchronous machine (PMSM), and the other competitive machine is called the brushless DC machine that has a trapezoidal back EMFs and pulses of current. Both types of PM drives have much in common practically [5]. BLDC have trapezoidal back-emf waveforms and use a rectangular current which allows simpler rotor position estimation. The rotor generally uses surface-mounted permanent magnets (PMs). Rare-earth PMs allow BLDC machines to achieve high efficiency and power density [23-25].

IX. CONTROL AND MANAGEMENT SYSTEM OF PM MOTORS

Essentially, the PM synchronous motor can adopt those control strategies that have been developed for the induction motor because both types of motors are based of sinusoidal waveforms, whereas the PM brushless motor needs to adopt dedicated control strategies because of its non-sinusoidal operating waveforms [26].

PM Synchronous Motor Control

As mentioned earlier, the PM synchronous motor can adopt those sophisticated control strategies that have been developed for the induction motor, such as the FOC and direct torque control. In order to provide the constant-power operation for EV cruising, the flux-weakening control of the PM synchronous motor is highly desirable. On the other hand, in order to get rid of the costly position encoder, the position sensorless control has been actively developed for the PM synchronous motor [26]. Therefore, these three prominent control strategies are:

1. Field-Oriented Control of PM Synchronous Motor
2. Flux-Weakening Control of PM Synchronous Motor
3. Position Sensorless Control of PM Synchronous Motor

There are many position sensorless techniques that have been developed for the PM synchronous motor. These techniques can beclassified by various ways. [27] Typically, they can be classified into four main methods. [28]

- Current model adaptive scheme
- PWM carrier component scheme
- External signal injection scheme
- Current model-based injection scheme

PM Brushless DC Motor Control

1. Phase-Advance Angle Control of PM Brushless DC Motor
2. Position Sensorless Control of PM Brushless DC Motor

There are many position sensorless techniques that have been developed to estimate the commutation signals for the PM BLDC motor [29]. Typically, they can roughly be classified into five main methods [28]:

- Estimation using machine model
- Induced EMF from sensing coils
- Inactive phase EMF sensing
- Third harmonic-induced EMF detection
- Artificial intelligent control

X. SWITCHED RELUCTANCE (SRM) AND SYNCHRONOUS RELUCTANCE MOTOR (SynRM)

Two important machine topologies that operate on the reluctance principle to produce torque are the synchronous reluctance (SynRM) machine and switched reluctance machine (SRM) [30]. SRMs are known for their simple construction, robustness, inherent fault-tolerant structure and low production and maintenance costs. Moreover, the machine has gained interest due to the absence of permanent magnets or windings in the rotor structure, which significantly reduces production costs when compared to other electric motors [31]. Despite all the advantages of SRMs, they have some disadvantage such as the difficulty of their manufacturing due to the small air gap required, they require a large inverter when it comes to the control strategy which can increase the cost of the system as a whole, they also exhibit acoustic-noise problems and high torque ripples and the iron loss is high in these machine at high speeds [4][32].

XI. CONTROL AND ENERGY MANAGEMENT SYSTEM OF SWITCHED RELUCTANCE MOTORS (SRM)

The switched reluctance machine, however, presents some known drawbacks. The SRM is prone to high torque ripple, because of the switched nature of the machine being the most contributing factor. In the flowchart of Fig.4 is dressed the main control techniques used in reluctance synchronous machines.

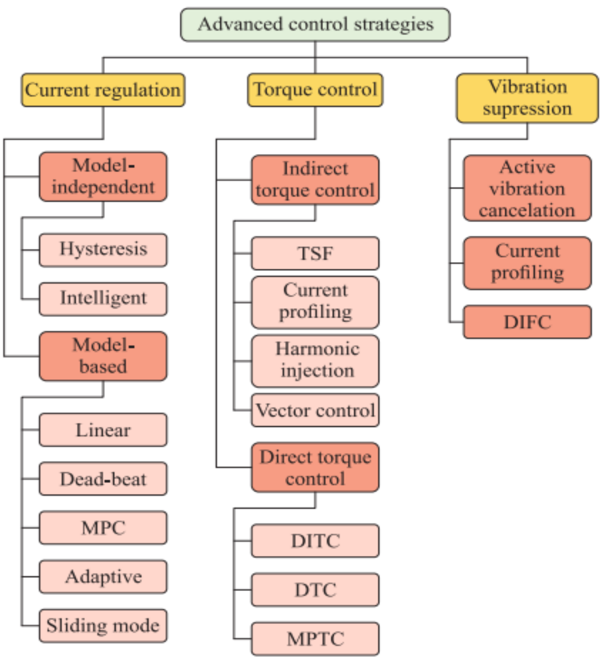

Fig 4. Classification of advanced control strategies for SRMs [31].

With the soaring development of transportation electrification, SRMs are gaining much interest in this field because of its rare-earth-free feature, simple and robust structure, and high reliability. Nevertheless, the high nonlinearity, pulsed torque feature, and unpleasant acoustic noise are barriers for the widespread use of SRMs [31].

XII. COMPARISON AND MULTI-CRITERIA ANALYSIS AND TRENDS OF ELECTRIC MOTORS FOR ELECTRIC VEHICLES

In this section, we analyse and evaluate five types of electric motors for electric vehicle applications based on various paradigms, The criteria are determined from the factors below. They are divided into those that have an impact on the performance, reliability, and efficiency of the model:

Performance: This is the set of actions that each motor can perform as a task.

Reliability: the reliability factor is based on the faithfulness of the motor, which is its immunity against rapid breakdowns and supports continuous operation without any regular maintenance.

Efficiency: this factor determines the capacity of the model to be more efficient with a minimum of resources relating to power sources and electronic systems; electric motor efficiency provides a connection between the electrical and mechanical yield [33].

Comparative studies on different topologies of electric motors for EVs

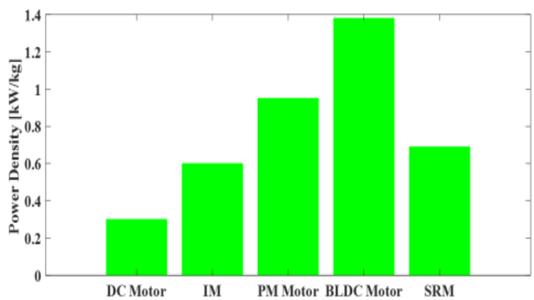

Fig 5. Power Density Cumulative Correlations of different topologies [34]

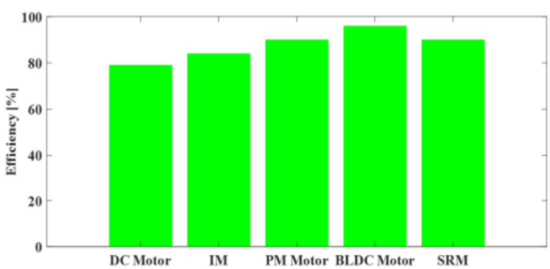

Fig 6. Efficiency Cumulative Correlations of different topologies [34]

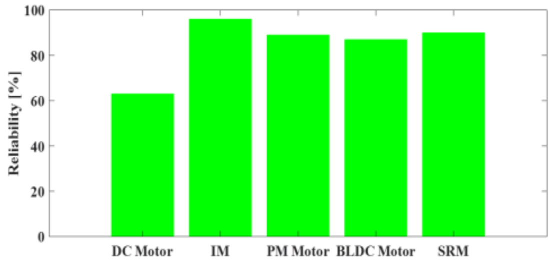

Fig. 7 Reliability Cumulative Correlations of different topologies [34]

Power density is an important performance parameter for electric motors for EV applications. It is the power output (kW) divided by the motor weight (kg). Fig. 5 presents the power density for five different motor topologies. The DC motor has the lowest power density while the BLDC motor shows the highest value. Fig. 6 shows a similar result is found for the efficiency, which is also important for EV applications. Fig. 7 provides the reliability comparisons. It is observed that the most reliable motors are the IM and SRM with the PM motor not far behind. The DC motor shows the lowest reliability [35].

XIII. FUTURE TRENDS AND RESEARCH GAPS

1.IPM Machines with Rare-Earth Magnets

The new topology of permanent magnet machine is called **AFPM**, which is increasingly being attracted by researchers and machine designers. Comparing with conventional topology, AFPM provides better characteristics for EV application in terms of higher power density, efficiency, compact structure, and lower weight [36].

2.Traction Machines without Rare-Earth Magnets

It appears that with significant research, SynRM and SRMs can provide a path to obtain high performance traction machines without rare earth content. The research to improve SRM and SynRM may be a worthwhile pursuit for non-rare-earth or reduced rare-earth drivetrains [37].

XIV. CONCLUSION

The present paper provides an explicit study of the various electrical machines employed in electrical machines. It is important to note that the study is not limited to permanent magnet and reluctance-based machines, but also includes other types of machines such as induction machines, synchronous machines, and brushless DC machines. The paper provides a brief description of each machine, including its advantages and drawbacks, as well as some control techniques and novel architectures to overcome these disadvantages. The permanent magnet and reluctance-based machines are particularly interesting due to their various skills. Permanent magnet machines are known for their high power density, low cost, and low maintenance requirements. They are also highly efficient and can be used in a wide range of applications. On the other hand, reluctance-based machines are known for their high torque density, low noise, and low vibration. They are also highly efficient and can be used in a wide range of applications. The paper also discusses some control techniques and novel architectures to overcome the disadvantages of these machines. For example, the paper discusses the use of vector control techniques to improve the performance of permanent magnet machines. Vector control techniques can be used to improve the torque and speed control of the machine, as well as to reduce the losses associated with the machine. Similarly, the paper discusses the use of advanced control techniques such as model predictive control and fuzzy logic control to improve the performance of reluctance-based machines. Overall, the present paper provides an explicit study of the various electrical machines employed in electrical machines. It provides a brief description of each machine, including its advantages and drawbacks, as well as some control techniques and novel architectures to overcome these disadvantages. The permanent magnet and reluctance-based machines are particularly interesting due to their various skills, and the paper discusses some control techniques and novel architectures to improve their performance.

References

[1] Chand, P. A Survey of Motorhomes and Key Factors to Consider When Developing Electric Motorhomes. Int. J. Veh. Perform.**2019**, 5, 165–186

[2] A. Emadi, L. Young-Joo, and K. Rajashekara, "Power Electronics and Motor Drives in Electric, Hybrid Electric, and Plug-In Hybrid Electric Vehicles," Industrial Electronics, IEEE Transactions on, vol. 55, pp. 2237-2245, **2008**.

[3] Alamoudi, Y. A., Ferrah, A., Panduranga, R., Althobaiti, A., & Mulolani, F. (**2019,** March). State-of-the art electrical machines for modern electric vehicles. In *2019 Advances in Science and Engineering Technology International Conferences (ASET)* (pp. 1-8). IEEE.

[4] K. T. Chau, C. C. Chan, and L. Chunhua, "Overview of Permanent Magnet Brushless Drives for Electric and Hybrid Electric Vehicles," Industrial Electronics, IEEE Transactions on, vol. 55, pp. 2246-2257, **2008**.

[5] Agamloh, E., Von Jouanne, A., & Yokochi, A. (**2020**). An overview of electric machine trends in modern electric vehicles. *Machines*, *8*(2), 20.

[6] Boldea, I.; Tutelea, L.N.; Parsa, L.; Dorrell, D.G. Automotive Electric Propulsion Systems With Reduced or No Permanent Magnets: An Overview. IEEE Trans. Ind. Electron. **2014**, 61, 5696–5711.

[7] Z. Q. Zhu and D. Howe, "Electrical Machines and Drives for Electric, Hybrid, and Fuel Cell Vehicles," Proceedings of the IEEE, vol. 95, pp. 746-765, **2007**.

[8] J. Herbst, J. Hahne, H. Jordan, H. Liu, A. Gattozzi, and W. Ben, "Challenges in the design of a 100 kw induction motor for a PHEV application," in Vehicle Power and Propulsion Conference, 2009. VPPC '09. IEEE, **2009**, pp. 408-413.

[9] A. K. Singh, A. Dalal, and P. Kumar, “Analysis of induction motor for electric vehicle application based on drive cycle analysis,” in Proc. IEEE Int. Conf. Power Electron., Drives Energy Syst. (PEDES), Dec. **2014**, pp. 1–6.

[10] M. Farasat, A. M. Trzynadlowski, and M. S. Fadali, “Efficiency improved sensorless control scheme for electric vehicle induction motors,” IET Electr. Syst. Transp., vol. 4, no. 4, pp. 122–131, Dec. **2014**, doi: 10.1049/iet-est.2014.0018.

[11] V. T. Buyukdegirmenci, A. M. Bazzi, and P. T. Krein, “Evaluation of induction and permanent-magnet synchronous machines using drive-cycle energy and loss minimization in traction applications,” IEEE Trans. Ind. Appl., vol. 50, no. 1, pp. 395–403, Jan. **2014**, doi: 10.1109/TIA.2013.2266352.

[12] K. Rajashekara, “Present status and future trends in electric vehicle propulsion technologies,” IEEE J. Emerg. Sel. Topics Power Electron., vol. 1, no. 1, pp. 3–10, Mar. **2013.**

[13] Aazmi, M. A., Fahmi, M. I., Aihsan, M. Z., Liew, H. F., & Saifizi, M. (**2021**, November). A review on VFD Control and Energy Management System of Induction

[14] T. Mehtab et al., “Metal-organic frameworks for energy storage devices: Batteries and supercapacitors,” J. Energy Storage, vol. 21, no. December 2018, pp. 632–646, **2019**.

[15] Z. Lin et al., “Materials for supercapacitors: When Li-ion battery power is not enough,” Mater. Today, vol. 21, no. 4, pp. 419–436, **2018**.

[16] F. Tazerart, Z. Mokrani, D. Rekioua, and T. Rekioua, “Direct torque control implementation with losses minimization of induction motor for electric vehicle applications with high operating life of the battery,” Int. J. Hydrogen Energy, vol. 40, no. 39, pp. 13827– 13838, **2015**.

[17] H. Shareef, M. M. Islam, and A. Mohamed, “A review of the stage-of-the-art charging technologies, placement methodologies, and impacts of electric vehicles,” Renew. Sustain. Energy Rev., vol. 64, pp. 403–420, **2016**.

[18] Z. Liang, L. Mu, F. Zhang, H. Zhou, and X. Zhang, “The fault detection method of islanded microgrid with the V/f controlled distributed generation,” Int. J. Electr. Power Energy Syst., vol. 112, no. April, pp. 28–35, **2019**.

[19] J. Jacob et al., “ScienceDirect ScienceDirect Field Oriented Control of Space Vector Modulated Multilevel Field Oriented Control of Space Vector Modulated Multilevel Inverter fed PMSM Drive Inverter fed PMSM Drive Assessing the feasibility of using the heat demand-outdoor,” Energy Procedia, vol. 117, pp. 966–973, **2017**.

[20] M. A. Hannan, J. A. Ali, A. Mohamed, and A. Hussain, “Optimization techniques to enhance the performance of induction motor drives: A review,” Renew. Sustain. Energy Rev., no. April, pp. 1–16, **2017**.

[21] S. Ram, O. P. Rahi, and V. Sharma, “A comprehensive literature review on slip power recovery drives,” Renew. Sustain. Energy Rev., vol. 73, no. November 2016, pp. 922–934, **2017**.

[22] G. Jinyun, K. T. Chau, C. C. Chan, and J. Z. Jiang, "A new surfaceinset, permanent-magnet, brushless DC motor drive for electric vehicles," Magnetics, IEEE Transactions on, vol. 36, pp. 3810-3818, **2000**.

[23] Chan, C.C. The state of the art of electric and hybrid vehicles. Proc. IEEE **2002**, 90, 247–275.

[24] F. Un-Noor, S. Padmanaban, L. Mihet-Popa, M. Mollah and E. Hossain, "A Comprehensive Study of Key Electric Vehicle (EV) Components, Technologies, Challenges, Impacts, and Future Direction of Development", Energies, vol. 10, no. 8, p. 1217, **2017**. Available: 10.3390/en10081217.

[25] P. C. Sen, "Electric motor drives and control-past, present, and future," Industrial Electronics, IEEE Transactions on, vol. 37, pp. 562-575, **1990**.
[26] Chau, K. T. (**2015**). *Electric vehicle machines and drives: design, analysis and application*. John Wiley & Sons.
[27] Yongdong, L., & Hao, Z. (**2008**, September). Sensorless control of permanent magnet synchronous motor—a survey. In *2008 IEEE Vehicle Power and Propulsion Conference* (pp. 1-8). IEEE.
[28] Krishnan, R. (**2017**). *Permanent magnet synchronous and brushless DC motor drives*. CRC press.
[29] Kim, T., Lee, H. W., & Ehsani, M. (**2007**). Position sensorless brushless DC motor/generator drives: review and future trends. *IET Electric Power Applications*, *1*(4), 557-564.
[30] Kabir, M. A. (**2017**). *High performance reluctance motor drives with three-phase standard inverter*. North Carolina State University.
[31] Fang, G., Scalcon, F. P., Xiao, D., Vieira, R. P., Gründling, H. A., & Emadi, A. (**2021**). Advanced control of switched reluctance motors (SRMs): A review on current regulation, torque control and vibration suppression. *IEEE Open Journal of the Industrial Electronics Society*, *2*, 280-301.
[32] P. C. Desai, M. Krishnamurthy, N. Schofield, and A. Emadi, "Novel Switched Reluctance Machine Configuration With Higher Number of Rotor Poles Than Stator Poles: Concept to Implementation," Industrial Electronics, IEEE Transactions on, vol. 57, pp. 649-659, **2010**.
[33] El Hadraoui, H., Zegrari, M., Chebak, A., Laayati, O., & Guennouni, N. (**2022**). A Multi-Criteria Analysis and Trends of Electric Motors for Electric Vehicles. *World Electric Vehicle Journal*, *13*(4), 65.
[34] P. Bhatt, H. Mehar and M. Sahajwani, "Electrical Motors for Electric Vehicle – A Comparative Study", SSRN Electronic Journal, **2019**. Available: 10.2139/ssrn.3364887
[35] Cao, Z., Mahmoudi, A., Kahourzade, S., & Soong, W. L. (**2021**, September). An overview of electric motors for electric vehicles. In *2021 31st Australasian Universities Power Engineering Conference (AUPEC)* (pp. 1-6). IEEE.
[36] A. Credo, M. Tursini, M. Villani, C. Di Lodovico, M. Orlando and F. Frattari, "Axial Flux PM In-Wheel Motor for Electric Vehicles: 3D Multiphysics Analysis", Energies, vol. 14, no. 8, p. 2107, **2021**. Available: 10.3390/en14082107.
[37] Jahns, T.M. Getting Rare-Earth Magnets Out of EV Traction Machines: A review of the many approaches being pursued to minimize or eliminate rare-earth magnets from future EV drivetrains. IEEE Electrif. Mag.**2017**, 5, 6–18.

Chapter 2

An Accurate Study of the Characteristics of the Photovoltaic Cells of the Kc200gt Panel and the Effect of Climatic Factors on Them Using Matlab Software

Siham AISSANI[1]

Mohcene BECHOUAT[2]

Moussa SEDRAOUI[3]

Toufik AMIEUR[4]

---

[1] Département Électronique et Télécommunications / Laboratoires des Télécommunications LT, University 8 May 1945 of Guelma,Algeria Guelma, Algeria,
aissanisiham24@gmail.com

[2] Département d'automatique et d'électromécanique, Faculté dessciences et de la technologie / Université de Ghardaïa, Algeria,
mohcene.oui@gmail.com

[3] Département Électronique et Télécommunications / Laboratoires des Télécommunications LT, University 8 May 1945 of Guelma,Algeria Guelma, Algeria,
sedraoui.moussa@univ-guelma.dz

[4] Département de Génie Électrique / Université de Larbi Tebessi Tebessa, Algeria,
amieur.to@gmail.com

I.INTRODUCTION

Non-renewable energy sources: Fossil fuels and their derivatives are witnessing a significant decrease over time, meaning they are on the way to disappear due to the increasing demand for them, especially in developed countries, and due to their negative effects on human health, animals and the environment. Pushing the world to exploit other sources of clean and renewable energies provided by nature, the most important of which is solar energy, which is characterized by low production and maintenance costs and does not pollute the environment.

Where solar energy is converted into electrical energy through photovoltaic panels, the efficiency of its

production is affected by several factors, including tilt angle, shading, dust, level of solar radiation, temperature, and wire loss. Solar radiation and temperature are the most important factors affecting cell properties.

The optimal exploitation of solar energy requires understanding the behavior of electric cells by studying their properties, many studies have been conducted in the literature on studying the properties of the photovoltaic cell, including Dorjadevi, A. and others studied mathematical modeling and studied the V-I and P-V properties of photovoltaic cells for different temperatures and radiation using two models: the experimental model and the ANFIS model. These last two have been compared and prove that ANFIS gives a better result [1]. Karafil, A, and others studied temperature and the effects of solar radiation on the resistance of photovoltaic panels using PSIM and MATLAB equivalent circuit simulations [2]. In the same direction Fesharaki, V and others suggested a relationship between efficiency, solar radiation, and temperature the simulation was performed in a cloudy climate to obtain the ambient temperature to achieve the desired efficiency of the photovoltaic panel [3].

The photovoltaic panel operates at its maximum power at MPP that is the characteristics of the photovoltaic cell must be studied at this point.

This paper is organized as follows: First: the photovoltaic cell model is designed and its characteristics determined, and the effect of climatic changes (ambient temperature and solar radiation) on these characteristics has been studied. and finally, these characteristics were studied at MPP. By simulating the photovoltaic model in Matlab®.

II. MODELING OF PV PANEL

In general, the actual PV cell behavior can be described by an equivalent electrical circuit based-single [6- 10]. Accordingly, for the PV panel arranged in N_p parallel strings and N_s series cells, the corresponding equivalent electrical circuit can be presented in Figure.1. It consists of N_p photocurrent sources, $\frac{N_s}{N_p}$ parallel resistors representing a leakage current, $N_p \times N_s$ diodes, and $\frac{N_s}{N_p}$ series resistors describing an internal resistance to the current flow [5, 11].

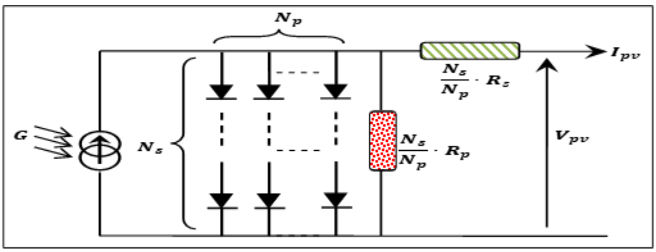

Fig.1.uivalent electrical circuit of the PV panel model

According to Fig.1, the predicted PV current model is given by (Bechouat, M., et al., 2017 and Bechouat, M., et al., 2019):

$$I_{pv} = N_p \cdot I_{ph} - N_p \cdot I_D - \frac{N_p}{N_S \cdot N_C \cdot R_p} \cdot V_{pv} - \frac{R_S}{R_p} \cdot I_{pv} \tag{1}$$

Where I_D and I_0 are respectively defined by:

$$I_D = I_0 \left(-1 + e^{\frac{q}{n \cdot K \cdot T} \cdot \left(\frac{1}{N_C \cdot N_S} \cdot V_{pv} + \frac{R_S}{N_p} \cdot I_{pv} \right)} \right) \tag{2}$$

$$I_0 = \sqrt[n]{\left(\frac{T}{T_{stc}} \right)^3} \cdot \frac{I_{sc}}{-1 + e^{\frac{q}{n \cdot K \cdot T} \cdot \left(\frac{1}{N_C \cdot N_S} \cdot V_{pv} + \frac{R_S}{N_p} \cdot I_{pv} \right)}} \cdot e^{\frac{q \cdot V_g}{n} \cdot \left(\frac{1}{\frac{1}{T} - \frac{1}{T_{stc}}} \right)} \tag{3}$$

According to equation 1, the two features (V-I) can be plotted as shown in Figures 2 and 3.

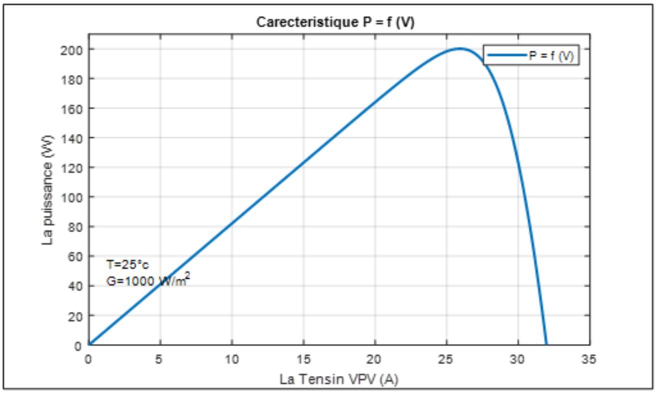

Fig. 2. P-V output characteristic of the PV panel KC200GT in stc.

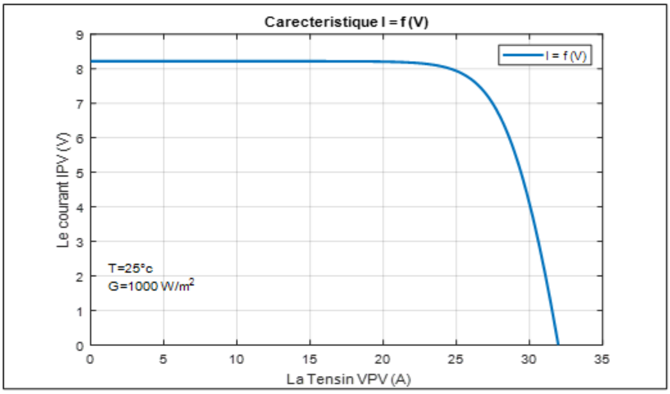

Fig.3. I-V output characteristic of the PV KC200GT module

III. NONLINEAR CHARACTERISTICS OF PHOTOVOLTAIC CELL

Photovoltaic cells have nonlinear V-I properties that depend on solar radiation and temperature. Their corresponding maximum power operating point varies non-linearly with environmental conditions and one of the main reasons for the low electrical efficiency of PV systems is the non-linear variation of output voltage and current.

In MATLAB and using the previous equation, we simulate the current, voltage and power characteristic curves of the KC200GT solar panel.

A. Effect of temperature

Two curves, the I-V and P-V characteristics are shown in Fig.4 and Fig.5 respectively. We take five temperatures: 5 ° C, 15 ° C, 25 ° C, 35 ° C and 45 ° When the temperature increases, the voltage decreases. The current increases with the temperature but very little and it does not compensate for the decrease in voltage caused by a given rise in temperature. This is why the power also decreases.

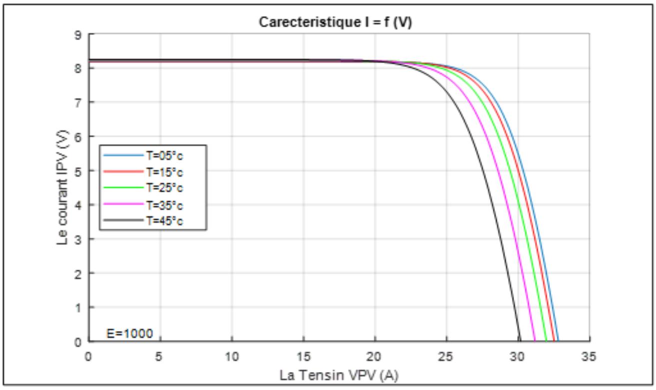

Fig.4. I-V output characteristics of the PV panel KC200GT with different temperatures

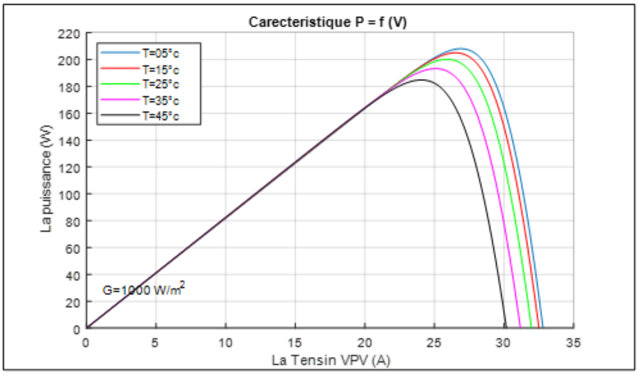

Fig.5. Output P-V characteristics of the PV panel KC200GT with different temperatures

B. Effect of irradiation

Two curves of I-V and P-V characteristics are shown in Fig. 6 and in Fig. 7. We choose five levels of radiation: 200 W / m2, 400 W / m2, 600 W / m2; 800 W / m 2 and 1000 W / m 2 The output current is directly proportional to the level of illumination, so an increase in radiation leads to a high current as shown in the figure.

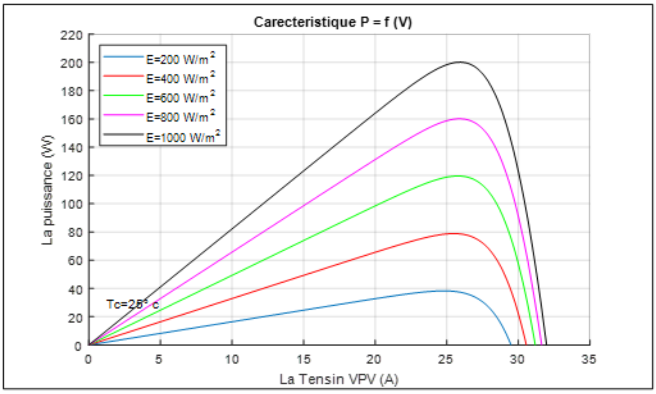

Fig.6. Output P-V characteristics of the PV panel KC200GT with different radiations.

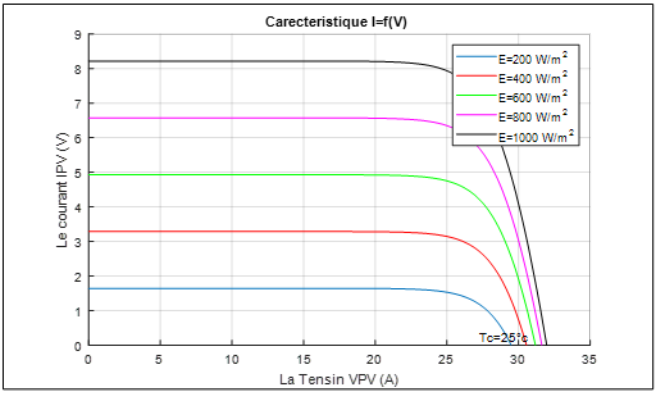

Fig.7. Output I-V characteristics of the PV panel KC200GT with different radiations.

IV. STUDY OF THE CHARACTERISTICS OF (I-V) AT MPP

Figure 8 shows that there are three main points that play an important role in determining the linearity $(I-V)$ of the characteristic about the nominal performance of the GPV, namely: the short circuit point $(I_{sc}, 0)$, the MPP point (I_{MPP}, V_{MPP}), and the open circuit point $(0, V_{oc})$. where energy extraction is maximum. Accordingly, the equivalent form of the nonlinear characteristic can be transformed into a straight line having the equation $i_{pv} = \alpha \cdot v_{pv} + \beta$ at point MPP.

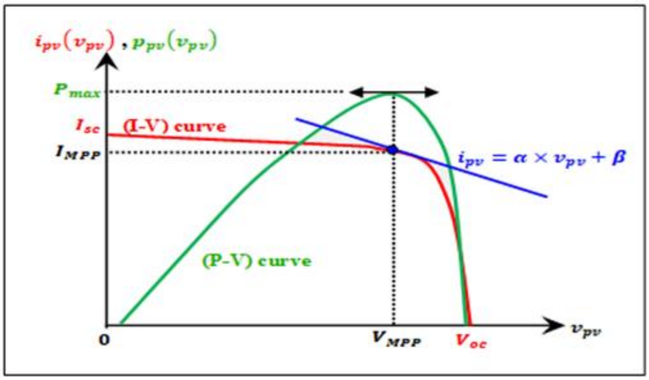

Fig.8. Nonlinear $(I-V)$ and $(P-V)$ characteristics of the PV panel

According to Fig.4 and Eq.1, the gradient α of the straight-line $i_{pv} = \alpha \cdot v_{pv} + \beta$ corresponding to the linear functioning of the *GPV* at *MPP* is given from computing the derivative $\dfrac{\partial i_{pv}}{\partial v_{pv}}$ at the point (V_{MPP}, I_{MPP}). It yields.

$$\alpha = -\frac{N_P}{N_s}\left[\frac{I_0}{aV_t}\exp\left(\frac{V_{MPP}}{N_s aV_t} + \frac{R_s I_{MPP}}{N_P aV_t}\right) - \frac{1}{R_p}\right] \tag{4}$$

where the second parameter β of the same preceding straight-line is given by

$$\beta = I_{MPP} - \alpha \cdot V_{MPP} \tag{5}$$

Let's consider the two parameters R_{eq} and V_{eq} that are assumed respectively by

$$R_{eq} = -\frac{1}{\alpha}$$
$$V_{eq} = V_{MPP} + R_{eq} I_{MPP} \tag{6}$$

From equations 5-6, the output current i_{pv} at the point (V_{MPP}, I_{MPP}) can be written in the general form, given by

$$i_{pv}(t) = \frac{1}{R_{eq}}\left(V_{eq} - v_{pv}(t)\right) \tag{7}$$

At MPP, the current-voltage characteristics become linear as shown in Figure 9

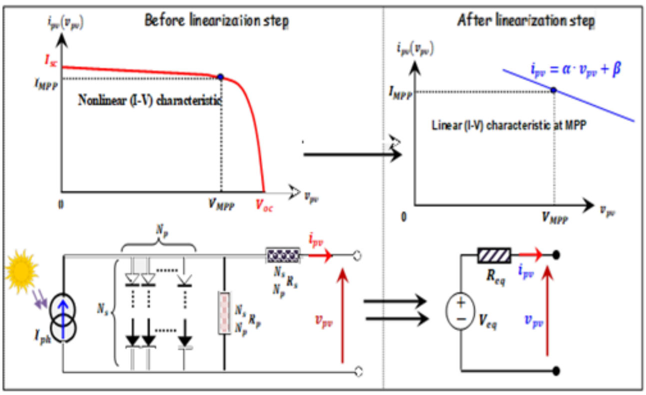

Fig.9. The equivalent electrical circuit provided through the $(I-V)$ characteristic linearization at *STC*

V. CONCLUSION

Climatic conditions (temperature and solar radiation) affect the properties of photovoltaic cells what affects the performance of the photovoltaic panel, in MPP, the photovoltaic properties change from nonlinear to linear. The study of the characteristics of photovoltaic cells makes it possible to understand the behavior of the cells and therefore the optimal use of the photovoltaic panel to extract the maximum energy P.

VI. REFERENCES

[1] Durgadevi, A., Arulselvi, S., & Natarajan, S. P. (2011, March). Photovoltaic modeling and its characteristics. In *2011 International Conference on Emerging Trends in Electrical and Computer Technology* (pp. 469-475). IEEE.

[2] Karafil, A., Ozbay, H., & Kesler, M. (2016). Temperature and solar radiation effects on photovoltaic panel power. *Journal of New Results in Science*, *5*, 48-58.

[3] Fesharaki, V. J., Dehghani, M., Fesharaki, J. J., & Tavasoli, H. (2011, November). The effect of temperature on photovoltaic cell efficiency. In *Proceedings of the 1stInternational Conference on Emerging Trends in Energy Conservation–ETEC, Tehran, Iran* (pp. 20-21).

[4] Amelia, A. R., Irwan, Y. M., Leow, W. Z., Irwanto, M., Safwati, I., & Zhafarina, M. (2016). Investigation of the effect temperature on photovoltaic (PV) panel output performance. *Int. J. Adv. Sci. Eng. Inf. Technol*, *6*(5), 682-688.

[5] Dolara, A., Leva, S., & Manzolini, G., (2015), Comparison of different physical models for PV power output prediction. Solar energy, 119: 83-99. [2]

[6] Du, Y., Fell, C. J., Duck, B., Chen, D., Liffman, K., Zhang, Y., ... & Zhu Y. (2016). Evaluation of photovoltaic panel temperature in realistic scenarios. *Energy Conversion and Management*, *108*, 60-67.

[7] Villalva, M. G., De Siqueira, T. G., & Ruppert, E. (2010). Voltage regulation of photovoltaic arrays: small-signal analysis and control design. IET Power Electronics, 3(6), 869-880

[8] Kollimalla, S. K., & Mishra, M. K. (2014). A novel adaptive P&O MPPT algorithm considering sudden changes in the irradiance. IEEE Transactions on Energy conversion, 29(3), 602-610.

[9] Althobaiti, A., M. Armstrong, and M. A. Elgendy. "Space vector modulation current control of a three-phase PV grid-connected inverter." 2016 Saudi Arabia Smart Grid (SASG). IEEE, 2016.

[10] Lasheen, M., Rahman, A. K. A., Abdel-Salam, M., & Ookawara, S. (2017). Adaptive reference voltage-based MPPT technique for PV applications. IET Renewable Power Generation, 11(5), 715-722.

[11] Belaout, A. (2018). Etude et diagnostic des défauts fréquents aux systèmes photovoltaïques (PV) par emploi de la caractéristique courant-tension (Doctoral dissertation).

[12] Mohapatra, A., Nayak, B., & Saiprakash, C. (2019, February). Adaptive perturb & observe MPPT for PV system with experimental validation. In *2019 IEEE International Conference on Sustainable Energy Technologies and Systems (ICSETS)* (pp. 257-261). IEEE.

[13] Talbi, B., Krim, F., Rekioua, T., Mekhilef, S., Laib, A., & Belaout, A. (2018). A high-performance control scheme for photovoltaic pumping system under sudden irradiance and load changes. *Solar Energy*, *159*, 353-368.

[14] Kumar, P., Jain, G., & Palwalia, D. K. (2015, August). Genetic algorithm based maximum power tracking in solar power generation. In *2015 International Conference on Power and Advanced Control Engineering (ICPACE)* (pp. 1-6). IEEE.

Chapter 3

Examining the Feasibility of Solutions to the Operations Research Problems with D-wave Quantum Annealing Services

Ege Dogan DURSUN[1]

Aysegul ALAYBEYOGLU[2]

[1] Izmir Katip Celebi University Graduate School of Natural and Applied Sciences Robotics Engineering Department.

edogandursun@gmail.com ORCID No: 0000-0003-1835-1207

[2] Prof. Dr.; Izmir Katip Celebi University Faculty of Engineering and Architecture Computer Engineering Department.

alaybeyoglu@gmail.com ORCID No: 0000-0001-9204-7356

1- INTRODUCTION

In every decade that has passed since the 1940s, the place of computers in our lives has gradually increased and their scope of use has expanded with the increased processing power. Computers, which have undergone significant improvements not only in terms of performance but also in terms of the area they cover, were only a few rooms in size in the first period of their production, but today they can provide thousands of times more effective working performance compared to those times, with devices the size of a matchbox.

The biggest reason for the reduction in the size of computers is the developments in transistor technology. Reducing the size of transistors over time, and increasing the number of transistors that can be placed per unit area, has also positively affected the processing performance of computers per unit time. Gordon E. Moore, who discovered the contraction rate of transistors over time, put forward Moore's law (Moore, 1965). According to Moore's law, the number of transistors per integrated circuit doubles every year. Thinking that this prediction, which was put forward in 1965, will remain valid for the next 10 years, Moore updated Moore's law in 1975 to double the number of transistors that can be placed in integrated circuits every 2 years instead of every year (Moore, 1975). Although Moore did not provide any empirical study or evidence for his prediction, this prediction continued to be valid in the industry for more than 50 years, and studies on the performance of existing processors revealed the approximate validity of Moore's law (IEEE, 2021) (Moore, 2021) (Schaller, 1996). A consensus has not yet been reached by academic or sectoral circles about how long Moore's law will remain valid, but observations reveal that the developments in transistor technology since the 2010s are not as rapid as before (Hennessy, 2018).

Considering that the current technological developments are slowing down, it is inevitable that Moore's law will lose its functionality in the long run. One of the biggest reasons for this is the unexpected side effects of reducing the size of transistors. As the size of the transistors decreases, the effect of the laws of classical physics decreases, and the effect of the laws of quantum physics, which is felt more actively, the smaller the size of the objects (Sciencedirect, 2021). In addition, since the size of transistors, whose main function is to control the flow of electrons, is smaller than one atom, they will be useless, so the minimum size they can reach is limited. The smallest transistor produced today is 2.5 nanometers in size (Saracco, 2021), which is between 5 and 25 times the approximate diameter of an atom (Basdevant and Spiro, 2005). If Moore's law were to progress at similar rates, the point at which transistor technology could advance after the next 10-20 years would be a predictable and inevitable deadlock. This problem was noticed by many academic and industrial circles years ago and a search for a solution was started.

Integrated circuit companies, which have problems in increasing the frequencies of the processors after a certain point, have started to increase the number of processor cores first.

One of the solutions produced for transistors is graphene, which is as conductive as silicon, but is much more resistant to heat than silicon, and can function stably even when it is a single atom thick (Lee, 2008). Graphene technology is expected to delay the inevitable doom of Moore's law for a while due to the increase in processor frequencies together with more efficient heat control.

The idea that a more revolutionary and innovative approach should be realised rather than saving the development of classical computers first emerged with the concept of a quantum computer after Paul Benioff designed the quantum mechanical equivalent of the Turing machine in the early 1980s (Benioff, 1980). According to Richard Feynman, who later expressed his views on this subject (Feynman, 1982), quantum computers would be very advantageous in solving certain problems that classical computers could not solve. In addition, the quantum phenomena, which caused the effect of getting smaller and smaller transistors to increase, would be used for the benefit of using quantum computers rather than classical computers, which would pave the way for new technological developments and provide an advantage in solving difficult problems. In 1994, Peter Shor developed a quantum algorithm with the potential to decrypt RSA-encrypted communications using integer factorization (Mermin, 2006). Although there have been serious developments regarding quantum computers since the 1990s; Fault-tolerant quantum computers are still a distant dream in certain academic circles. High fault tolerance is one of the most important criteria for the potential of quantum computers because this factor determines how much more efficient quantum computers can work compared to classical computers, especially in processes with NP-Complete and NP-Hard problem complexities.

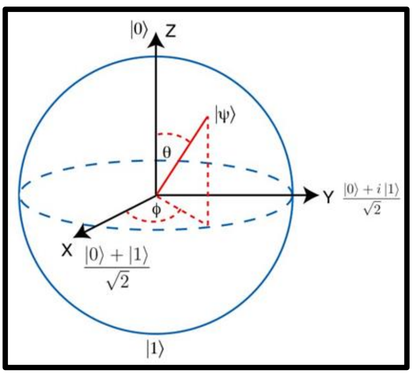

Figure 1: Bloch Sphere

The working method of quantum computers differs from classical computers in certain aspects. Data expressed in classical computers are expressed in bits in the binary number system, while data expressed in quantum computers are expressed in qubits. The most basic difference between qubits and bits is that they can take 1 or 0 values like bits; is that they can carry both of these values simultaneously in superposition. This state of qubits in superposition is valid only when they are not measured. While unmeasured qubits are expressed as probabilities of being 1 or 0 when in superposition, they will turn into either 1 or 0 expressions depending on these probabilistic values as a result of the collapse of the wave function in the case they are measured. This situation is expressed with the example of Schrödinger's cat in quantum physics (Schrödinger, 1935). According to this example, there is a cat standing in a box that cannot be observed from the outside with any sense organs. Inside the same box is a radioactive isotope with exactly a 50% probability of decay. If radioactive decay occurs, the cat dies. If not, the cat lives. Since it is known that what is inside the box can never be observed from the outside, according to quantum laws, the cat is both alive and dead at the same time. But as soon as the box is opened and the cat's condition is observed, the wave function collapses and as a result, the cat is seen as either alive or dead.

The existence of superposition-based probabilistic values other than 1 and 0 made it advantageous to use the Bloch Sphere when expressing Qubits. Classical bits and qubits also differ in their data storage properties. (Figure 1) For example, 2 classical bits can store 2 bits of data. Whereas, a 2-bit Qubit represents 4-bit data since it requires 4 variables to measure their value. Based on this, in ideal conditions, it is the classical number of bits expressed by N Qubits. However, there are several factors that prevent such an ideal scenario from being achieved in today's quantum computers. Examples of these are noise, decay time, poor fault tolerance, and the difficulty of entangling a large number of Qubits. In order to achieve an ideal performance increase in expressing the data as indicated in the formula above, it is essential that all of the Qubits be ideally entangled with each other. Entanglement is another concept in quantum physics and refers to the ability of a particle to act on another particle, regardless of the distance between them. According to quantum laws, a change in the spin of an electron located at any point in the universe will be observed in any corner of the universe with which its entangled pair is located. This interesting situation has led to the curiosity that Quantum computers can be used in subjects such as fast data transfer or data beaming, in addition to solving NP-Complete and NP-Hard problems that are difficult to solve with classical methods. Map Colouring problem, Travelling Salesperson problem, Minimum Vertex Cover problem, and

Social Graph problem can be shown as examples of problems that classical computers have difficulty solving and quantum computers can provide solutions to. Contrary to classical computers that can solve these problems in exponential time in practice, quantum computers can theoretically solve these problems in linear time. In addition, the uncertainty created by the superposition makes quantum computers a unique candidate for cryptography, since within quantum physics encrypted data completely loses its true nature when observed. In practice, cracking data encrypted with quantum cryptography is only possible by circumventing the laws of quantum physics.

Examples of issues that quantum computers can provide more effective solutions than classical computers are as follows:

1. Particle Physics Simulations
2. Chemical Interaction Simulations
3. Solving NP-Complete and NP-Hard Time Complex Problems
4. Medicinal Drug Formulations
5. Quantum Machine Learning
6. Cyber Security and Cryptography
7. Financial Modeling and Forecasting.

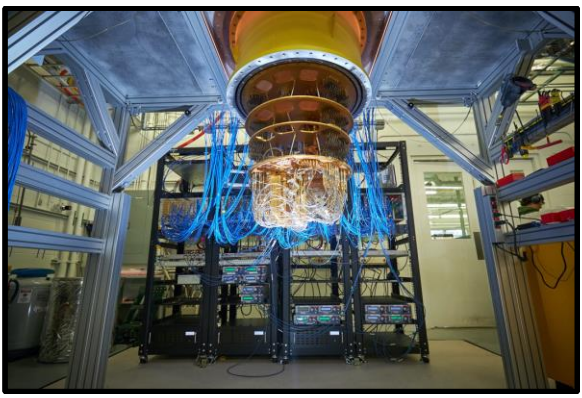

Figure 2: Digital Quantum Computer

Efforts to develop technology for the creation of digital quantum computers are still ongoing. However, as of 2022, the point reached is still not at a level that will allow the industrial use of digital quantum computers. Efforts to develop quantum computers are actively carried out and supported, particularly within the European Union, the United States, Russia, and China. IQM, which works in Finland and Germany, can be shown to companies that strive against the development of digital quantum computers, especially industry giants such as

IBM, Google, and Microsoft (García-Martín and Sierra, 2021) (Jones and Hansen, 2021) (Schuld, Borcharov, Svore and Wiebe, 2021) (Yang et al., 2021). The difficulty of creating quantum logic gates and the very short decay times of Qubits can be shown as examples of the main problems that hinder the creation of digital quantum computers. Due to various feasibility problems, the technology and materials used to build digital quantum computers differ. Two examples of these technologies are ion traps and superconductors. Superconductors are believed to be the most promising of these technologies. Superconductors are materials that exhibit zero resistance below the critical temperature. In the case of digital quantum computers, superconductors are in an advantageous position due to the previously mentioned quantum physical properties and prolonging the decay times of Qubits. The processing units of such quantum computers are located in special cooling units called cryostats. (Figure 2)

Another type of quantum computer that is being developed alongside digital quantum computers is the analog quantum computer. Analog quantum computers are thermal annealing devices that work on the principle of bringing fundamental particles such as electrons or photons, which act as qubits, to a position to interact with each other in certain patterns. Quantum thermal annealing is a method similar to the classical annealing method in data science.

Figure 3: D-Wave Analog Quantum Computer

D-Wave company in the United States develops analog quantum computers and makes the use of these computers available to users over the cloud. (Figure 3) In this study, it is tried to find solutions to certain operational problems using D-Wave's cloud quantum annealing services on various sample graphs. Examples of these problems are Maximum Cut, Map Colouring, Travelling Salesperson, Social Graph, and Clique. It has been compared the solutions generated using quantum annealing services with the solutions obtained using classical processors and reported the performance differences between classical and quantum computers.

Since quantum computers do not work effectively yet, it is difficult to test their performance on real operations problems. In order to solve this problem, D-Wave has offered an option where only Quantum Processing Units (QPU) can be used in the services it offers on the cloud, as well as an option where Classic CPUs and QPUs can work as hybrids. In the next stage of the study, the operations problems in question were approached with hybrid analyzers; and the obtained performances are again compared with the performances of CPU-only parsers.

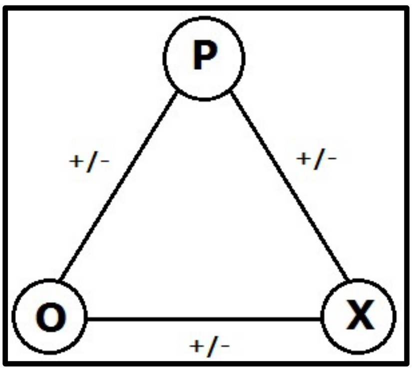

Figure 4: Signed Social Graph

Then, studies were carried out to create sample problems related to the Structural Imbalance problem based on the Signed Social Graph problem, which is the main subject of the study; tried to create real-world problems. In the next stage, these problems were solved with QPU, CPU, and QPU/CPU hybrid processing units, and the results were reported together with the performance times. The main factors taken into account during the creation of the sample problems are the areas where it would be advantageous to use the Signed Social Graph problem in daily life. Examples of these areas are logistics, public order, internal/external security, and social order.

Signed social graphs are structures that have advantages in many different disciplines such as social psychology, spin glasses, complex systems, and data clustering (Cartwrigh and Harary, 1956) (Cao, Fan, and Di, 2018) (Puccia, Charles, and Levins, 1986) (Kunegis et al., 2010). When it comes to signed social graphs, the most important question to answer is whether the graph is in a balanced state. This concept can be explained more effectively through figures.

Let's examine the Social Diagrams in Figure 5, which consist of three units. All of the relations (a, b), (b, c), and (a, c) in diagram (a) are positive. In the case of a possible grouping, the units a, b, and c are in the same team and naturally, this graph is a stable and balanced graph in itself. In diagram (b), the relation (a, b) is in the positive direction, while the relations (a,c) and (b,c) are in the negative position. In this case, in a possible grouping, units a and b will take place in different teams with unit c. When it is evaluated structurally, there is still a balanced graph. When the graph (c) is examined, it is observed that the relations (a,b) and (b,c) are positive while the relation (a,c) is negative. In that case, while these individuals are grouped, in a possible teaming, although c from the units included in the team shows a negative relationship with a, b in the same team is in a positive relationship with a. This situation turns graph (c) into a structurally unstable graph. The same situation can be observed in the diagram (d), which has a negative relationship between them despite being in the same team.

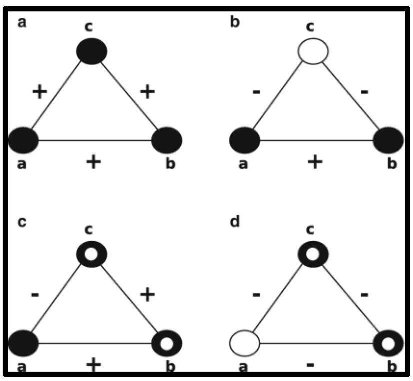

Figure 5: Unit Social Graph Examples

Research on social psychology suggests that when a social environment is expressed as a signed graph, a possible imbalance is a piece of evidence that that social environment is unstable (Uni Chicago, 2021). Social environments that are not in equilibrium experience various changes in order to move to a more balanced state. These changes can be a positive change in which negative relationships turn into positive relationships, negative change in which positive relationships turn into negative relationships, and group change or group increase.

In order to understand the structural imbalance problem, the closest situation that can be given through popular culture is love triangles. This situation can be explained with the following metaphor:

1. Alice and Bob are lovers.
2. Bob is attracted to a woman named Cassandra.
3. Naturally, Alice and Cassandra do not like each other.
4. Due to this situation, the problem of structural imbalance arises in the interaction of these three units.
5. The solution to the problem can occur in the following ways:
   a. Alice and Bob break up. (The Alice-Bob relationship turns negative.)
   b. Bob stops seeing Cassandra. (The Bob-Cassandra relationship turns negative.)
   c. Alice and Cassandra come to an agreement and leave Bob. (The Alice-Bob and Bob-Cassandra relationship turns negative, while the Alice-Cassandra relationship turns positive.)
   d. Alice and Cassandra continue to see Bob and stop loving each other. (The Alice-Cassandra relationship turns positive.)

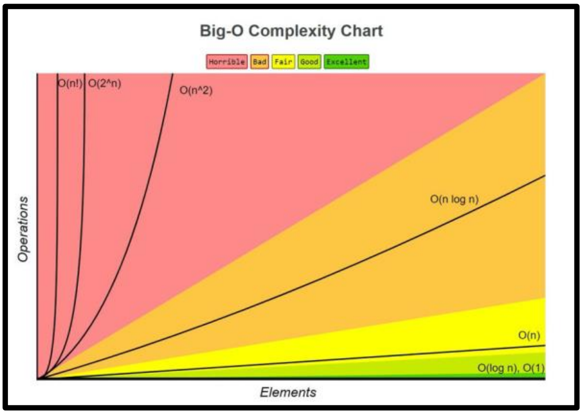

Figure 6: Big-O Time Complexity Chart

As it can be understood from the example given above, there may be more than one solution to the structural imbalance problems encountered in signed social diagrams. However, while it may be easy to analyse a graph with three units as in the example, the number of relations increases as the number of units included in the graph increases. This makes the time complexity of the problem O(N-Squared), which can be problematic for large problems. (Figure 6)

Examples of situations where structural imbalance problems can be used in daily life are the detection of structural imbalances within terrorist organisations and the development of more effective strategies to eliminate the organisation, and the achievement of healthier ecosystems by observing the relations within the society and other types of organisations and solving possible structural imbalances.

The time complexity of the structural imbalance problems causes the existing classical processors to be inefficient when it comes to very large problems. However, quantum computers, by their design, can have the efficiency to solve these problems in linear time. The main purpose of this study is to test the feasibility of Quantum Annealing services offered by D-Wave on Signed Social Diagrams and structural imbalance problems. Necessary sample problems related to this subject were designed, and their performances were reported by measuring with CPU, QPU, and CPU/QPU hybrid analysis tools.

Main aim of the study is to create exemplary work for other academic and industrial circles who want to work in this field and to experimentally test the feasibility of analog quantum computer technologies in real-world problems. This study aims to be an incentive for other circles to work in this field and to accelerate the development of applications that will solve operations problems in the field in more depth and detail.

RESULTS

In the experiments conducted within this study, it was observed that the QPU and the QPU/CPU hybrid are faster in many ways compared to the CPU. There is one problem dimension where the QPU and the QPU/CPU hybrid are more advantageous than the CPU. While up to this point, the CPU is more advantageous, after this point the CPU's processing time enters an exponential increase and reaches non-feasibility times after a point. At such points, QPU and QPU/CPU services can produce very fast results.

In the experiments conducted within this study, it was observed that the QPU and the QPU/CPU hybrid are faster in many ways compared to the CPU. There is one problem dimension where the QPU and the QPU/CPU hybrid are more advantageous than the CPU. While up to this point, the CPU is more advantageous, after this point the CPU's processing time enters an exponential increase and reaches non-feasibility times after a point. At such points, QPU and QPU/CPU services can produce very fast results.

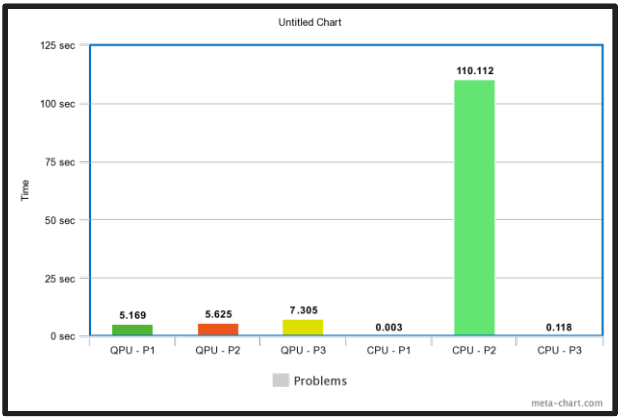

Figure 7: Map Colouring Problem, Solution Time Comparison

Of course, consistency and accuracy are as important as speed in order to ensure that QPUs instead of CPUs become widespread in operations research. During the experiments, it is observed that the solutions produced by the QPU and the CPU do not always fully overlap. These mismatches may be due to noise, singular metering, or simply not having enough of the QPU hardware yet. It may be possible for multiple measurements to increase the accuracy of the solutions of probabilistic working quantum computers. The reasons why the resolutions produced by the QPU and the QPU/CPU hybrid at the current technological level do not overlap with each other should be more effectively investigated by further studies.

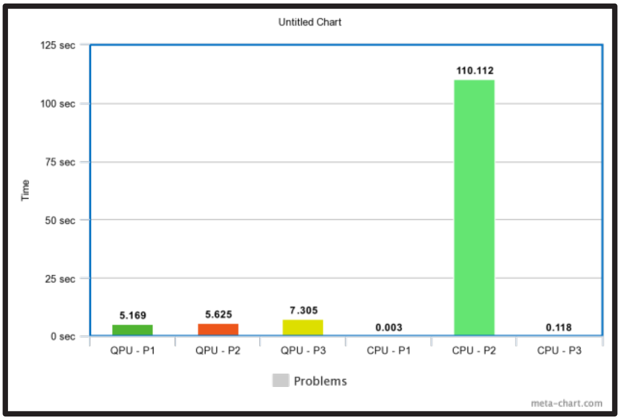

Figure 8: Maximum Clique Problem, Solution Time Comparison

In addition to QPU, QPU/CPU hybrid solvers are important in the sectoral use of quantum computers in the upcoming medium-term timeframe. The main reason for this is that the current quantum computer technology is still in its infancy, and at many points, the processing power of CPUs can still provide high benefits. Combining the strengths of QPUs and CPUs with appropriate infrastructures can provide advantages in many areas of the industry as quantum computing technologies evolve.

The increase in the number of Qubits, which is another factor that directly affects the performance of quantum computers, will increase the advantage of quantum computers and accelerate their use in many industrial areas, assuming that the noise level can be reduced.

In addition to the analog quantum computers offered by D-Wave, digital quantum computers also show great promise. In the next 30-40 years, digital quantum computers will reach the point where they can work more effectively and will provide great returns to the countries and companies that invest in this field.

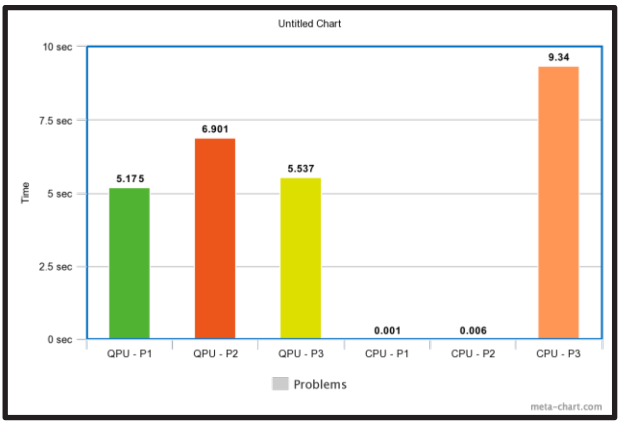

Figure 9: Minimum Maximal Matching Problem, Solution Time Comparison

Another limiting factor encountered in the study is the network-related delays caused by accessing quantum computers over the cloud. These delays are often unpredictable, but they constitute a large part of the resolution process one produces for problems. When network delays are not taken into account, quantum computers can solve existing problems much faster than a CPU. Since total resolution time was a controlled factor in this work, it’s chosen to include network-related delays in the time.

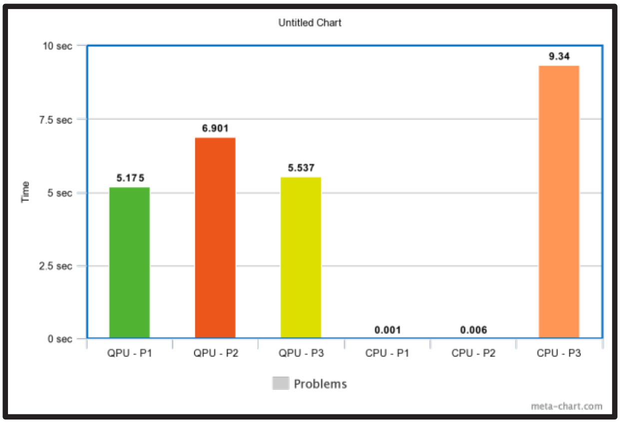

Figure 10: Maximum Cut Problem, Solution Time Comparison

One of the surprising results during the study was that the QPU/CPU hybrid resolved slower than the QPU for certain problems. The main reason for this may be the incompatibility of the problem produced with the QPU/CPU infrastructure, or there may be other reasons that can be understood with further research.

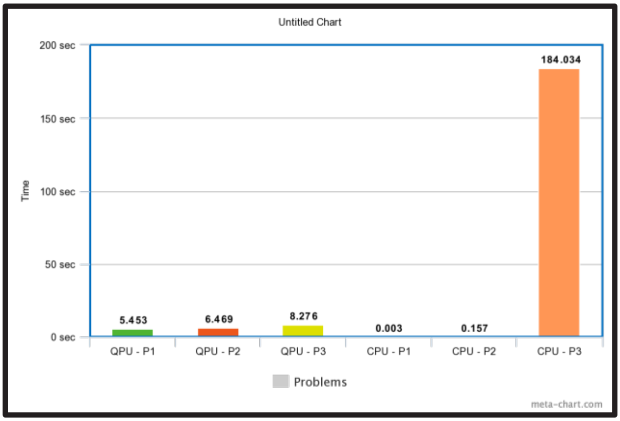

Figure 11: Travelling Salesperson Problem, Solution Time Comparison

Finally, humanity will witness in the near future that quantum computers will solve problems that are either very costly or impossible to solve with existing CPUs, along with advancing technology. In this study, it was aimed to express this with small examples and aimed to be a source of inspiration for academic and commercial circles who want to do more detailed research on the subject.

REFERENCES

Basdevant, J.-L.; Rich, J.; Spiro, M. (2005). Fundamentals in Nuclear Physics. Springer. p. 13, fig 1.1. ISBN 978-0-387-01672-6.

Benioff, Paul (1980). The computer as a physical system: A microscopic quantum mechanical Hamiltonian model of computers as represented by Turing machines. Journal of Statistical Physics. 22 (5): 563–591. Bibcode:1980JSP....22..563B. doi:10.1007/bf01011339. S2CID 122949592.

Cao, Jiayu; Fan, Ying; Di, Zengru. (2018). Frustration of signed networks: How does it affect the thermodynamic properties of a system?.

Cartwright, D.; Harary, Frank (1956). Structural balance: a generalisation of Heider's theory (PDF). Psychological Review. 63 (5): 277–293. doi:10.1037/h0046049.

Feynman, Richard (June 1982). Simulating Physics with Computers (PDF). International Journal of Theoretical Physics. 21 (6/7): 467–488. Bibcode:1982IJTP...21..467F. doi:10.1007/BF02650179. S2CID 124545445. Archived from the original (PDF) on 8 January 2019. Retrieved 28 February 2019.

García-Martín, D. and Sierra, G., 2021. Five Experimental Tests On The 5-Qubit IBM Quantum Computer. Accessed 7 January 2021.

Ieeexplore.ieee.org. 2021. Moore's Law: Past, Present, And Future - IEEE Journals & Magazine. (online) Available at: https://ieeexplore.ieee.org/abstract/document/591665 (Accessed 7 January 2021).

John L. Hennessy; David A. Patterson (June 4, 2018). A New Golden Age for Computer Architecture: Domain-Specific Hardware/Software Co-Design, Enhanced Security, Open Instruction Sets, and Agile Chip Development. International Symposium on Computer Architecture - ISCA 2018. In the later 1990s and 2000s, architectural innovation decreased, so performance came primarily from higher clock rates and larger caches. The ending of Dennard Scaling and Moore's Law also slowed this path; single-core performance improved only 3% last year!

Jones, J., Mosca, M. and Hansen, R., 2021. Implementation Of A Quantum Search Algorithm On A Quantum Computer. Accessed 7 January 2021.

Journals.uchicago.edu. 2021. The Structural Balance Theory Of Sentiment Networks: Elaboration And Test | American Journal Of Sociology: Vol 123, No 2. (online) Available at: https://www.journals.uchicago.edu/doi/full/10.1086/692757 (Accessed 7 January 2021).

Kunegis, Jérôme; Schmidt, Stephan; Lommatzsch, Andreas; Lerner, Jürgen; De Luca, Ernesto; Albayrak, Sahin. (2010). Spectral Analysis of Signed Graphs for Clustering, Prediction, and Visualization. Proc SDM. 559-. 10.1137/1.9781611972801.49.

Lee, Changgu (2008). Measurement of the Elastic Properties and Intrinsic Strength of Monolayer Graphene" Science. 321 (385): 385–388. Bibcode:2008Sci...321..385L. doi:10.1126/science.1157996. PMID 18635798. S2CID 206512830.

Mermin, David (March 28, 2006). Breaking RSA Encryption with a Quantum Computer: Shor's Factoring Algorithm (PDF). Physics 481-681 Lecture Notes. Cornell University. Archived from the original (PDF) on 2012-11-15.

Moore, Gordon E. (1965-04-19). Cramming more components onto integrated circuits (PDF). intel.com. Electronics Magazine. Retrieved April 1, 2020.

Moore, Gordon E. (1975). Progress in digital integrated electronics (http://ieeexplore.ieee.org/xpls/abs_all.jsp?arnumber=1478174). IEEE. . Retrieved 2011-11-27.

Moore, Gordon E. 2021. Lithography And The Future Of Moore's Law. Accessed 7 January 2021.

Puccia, Charles J. and Levins, Richard (1986). Qualitative Modelling of Complex Systems: An Introduction to Loop Analysis and Time Averaging. Harvard University Press, Cambridge, MA.

Saracco, R., 2021. Tiniest Transistor – Yet: 2.5 Nm - IEEE Future Directions. (online) IEEE Future Directions. Available at: https://cmte.ieee.org/futuredirections/2019/03/13/tiniest-transistor-yet-2-5-nm (Accessed 7 January 2021).

Schaller, Bob (September 26, 1996). The Origin, Nature, and Implications of MOORE'S LAW. Microsoft. Retrieved September 10, 2014.

Schrödinger, Erwin (November 1935). Die gegenwärtige Situation in der Quantenmechanik (The present situation in quantum mechanics). Naturwissenschaften. 23 (48): 807–812. Bibcode:1935NW.....23..807S. doi:10.1007/BF01491891. S2CID 206795705

Schuld, M., Bocharov, A., Svore, K. and Wiebe, N., 2021. Circuit-Centric Quantum Classifiers. Accessed 7 January 2021.

Sciencedirect.com. 2021. Quantum Size Effect - An Overview | ScienceDirect Topics. (online) Available at: https://www.sciencedirect.com/topics/chemistry/quantum-size-effect (Accessed 7 January 2021).

Yang, C., Leon, R., Hwang, J., Saraiva, A., Tanttu, T., Huang, W., Camirand Lemyre, J., Chan, K., Tan, K., Hudson, F., Itoh, K., Morello, A., Pioro-Ladrière, M., Laucht, A. and Dzurak, A., 2021. Operation Of A Silicon Quantum Processor Unit Cell Above One Kelvin. Accessed 7 January 2021. [Original source: https://studycrumb.com/alphabetizer]

Chapter 4

Shallow Transfer Learning Models

Muhammet ÇAKMAK[1]

[1] Dr. Öğr. Üyesi, Karabük Üniversitesi Mühendislik Fakültesi, Elektrik-Elektronik Mühendisliği
muhammetcakmak@karabuk.edu.tr, ORCID: 0000-0002-3752-6642

Shallow transfer learning is a technique in machine learning that aims to transfer knowledge acquired from a related task or domain to a new task or domain. In this approach, the pre-trained model's higher-level layers are employed, while the lower-level layers are generally re-initialized or fine-tuned for the new task. This approach enables the model to exploit the learned features from the pre-trained model, thus enhancing the performance on the new task while adjusting to the unique characteristics of the new dataset. Shallow transfer learning has found widespread usage in various fields, such as natural language processing, speech recognition, computer vision, and time series analysis . For instance, in natural language processing, a pre-trained language model on a large corpus of text can be adapted for a specific downstream task, including sentiment analysis or text classification. Similarly, in computer vision, a pre-trained convolutional neural network (CNN) can be fine-tuned for specific tasks like semantic segmentation or object detection. Shallow transfer learning offers several benefits, including faster and more efficient training compared to building a model from the beginning. Furthermore, it can enhance performance on a new task even when the labeled data is scarce. Shallow transfer learning is also valuable for knowledge transfer between associated tasks or domains. All in all, shallow transfer learning is a potent approach in machine learning and has extensive applications in both research and industry.

1. Introduction to Shallow Transfer Learning Models

Transfer learning is a subfield of machine learning that has gained popularity in recent years due to its ability to leverage knowledge learned from one task to improve the performance of another related task [1]. Shallow transfer learning models are a specific type of transfer learning approach that involves transferring knowledge from a pre-trained model to a new model that is designed to solve a similar task [2].

The idea behind shallow transfer learning is that the pre-trained model has already learned a lot of relevant features and patterns from a large and diverse dataset that is related to the new task [3]. By fine-tuning the pre-trained model on the new task, we can leverage this knowledge to improve the performance of the model on the new task, even with limited labeled data.

In shallow transfer learning, the pre-trained model can be trained on various tasks, including speech recognition, natural language processing, image classification, object detection and more. The pre-trained model can be trained on a large dataset, such as ImageNet or Common Objects in Context (COCO), or a smaller dataset that is specific to the task [4]. Shallow transfer learning models can be categorized into two main types: feature extraction and fine-tuning.

Feature extraction involves fixing the pre-trained model's weights and utilizing the final layer's output as input for a new model [5]. The new model's layers are then trained to solve the new task . This approach is useful when the pre-trained model has learned a set of generic features that are relevant to the new task.

In fine-tuning, the pre-trained model's weights are updated during training on the new task . The last few layers of the model are typically replaced with new layers that are initialized randomly and then trained on the new task. This approach is useful when the pre-trained model needs to be adapted to the specific characteristics of the new task.

Shallow transfer learning models have several advantages over traditional machine learning models. Firstly, they require less labeled data to achieve high performance, which is particularly useful in scenarios where labeled data is expensive or difficult to obtain. Secondly, they can improve the performance of the model by leveraging the knowledge learned from a large and diverse dataset, which can result in more accurate predictions. Finally, they can reduce the training time and computation resources required to train a new model from scratch, as the pre-trained model has already learned a set of relevant features.

The fundamental objective of shallow transfer learning is to enhance the performance of machine learning models on novel tasks through the utilization of pre-existing models. The premise of transfer learning is founded on the realization that numerous tasks share common underlying patterns and structures. Consequently, by transferring the knowledge acquired from one task to another, we can harness the shared structures and patterns to enhance the model's performance on the new task.

Shallow transfer learning is particularly useful in scenarios where the new task has limited labeled data. Fine-tuning a pre-trained model on the new task can improve the model's performance by leveraging the knowledge learned from the large and diverse dataset used to train the pre-trained model.

In summary, shallow transfer learning models represent a potent technique to enhance the performance of machine learning models on fresh tasks. By capitalizing on knowledge acquired from pre-existing models, the performance of the new model can be improved, even in the presence of restricted labeled data. This technique has proven to be effective across multiple domains, such as natural language processing computer vision, and speech recognition.

2. Overview of Shallow Transfer Learning Models

Shallow transfer learning models can be categorized into two main types: feature extraction and fine-tuning. In this chapter, we will discuss each of these types in more detail, including their advantages and limitations.

2.1 Feature Extraction

Feature extraction is a popular technique in shallow transfer learning that has been widely used in various applications. It has been applied to many different types of data, including images, text, and audio [6]. One of the main advantages of feature extraction is that it allows us to leverage the knowledge learned from large-scale pre-training datasets. This knowledge can then be transferred to new, smaller datasets, where it can help improve the performance of models.

In computer vision, feature extraction has been used to improve the performance of image classification, object detection, and segmentation models . For example, AlexNet, Visual Geometry Group (VGG), and Residual Networks (ResNet) are pre-trained models that have learned to extract generic features from images. These features can then be used as input to new models, such as Support Vector Machines (SVM), which are trained on smaller datasets specific to a new task. This approach has been shown to be effective in improving the accuracy of image classification models, especially when the new dataset is small.

Feature extraction has been utilized in natural language processing to boost the accuracy of sentiment analysis, text classification, and named entity recognition models [7]. Pre-trained models, such as Bidirectional Encoder Representations from Transformers (BERT), Generative Pre-trained Transformer 2 (GPT-2), and XLNet, have been trained on massive text datasets to acquire generic features. These models can subsequently serve as feature extractors to acquire embeddings for new datasets, which can then be employed as input to new models, such as logistic regression or SVMs. This methodology has been demonstrated to be effective in enhancing the accuracy of text classification models, particularly when the new dataset is limited in size.

One of the primary challenges of feature extraction is that the pre-trained model's features may not be tailored to the new task's specific requirements. For instance, a pre-trained model trained on a vast image dataset may have acquired general features, such as edges, corners, and textures, that are beneficial for image classification but not necessarily for object detection or segmentation [8]. To mitigate this challenge, hybrid approaches can be employed, where only specific layers of the pre-trained model are utilized as feature extractors, while the remaining layers are fine-tuned for the new task. This can help to balance the use of pre-existing knowledge while adapting it to the unique attributes of the new task.

In conclusion, feature extraction is a potent methodology in shallow transfer learning that enables us to utilize the knowledge acquired from pre-training on extensive datasets. It has been widely implemented in various applications, such as computer vision and natural language processing [9]. Despite its limitations, hybrid approaches can be employed to balance the use of pre-existing knowledge and adapt it to the unique characteristics of the new task. Overall, shallow transfer learning has proven to be an effective approach to improve model performance in new tasks with limited labeled data, and it is expected to play a critical role in future machine learning research.

2.2 Fine-Tuning

Fine-tuning is another popular technique in shallow transfer learning that has been widely used in various applications. In contrast to feature extraction, fine-tuning involves training the entire pre-trained model on a new task-specific dataset [10]. This approach has been shown to be effective in improving the accuracy of models, especially when the new dataset is large and similar to the pre-training dataset.

In computer vision, fine-tuning has been used to improve the performance of image classification, object detection, and segmentation models. For example, after pre-training on large-scale image datasets, models such as VGG, ResNet, and Inception can be fine-tuned on smaller, task-specific datasets to improve their accuracy on the new task. Fine-tuning typically involves freezing the lower layers of the pre-trained model, which have learned generic features, and only training the higher layers, which are specific to the new task [11]. This allows the model to adapt its learned features to the specific characteristics of the new task while retaining the generic features learned from the pre-training dataset.

In natural language processing, fine-tuning has been used to improve the performance of text classification, sentiment analysis, and language modeling models. For example, after pre-training on large-scale text datasets, models such as BERT, GPT-2, and XLNet can be fine-tuned on smaller, task-specific datasets to improve their accuracy on the new task [12]. Fine-tuning involves updating the parameters of the pre-trained model by training it on the new task-specific dataset. This allows the model to adapt its learned representations to the specific characteristics of the new task.

One of the advantages of fine-tuning is that it allows us to leverage the pre-trained model's knowledge more effectively than feature extraction, especially when the new dataset is similar to the pre-training dataset. Fine-tuning also allows us to train models on smaller datasets, which is particularly useful in applications where collecting large amounts of data is challenging or expensive [13].

However, fine-tuning has some limitations. One challenge is overfitting, which occurs when the model is too complex or when the new dataset is too small. Overfitting can be mitigated by using techniques such as regularization or early stopping [14]. Another challenge is catastrophic forgetting, which occurs when the model forgets the knowledge learned from the pre-training dataset as it learns new knowledge from the new task-specific dataset. To address this challenge, techniques such as knowledge distillation or multi-task learning can be used.

In conclusion, fine-tuning is a potent methodology in shallow transfer learning that enables us to leverage the pre-trained model's knowledge more effectively than feature extraction. It has been widely implemented in various applications, such as computer vision and natural language processing. Despite its limitations, techniques such as regularization, early stopping, knowledge distillation, and multi-task learning can be employed to mitigate these challenges. Overall, shallow transfer learning has proven to be an effective approach to improve model performance in new tasks with limited labeled data, and it is expected to play a critical role in future machine learning research..

2.3 Hybrid Approaches

As mentioned earlier, both feature extraction and fine-tuning have their own advantages and limitations. While feature extraction allows us to leverage the pre-trained model's knowledge effectively, it may not be specific enough to the new task. On the other hand, while fine-tuning allows us to adapt the pre-trained model to the new task-specific dataset, it may require a large amount of data and can suffer from overfitting [15].

To overcome the limitations of feature extraction and fine-tuning, a hybrid approach has been introduced. Hybrid approaches aim to strike a balance between these techniques by utilizing certain layers of the pre-trained model as feature extractors and fine-tuning the remaining layers on the new task-specific dataset [16].

Hybrid techniques have been proposed in the field of computer vision to enhance the effectiveness of object detection and segmentation models [17]. Faster Region-based Convolutional Neural Network (R-CNN) and Mask R-CNN models, for instance, take advantage of a pre-trained ResNet model to extract image features, which are then fine-tuned in the fully connected layers to perform object detection or segmentation [18]. This strategy permits the model to exploit the pre-trained model's familiarity with features such as corners, edges, and textures, while also adapting to the unique properties of the new task.

In the domain of natural language processing, a combination of techniques has been employed to enhance the performance of text classification and named entity recognition models. To illustrate, the Universal Language Model Fine-tuning (ULMFiT) method leverages a pre-trained language model like ASGD Weight-Dropped LSTM (AWD-LSTM) or Embeddings from Language Models (ELMo) for feature extraction from the text, which is then fine-tuned on the new task-specific dataset . This approach enables the model to take advantage of the pre-trained model's expertise in language structures and semantics while also adapting to the particular features of the new task[9].

In addition, hybrid approaches have been applied in various other fields, including speech recognition and recommender systems. For instance, in speech recognition, a hybrid approach entails utilizing a pre-trained deep neural network model to extract audio features, which is then fine-tuned on the task-specific dataset. In the case of recommender systems, a hybrid approach involves using a pre-trained collaborative filtering model to extract user and item embeddings, which are then fine-tuned on the new task-specific dataset.

One of the benefits of hybrid approaches is that they allow us to leverage the pre-trained model's knowledge more effectively than feature extraction alone, while also adapting the model to the specific characteristics of the new task more effectively than fine-tuning alone [19]. Hybrid approaches can also be useful in cases where the pre-trained model is not specific enough to the new task, but still provides a useful starting point for learning the new task.

In summary, hybrid approaches are a powerful technique in shallow transfer learning that strike a balance between feature extraction and fine-tuning. They have been widely used in various applications, including computer vision, natural language processing, speech recognition, and recommender systems. Hybrid approaches allow us to leverage the pre-trained model's knowledge more effectively than feature extraction alone, while also adapting the model to the specific characteristics of the new task more effectively than fine-tuning alone.

3. Applications of Shallow Transfer Learning Models

Shallow transfer learning models have become increasingly popular in recent years due to their ability to learn from one task and apply that knowledge to a different but related task. In this chapter, we will explore some of the common applications of shallow transfer learning models in various fields.

Shallow transfer learning models are widely used in the field of Natural Language Processing (NLP). These models are trained on large datasets of text and fine-tuned on specific tasks, such as sentiment analysis, text classification, and named entity recognition. Bidirectional Encoder Representations from

Transformers (BERT) is a popular shallow transfer learning model used in NLP, and it has demonstrated excellent performance on a variety of NLP tasks, making it one of the most popular models in the field.

Shallow transfer learning models are also widely used in computer vision. These models are trained on a large dataset of images, such as ImageNet, and then fine-tuned on a specific task, such as object detection, image classification, or image segmentation. Some of the popular shallow transfer learning models used in computer vision include VGG16, InceptionV3, and ResNet.

To tackle speech recognition tasks, shallow transfer learning models are also employed. These models are trained on large datasets of audio data and then fine-tuned on specific speech recognition tasks like speaker identification or speech-to-text conversion. DeepSpeech is one of the most widely used shallow transfer learning models in speech recognition and has achieved exceptional performance on a range of speech recognition tasks.

Shallow transfer learning models are also used in recommendation systems, where they are trained on a large dataset of user behavior data and then fine-tuned on a specific recommendation task, such as movie or product recommendations. These models can also be used for personalized recommendations, where the model is fine-tuned on a specific user's behavior data to provide personalized recommendations.

Shallow transfer learning models are also used in time series analysis, where they are trained on a large dataset of time series data and then fine-tuned on a specific time series analysis task, such as forecasting or anomaly detection. These models can also be used for multi-step forecasting, where the model is fine-tuned on a specific time series dataset to predict multiple steps ahead.

3.1 Natural Language Processing (NLP):

In addition to the applications mentioned earlier, shallow transfer learning models have been used in a wide range of NLP tasks. One of the most notable applications is in machine translation, where these models are used to translate text from one language to another [20]. In this use case, the model is initially trained on a vast amount of text data in a particular language and then fine-tuned on a specific translation task, such as the task of translating from English to Spanish or the reverse. Some popular shallow transfer learning models used for machine translation include Transformer, BERT, and GPT-2. Another application of shallow transfer learning models in NLP is in question answering. These models are trained on a large corpus of text, such as Wikipedia or other knowledge bases, and then fine-tuned on a specific question-answering task [21]. One example of this is the Stanford Question Answering Dataset (SQuAD), which is a popular benchmark for question-answering models. These models are also used in chatbots and conversational agents, where they are trained on a large dataset of conversational data and then fine-tuned on a specific conversational task.

Text summarization is another application where shallow transfer learning models are commonly utilized. These models are initially trained on a vast dataset of textual content and then fine-tuned on a specific summarization task, such as creating summaries of news articles or scientific publications [21]. Some popular shallow transfer learning models used for text summarization include Bidirectional and Auto-regressive Transformers (BART) and Text-to-Text Transfer Transformers (T5). Lastly, shallow transfer learning models are also used in sentiment analysis, where they are trained on a large corpus of text and then fine-tuned on a specific sentiment analysis task, such as predicting whether a piece of text is positive, negative, or neutral. These models are used in various applications, including social media analysis, brand monitoring, and customer feedback analysis[22].

In conclusion, shallow transfer learning models have proven to be highly effective in various NLP tasks, including question-answering, machine translation, text summarization, and sentiment analysis. As the field of NLP continues to grow, we can expect to see even more innovative applications of shallow transfer learning models in the future.

3.2 Computer Vision

In addition to the applications mentioned earlier, shallow transfer learning models have been used in a wide range of computer vision tasks. One notable application is in image captioning, where these models are used to generate a textual description of an image [23]. In this application, the model is first trained on a large dataset of image-caption pairs and then fine-tuned on a specific image captioning task. Some popular shallow transfer learning models used for image captioning include Show and Tell, NeuralTalk, and Bottom-Up Top-Down.

Image generation is another field where shallow transfer learning models are applied in computer vision. In this application, these models are utilized to create new images that are similar to a given input image or set of images [24]. The models are first trained on a large dataset of images and then fine-tuned on a specific image generation task such as image-to-image translation, super-resolution, or style transfer. Cycle Generative Adversarial Network (CycleGAN), Pixel to Pixel (Pix2Pix), and Adaptive Instance Normalization (AdaIN) are some of the most popular shallow transfer learning models used for image generation.

Shallow transfer learning models are utilized in object detection as well, which involves training them on a vast image dataset, followed by fine-tuning for detecting and locating objects in an image [25]. Several shallow transfer learning models used for object detection are prevalent, such as You Only Look Once (YOLO), Faster R-CNN, and Single Shot Detector (SSD).

Another application of shallow transfer learning models in computer vision is in video analysis, where these models are used to analyze and understand the content of videos. In this application, the model is first trained on a large dataset of videos and then fine-tuned on a specific video analysis task, such as action recognition, video segmentation, or video captioning [26]. Some popular shallow transfer learning models used for video analysis include Two-Stream Convolutional Networks, 3D Convolutional Networks, and Temporal Segment Networks.

To summarize, shallow transfer learning models have demonstrated remarkable performance in different computer vision tasks, such as image captioning, object detection, image generation, and video analysis. As the field of computer vision advances, it is anticipated that shallow transfer learning models will be applied in more innovative ways in the future.

3.3 Speech Recognition

Shallow transfer learning models have also been successfully applied in the field of speech recognition. In speech recognition, these models are used to convert spoken words into text. One of the most notable applications of shallow transfer learning models in speech recognition is in automatic speech recognition (ASR) systems [27].

Automatic Speech Recognition (ASR) systems typically undergo a training process on a large corpus of speech recordings and their corresponding transcriptions [28]. Subsequently, the model is fine-tuned on a specific speech recognition task, such as identifying the speech of a particular speaker or recognizing speech within a specific domain. Some popular shallow transfer learning models used for ASR include Deep Speech, Kaldi, and Wav2Letter.

Shallow transfer learning models are also used in speaker recognition, where they are used to identify and verify the identity of a speaker based on their voice. In this application, the model is first trained on a large dataset of speaker voice recordings and then fine-tuned on a specific speaker recognition task. Some popular shallow transfer learning models used for speaker recognition include x-vector, i-vector, and Deep Speaker Embeddings [25].

Another application of shallow transfer learning models in speech recognition is in emotion recognition, where they are used to recognize the emotional state of a speaker based on their voice. In this application, the model is first trained on a large dataset of emotional speech recordings and then fine-tuned on a specific emotion recognition task. Some popular shallow transfer learning models used for emotion recognition include Deep Emotion Recognition, AffectNet, and EmoReact [29].

Lastly, shallow transfer learning models are also used in accent recognition, where they are used to identify the accent of a speaker based on their voice. In this application, the model is first trained on a large dataset of speech recordings from speakers with different accents and then fine-tuned on a specific accent recognition task. Some popular shallow transfer learning models used for accent recognition include Deep Accent Recognition, VoxCeleb, and AccentDB.

Consequently, it is evident that shallow transfer learning models have demonstrated remarkable efficiency in several speech recognition tasks, including automatic speech recognition, speaker recognition, emotion recognition, and accent recognition. As the domain of speech recognition continues to expand, we anticipate more creative applications of shallow transfer learning models in the future.

3.4 Recommendation Systems

Shallow transfer learning models have also been widely used in recommendation systems, which are designed to recommend items to users based on their past behavior, preferences, and interactions [30]. One notable application of shallow transfer learning models in recommendation systems is in collaborative filtering, where the model is used to predict the preferences of a user for a given item based on the preferences of other users with similar interests.

To perform collaborative filtering, a shallow transfer learning model is trained on a large dataset of user-item interactions, such as purchase histories or ratings. After training, the model is fine-tuned for a specific recommendation task, such as predicting a user's rating for a new item or suggesting a set of items based on past user behavior. Common shallow transfer learning models utilized for collaborative filtering include Matrix Factorization, Neural Collaborative Filtering, and Factorization Machines [31].

Another application of shallow transfer learning models in recommendation systems is in content-based recommendation, where the model is used to recommend items to users based on their content features, such as genre, author, or keywords. In this application, the model is first trained on a large dataset of item content features and then fine-tuned on a specific recommendation task. Some popular shallow transfer learning models used for content-based recommendation include Word2Vec, Doc2Vec, and FastText [31], [32].

Hybrid recommendation systems, which integrate collaborative filtering and content-based recommendation, can benefit from shallow transfer learning models to deliver more diverse and precise recommendations. These models are initially trained on a comprehensive set of item content features and user-item interactions, and subsequently fine-tuned for a specific hybrid recommendation task. Popular shallow transfer learning models applied in hybrid recommendation systems encompass DeepFM, Wide and Deep, and AutoInt.

In context-aware recommendation systems, which consider the contextual information of both the user and the item for personalized recommendations, shallow transfer learning models are also employed. These models are trained on a vast dataset of user-item interactions and contextual information, such as location, time, or weather, and later fine-tuned for a specific context-aware recommendation task [33]. Prominent shallow transfer learning models applied in context-aware recommendation systems comprise Factorized Personalized Markov Chains (FPMC), CoFactor, and Context-aware Attentional Factorization Machines .

In conclusion, shallow transfer learning models have proven to be highly effective in various recommendation systems tasks, including collaborative filtering, content-based recommendation, hybrid recommendation, and context-aware recommendation. As the field of recommendation systems continues to grow, we can expect to see even more innovative applications of shallow transfer learning models in the future.

3.5 Time Series Analysis

The domain of time series analysis, which pertains to examining and predicting data points gathered over time, has also seen the successful implementation of shallow transfer learning models [33]. These models are particularly noteworthy in forecasting, as they enable the prediction of future values of a time series based on its historical data.

In time series forecasting, the model is first trained on a large dataset of historical time series data and then fine-tuned on a specific forecasting task, such as predicting the stock prices of a particular company or forecasting the demand for a particular product. Some popular shallow transfer learning models used for time series forecasting include Long Short-Term Memory (LSTM), Gated Recurrent Unit (GRU), and WaveNet [30].

Anomaly detection is yet another field of time series analysis where shallow transfer learning models have found their application. In this context, these models can identify uncommon patterns or outliers in time series data. To accomplish this, the model is initially trained on a vast dataset of regular time series data and later fine-tuned for a specific anomaly detection task. Notable shallow transfer learning models applied in anomaly detection in time series comprise AutoEncoder, Deep AR, and DeepAD [31].

Time series classification is another area where shallow transfer learning models are commonly utilized. These models can classify time series data into distinct categories based on their features or characteristics. To achieve this, the model is initially trained on a comprehensive dataset of labeled time series data, and then fine-tuned for a specific time series classification task. Prominent shallow transfer learning models used for time series classification encompass CNN, ResNet, and TimeLeNet.

Lastly, shallow transfer learning models are also used in time series clustering, where the model is used to group similar time series data into clusters based on their features or characteristics. In this application, the model is first trained on a large dataset of time series data without labels and then fine-tuned on a specific time series clustering task. Some popular shallow transfer learning models used for time series clustering include Dynamic Time Warping (DTW), k-means, and Symbolic Aggregate Approximation Vector Space Model (SAX-VSM) [32].

In conclusion, shallow transfer learning models have proven to be highly effective in various time series analysis tasks, including forecasting, anomaly detection, classification, and clustering. As the field of time series analysis continues to grow, we can expect to see even more innovative applications of shallow transfer learning models in the future.

5. Conclusion

In recent years, shallow transfer learning models have emerged as a powerful tool in machine learning, providing a flexible and efficient way to solve a wide range of tasks with limited labeled data. These models leverage the pre-trained knowledge learned from large datasets and transfer it to new tasks with less data, thereby reducing the need for expensive and time-consuming data collection and annotation.

Throughout this book chapter, we have explored the various applications of shallow transfer learning models in different domains, including natural language processing, computer vision, speech recognition, recommendation systems, and time series analysis. In each of these domains, we have seen how shallow transfer learning models have demonstrated impressive performance and outperformed traditional machine learning approaches.

While there are many benefits of using shallow transfer learning models, there are also some limitations and challenges that need to be addressed. One challenge is the selection of appropriate pre-trained models and fine-tuning strategies that can optimize the performance on a given task. Another challenge is the domain shift problem, where the pre-trained knowledge may not generalize well to the new task due to differences in the data distribution or feature space.

Despite these challenges, the future of shallow transfer learning models looks promising, and we can expect to see continued growth and development in this field. As more data becomes available, and computational power continues to improve, we can expect that shallow transfer learning models will become even more powerful and widely used in various applications.

In conclusion, this book chapter has provided an overview of shallow transfer learning models, their applications, and their limitations. We hope that this book has provided a useful resource for researchers, practitioners, and students interested in learning more about this exciting area of machine learning. We also hope that this book chapter has inspired new ideas and innovations in shallow transfer learning that will contribute to the advancement of machine learning as a whole.

Referencess

[1] J. Zhu, N. Chen, and C. Shen, "A New Deep Transfer Learning Method for Bearing Fault Diagnosis under Different Working Conditions," *IEEE Sens J*, vol. 20, no. 15, pp. 8394–8402, Aug. 2020, doi: 10.1109/JSEN.2019.2936932.

[2] M. Long, H. Zhu, J. Wang, and M. I. Jordan, "Deep Transfer Learning with Joint Adaptation Networks," 2017.

[3] F. Zhuang *et al.*, "A Comprehensive Survey on Transfer Learning," *Proceedings of the IEEE*, vol. 109, no. 1. Institute of Electrical and Electronics Engineers Inc., pp. 43–76, Jan. 01, 2021. doi: 10.1109/JPROC.2020.3004555.

[4] D. Impedovo, V. Dentamaro, G. Abbattista, V. Gattulli, and G. Pirlo, "A comparative study of shallow learning and deep transfer learning techniques for accurate fingerprints vitality detection," *Pattern Recognit Lett*, vol. 151, pp. 11–18, Nov. 2021, doi: 10.1016/j.patrec.2021.07.025.

[5] R. Alasbahi and X. Zheng, "An Online Transfer Learning Framework With Extreme Learning Machine for Automated Credit Scoring," *IEEE Access*, vol. 10, pp. 46697–46716, 2022, doi: 10.1109/ACCESS.2022.3171569.

[6] J. Xie, B. Huang, and S. Dubljevic, "Transfer Learning for Dynamic Feature Extraction Using Variational Bayesian Inference," *IEEE Trans Knowl Data Eng*, vol. 34, no. 11, pp. 5524–5535, Nov. 2022, doi: 10.1109/TKDE.2021.3054671.

[7] I. Patrini, M. Ruperti, S. Moccia, L. S. Mattos, E. Frontoni, and E. De Momi, "Transfer learning for informative-frame selection in laryngoscopic videos through learned features," *Med Biol Eng Comput*, vol. 58, no. 6, pp. 1225–1238, Jun. 2020, doi: 10.1007/s11517-020-02127-7.

[8] Md. A. Talukder, Md. M. Islam, M. A. Uddin, A. Akhter, K. F. Hasan, and M. A. Moni, "Machine Learning-based Lung and Colon Cancer Detection using Deep Feature Extraction and Ensemble Learning," Jun. 2022, [Online]. Available: http://arxiv.org/abs/2206.01088

[9] A. Carballal, C. Fernandez-Lozano, J. Heras, and J. Romero, "Transfer learning features for predicting aesthetics through a novel hybrid machine learning method," *Neural Comput Appl*, vol. 32, no. 10, pp. 5889–5900, May 2020, doi: 10.1007/s00521-019-04065-4.

[10] G. Vrbančič and V. Podgorelec, "Transfer learning with adaptive fine-tuning," *IEEE Access*, vol. 8, pp. 196197–196211, 2020, doi: 10.1109/ACCESS.2020.3034343.

[11] Y. H. Gu, H. Yin, D. Jin, J. H. Park, and S. J. Yoo, "Image-Based Hot Pepper Disease and Pest Diagnosis Using Transfer Learning and Fine-

Tuning," *Front Plant Sci*, vol. 12, Dec. 2021, doi: 10.3389/fpls.2021.724487.

[12] Y. Arase and J. Tsujii, "Transfer fine-tuning of BERT with phrasal paraphrases," *Comput Speech Lang*, vol. 66, Mar. 2021, doi: 10.1016/j.csl.2020.101164.

[13] A. Albayrak, "Classification of analyzable metaphase images using transfer learning and fine tuning," *Med Biol Eng Comput*, vol. 60, no. 1, pp. 239–248, Jan. 2022, doi: 10.1007/s11517-021-02474-z.

[14] A. Bashar and R. Nayak, "Active Learning for Effectively Fine-tuning Transfer Learning to Downstream Task."

[15] O. Day and T. M. Khoshgoftaar, "A survey on heterogeneous transfer learning," *J Big Data*, vol. 4, no. 1, Dec. 2017, doi: 10.1186/s40537-017-0089-0.

[16] Y. Tang, K. Yang, S. Zhang, and Z. Zhang, "Photovoltaic power forecasting: A hybrid deep learning model incorporating transfer learning strategy," *Renewable and Sustainable Energy Reviews*, vol. 162, Jul. 2022, doi: 10.1016/j.rser.2022.112473.

[17] J. T. Zhou, S. J. Pan, and I. W. Tsang, "A deep learning framework for Hybrid Heterogeneous Transfer Learning," *Artif Intell*, vol. 275, pp. 310–328, Oct. 2019, doi: 10.1016/j.artint.2019.06.001.

[18] N. A. Samee *et al.*, "Classification Framework for Medical Diagnosis of Brain Tumor with an Effective Hybrid Transfer Learning Model," *Diagnostics*, vol. 12, no. 10, Oct. 2022, doi: 10.3390/diagnostics12102541.

[19] R. K. Mishra, S. Urolagin, J. A. Arul Jothi, and P. Gaur, "Deep hybrid learning for facial expression binary classifications and predictions," *Image Vis Comput*, vol. 128, Dec. 2022, doi: 10.1016/j.imavis.2022.104573.

[20] I. Sarhan and M. Spruit, "Can we survive without labelled data in NLP? Transfer learning for open information extraction," *Applied Sciences (Switzerland)*, vol. 10, no. 17, Sep. 2020, doi: 10.3390/APP10175758.

[21] C. Shorten, T. M. Khoshgoftaar, and B. Furht, "Text Data Augmentation for Deep Learning," *J Big Data*, vol. 8, no. 1, Dec. 2021, doi: 10.1186/s40537-021-00492-0.

[22] R. Liu, Y. Shi, C. Ji, and M. Jia, "A Survey of Sentiment Analysis Based on Transfer Learning," *IEEE Access*, vol. 7. Institute of Electrical and Electronics Engineers Inc., pp. 85401–85412, 2019. doi: 10.1109/ACCESS.2019.2925059.

[23] X. Li *et al.*, "Transfer learning in computer vision tasks: Remember where you come from," *Image Vis Comput*, vol. 93, Jan. 2020, doi: 10.1016/j.imavis.2019.103853.

[24] K. Bayoudh, R. Knani, F. Hamdaoui, and A. Mtibaa, "A survey on deep multimodal learning for computer vision: advances, trends, applications, and datasets," *Visual Computer*, vol. 38, no. 8, pp. 2939–2970, Aug. 2022, doi: 10.1007/s00371-021-02166-7.

[25] W. Shen, INESC TEC (Organization), Universidade de Trás-os-Montes e Alto Douro, M. IEEE Systems, International Working Group on Computer Supported Cooperative Work in Design, and Institute of Electrical and Electronics Engineers, *Proceedings of the 2019 IEEE 23rd International Conference on Computer Supported Cooperative Work in Design (CSCWD) : May 6-8, 2019, Porto, Portugal*.

[26] C. Zhang, J. Wang, G. Lu, S. Fei, T. Zheng, and B. Huang, "Automated tea quality identification based on deep convolutional neural networks and transfer learning," *J Food Process Eng*, 2023, doi: 10.1111/jfpe.14303.

[27] V. Kadyan and P. Bawa, "Transfer learning through perturbation-based in-domain spectrogram augmentation for adult speech recognition," *Neural Comput Appl*, vol. 34, no. 23, pp. 21015–21033, Dec. 2022, doi: 10.1007/s00521-022-07579-6.

[28] D. Wang and T. F. Zheng, "Transfer learning for speech and language processing," in *2015 Asia-Pacific Signal and Information Processing Association Annual Summit and Conference, APSIPA ASC 2015*, Feb. 2016, pp. 1225–1237. doi: 10.1109/APSIPA.2015.7415532.

[29] T. A. Mariya Celin, P. Vijayalakshmi, and T. Nagarajan, "Data Augmentation Techniques for Transfer Learning-Based Continuous Dysarthric Speech Recognition," *Circuits Syst Signal Process*, vol. 42, no. 1, pp. 601–622, Jan. 2023, doi: 10.1007/s00034-022-02156-7.

[30] X. Li, Z. Wang, R. Hu, Q. Zhu, and L. Wang, "Recommendation algorithm based on improved spectral clustering and transfer learning," *Pattern Analysis and Applications*, vol. 22, no. 2, pp. 633–647, May 2019, doi: 10.1007/s10044-017-0671-2.

[31] X. Fang, "Making recommendations using transfer learning," *Neural Comput Appl*, vol. 33, no. 15, pp. 9663–9676, Aug. 2021, doi: 10.1007/s00521-021-05730-3.

[32] H. Xie, B. Liu, and Y. Xiao, "Transfer learning-based one-class dictionary learning for recommendation data stream," *Inf Sci (N Y)*, vol. 547, pp. 526–538, Feb. 2021, doi: 10.1016/j.ins.2020.08.091.

[33] D. Li, Z. Gong, and D. Zhang, "A common topic transfer learning model for crossing city POI recommendations," *IEEE Trans Cybern*, vol. 49, no. 12, pp. 4282–4295, Dec. 2019, doi: 10.1109/TCYB.2018.2861897.

Chapter 5

Study and Comparative Analysis of P&O-PID and FLC-PID Maximum Power Point Tracking Algorithms for a New Solar PV System

Siham AISSANI[1]

Mohcene BECHOUAT[2]

Moussa SEDRAOUI[3]

Toufik AMIEUR[4]

[1] Département Électronique et Télécommunications / Laboratoires des Télécommunications LT, University 8 May 1945 of Guelma,Algeria Guelma, Algeria,
aissanisiham24@gmail.com

[2] Département d'automatique et d'électromécanique, Faculté dessciences et de la technologie / Université de Ghardaïa, Algeria,
mohcene.oui@gmail.com

[3] Département Électronique et Télécommunications / Laboratoires des Télécommunications LT, University 8 May 1945 of Guelma,Algeria Guelma, Algeria,
sedraoui.moussa@univ-guelma.dz

[4] Département de Génie Électrique / Université de Larbi Tebessi Tebessa, Algeria,
amieur.to@gmail.com

I. INTRODUCTION

Due to the increasing demand for energy in the world, in addition to the many dangers left by fossil fuels and their derivatives, the world has moved to the use of renewable energies, which are many and varied and are not harmful to the environment,

in addition to being constantly renewed, the most important of which is solar energy, as it provides huge amounts of energy daily, which is exploited using solar panels Which has the ability to convert sunlight into electrical energy, the performance of this latter is ideal, at the point MPP and this point is not fixed but changes with the change of weather conditions and thus affects the current and output voltage of the photovoltaic panel so this point must be monitored and tracked, the main goal is to choose the algorithm that Provides dynamic tracking accurate and true for MPP regardless of the current climatic conditions such as absolute temperature and solar radiation to ensure maximum power extraction P from the solar panels,

For this; $MPPT$ technologies are used to track this point. The issue of $MPPT$ has been studied in many literatures among them Perturb Observe Algorithm and FLC Algorithm These two algorithms are the most used due to their ease of application and the good results they provide. The Perturb Observe algorithm is simple and easy to implement, and the $FLC\ fuzzy$ logic algorithm has a powerful feature of voltage regulation by automatic update duty cycle control, that is, it prevents us from making the mistake of choosing the update step that causes the entire system to malfunction; Many researchers have improved and developed these algorithms, as they have provided many simulations and experimental tests to control the transformer duty cycle, including:

Femia et al. (2005) implemented the direct $P\&O$ algorithm and improved it by defining its parameters .and energy extraction and improvement under changing weather conditions, where they succeeded in overcoming some of the shortcomings of this algorithm.[1]. Ngan & Tan (April 2011) also carried out the direct implementation of the $P\&O$ algorithm, where it calculated the duty cycle of the $Boost\ DC-DC$ converter and used: the generated power and the corresponding voltage.[2],

Algazar, M. et al. (2012), $Fuzzy-MPPT$ Control Strategy for Fast and Efficient MPP Tracking in Weather Conditions changing [3], Elgharbaoui E, et al; (2014) controlled the photovoltaic generator using MPP strategy based on INC and $Fuzzy$ algorithm [4]; Zaghba, L. and others; (2014) use an $MPPT$ algorithm based on fuzzy logic to improve the control performance of a PV system consisting of (PV panel, $Buck-Boost\ DC-DC$ converter, and load) and use Matlab/Simulink software to simulate and show results [5]. Kumar, M., and others; (2015) they compared the controller based on the additive conductivity algorithm and the controller based on the fuzzy logic controller algorithm in PV systems, and the comparison results showed that the performance of the fuzzy controller is superior in comparison with the additive conductivity. [6].

Both algorithms improve the performance of the PV system and give good MPP tracking dynamics, but there is a ripple problem, which leads to a large loss of output power and is a major problem for PV systems, to get rid of this problem, a PID controller is combined with $P\&O - MPPT$ algorithms and $Fuzzy - MPPT$ to design a powerful controller and achieve better and more accurate MPP tracking dynamics. $P\&O - PID$ and $FLC - PID$ control strategies allow us to regulate the PV system output voltage and power under rapid and sudden changes in climatic conditions This made many researchers focus on studying indirect control under changing weather conditions. between them; Harrag & Messalti (2015) implemented the standard $P\&O - MPPT$ control strategy based on variable step size. The parameters of the PID controller were modified and developed using the GA genetic algorithm [7].Subianto et al. (2010). used a closed-loop fuzzy logic algorithm and the proportional integral derivative (PID) and applied it to a new high-performance $DC - DC\ Boost$ converter [8]. In this paper, the two new control strategies consist of two steps : first: using the principle of small signal to design a mathematical model of the photovoltaic system, And second, to create an optimal reference voltage using both direct $P\&O$ and FLC algorithms as a function of solar radiation and absolute temperature. Finally, a comparison is made between the output reference voltage and the voltage provided by a model of the photovoltaic system based on the small signal. This comparison results in the voltage deviation and its reduction. The main task of the PID voltage control unit is that the correct adjustment of the PID parameters provides the required duty cycle. The latter should eliminate the oscillations that occurred during MPP tracking. Simulation results confirm that the proposed control strategies $P\&O\ - PID$ and $FLC - PID$ capture the required MPP under changes in solar radiation and temperature. The control strategy $P\&O - PID$ provides better tracking dynamics than the $FLC\ - PID$ control strategy

The rest of the paper will be organized as follows: The introduction is presented in Section 1. The equivalent electric circuit model is presented in Section 2. The linear small-signal solar system model is presented in Section 3. Section 4 and 5 will focus on tuning two voltage PID controllers for the algorithm $P\&O$ and FLC algorithm, simulation results are shown in Section 6. Finally, conclusions are drawn in Section 7.

II. MODELING OF PV PANEL

The nonlinear (voltage-current) behavior of photovoltaic cells is described by the equivalent electric circuit illustrated in Figure 1.

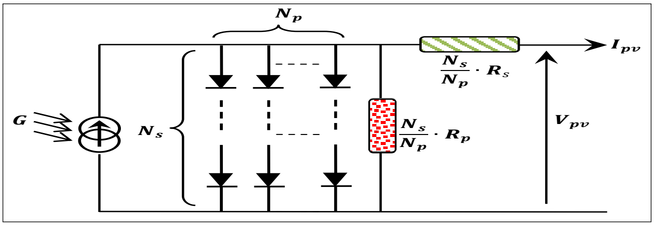

Fig.1. Equivalent electrical circuit of the PV panel model

According to Fig. 1, the nonlinear characteristic $(V - I)$ is derived where the photoelectric current expected is expressed by:

$$I_{pv} = N_p I_{ph} - N_p I_0 \left[exp\left(\frac{q\left(\frac{V_{pv}}{N_S} + \frac{R_S I_{pv}}{N_p}\right)}{a N_C K T} \right) - 1 \right] - \frac{\frac{N_p V_{pv}}{N_S} + R_S I_{pv}}{R_p} \tag{1}$$

Where T is the temperature of the PV cells constant, R_s is the equivalent series resistance, q is the electronic charge and k is the Boltzmann, $V_t = N_c kT / q$ is the thermal voltage, N_c is the number of cells connected in series, N_S and N_p are series and parallel string respectively, I_{Pv} and I_0 are the photovoltaic (PV) currents and saturation, a is the ideality constant of the diode, R_p is the equivalent shunt resistance.

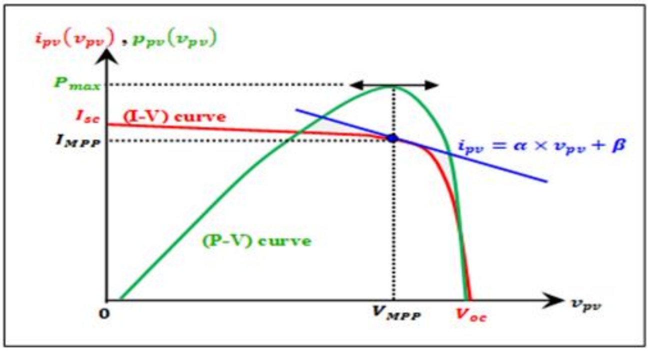

Fig.2. Nonlinear $i \times v$ characteristic of the $KC200GT$ solar panel and linear MPP equivalent model

III. MODELING OF GLOBAL SOLAR SYSTEM

Most real-world applications require more power than that produced by the GPV panel and to obtain greater power, the insertion of a $DC-DC\ Boost$ converter is necessary between the GPV panel and the electrical device to be driven. Figure 3 shows the equivalent electrical circuit used for the three aforementioned electrical devices.

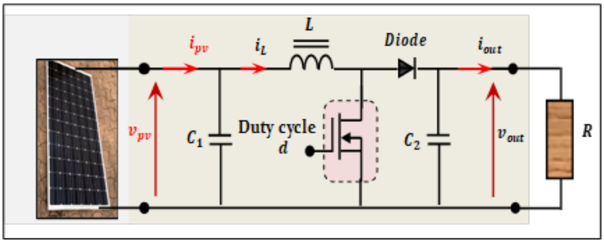

Fig.3. Interconnection system including the $PV, DC-DC$ boost ,and the resistive load

From Figure 3, to obtain the power required to feed the resistive load, the appropriate voltage supplied by the control switch (transistor) of the $DC-DC\ Boost$ converter must be regulated. Here, the appropriate voltage PID controller supplies the necessary pulse width modulation PWM signal, which has the preset frequency. As a result, tuning the PID voltage controller requires a linear preform that relates the PV output voltage to the input command of the $DC-DC\ Boost$ converter. Accordingly, the corresponding nonlinear space representation is given by:

$$\begin{aligned} \dot{V}_{pv} &= \frac{1}{C_1}.I_{PV} - \frac{1}{C_1}.I_L \\ \dot{I}_L &= \frac{1}{L}.V_{pv} - \left(\frac{1-d}{L}\right).V_{out} \\ \dot{V}_{out} &= \left(\frac{1-d}{C_2}\right).I_L - \frac{1}{R.C_2}.V_{out} \end{aligned} \tag{2}$$

The principle of small sign is applied to convert the previous non-linear space into a linear space. This is achieved by applying some steps described in [13]. The resulting linear state space representation is given by

$$\begin{bmatrix} \delta \dot{V_{pv}} \\ \delta \dot{I_L} \\ \delta \dot{V_{out}} \end{bmatrix} = \begin{bmatrix} -\frac{1}{R_{eq}C_1} & -\frac{1}{C_1} & 0 \\ \frac{1}{L} & 0 & \frac{1-D_{MPP}}{L} \\ 0 & \frac{1-D_{MPP}}{C_2} & -\frac{1}{RC_2} \end{bmatrix} \begin{bmatrix} \delta V_{pv} \\ \delta I_L \\ \delta V_{out} \end{bmatrix} + \begin{pmatrix} 0 \\ \frac{-V_{out_{MPP}}}{L} \\ -\frac{I_{L_{MPP}}}{C_2} \end{pmatrix} \delta d \qquad (3)$$

IV. SYNTHESIS OF VOLTAGE $P\&O - PID$ CONTROLLER

The indirect implementation of the $P\&O$ strategy, which highlights the new improved $P\&O - PID$ control, takes place is realized in two basic steps: First, the direct use of the $P\&O$ algorithm to produce the reference voltage using the current PV voltage and PV power. The latter is compared to the photovoltage obtained from the linear model and this produces a voltage error at each sampling time. This error is reduced in the second step by means of a composite PID controller whose parameters are modeled through the linear small-signal model which is given by "(3)". The general scheme of the optimized control strategy is shown in Figure 4 as follows

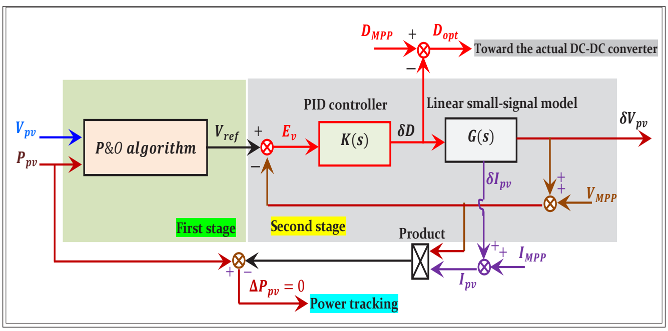

Fig.4. $P\&O - MPPT$ scheme equipped with a stabilized PID voltage controller

According to Figure 4, the reference voltage is generated using the rectified flow diagram shown in Figure 5 as follows:

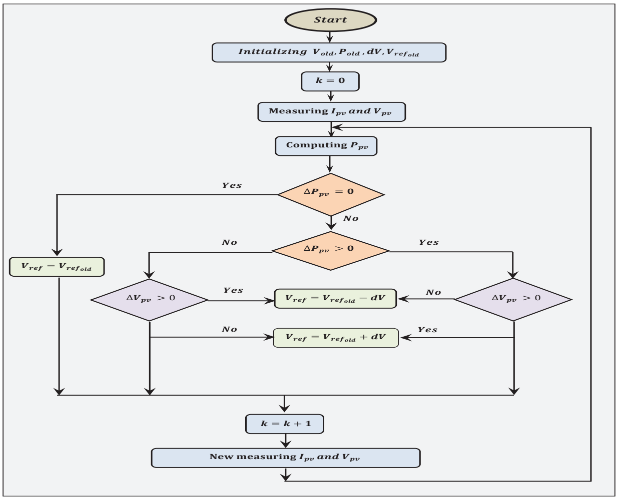

Fig.5. Flowchart of the $P\&O$ algorithm used to generate the reference PV voltage

V. SYNTHESIS OF VOLTAGE $FLC - PID$ CONTROLLER

The indirect implementation of the FLC strategy, which highlights the new improved control of the $FLC - PID$, takes place in two basic steps: first, the direct use of the FLC algorithm to produce $\Delta Vref$; The power change (ΔPPV) and the voltage change (ΔVPV) are used. $\Delta Vref$ is compared to the PV voltage obtained from the linear model and this produces an error in voltage at each sampling time. This error is reduced in the second step by means of a composite PID controller whose parameters are modeled by the linear small-signal model given by “(3)”. The general scheme of the optimal control strategy is shown in Figure 6 as follows

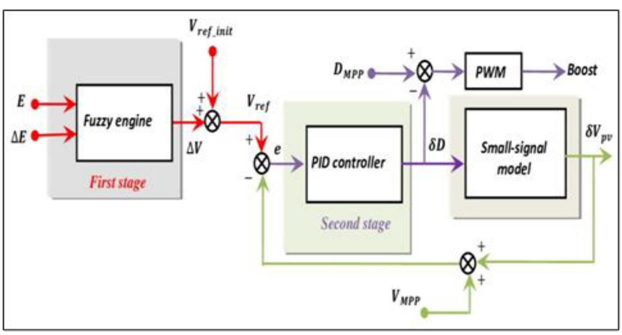

Fig.6. $FLC - MPPT$ scheme equipped with a stabilized PID voltage controller

According to Figure 6, the reference voltage is generated using the rectified flow diagram shown in Figure 7 as follows:

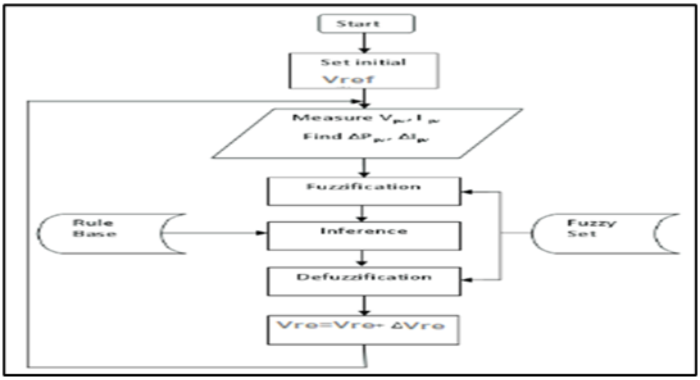

Fig.7. Flowchart of the FLC algorithm used to generate the reference PV voltage

VI. SIMULATION RESULTS AND DISCUSSION

To demonstrate the effectiveness of the improved $P\&O - MPPT$ and $FLC - MPPT$ control strategy, the $MATLAB® / SIMULINK$ package is used. Here, the solar system parameters are summarized in the table. Indeed, the transfer function describing the small-signal model is calculated using “(3)”. The latter relates the variation of the duty cycle input to the output PV voltage. given before:

$$G(s) = \frac{168.27\times10^{6}(s+3.333)}{(s+3.3104)(s+31.181-738.41i)(s+31.181+738.41i)} \tag{4}$$

Table1. system data

		Parameter	Value	Unit
Parameters of the KC200GT solar anel		I_0	$9.825 \times 10^{-8} A$	A
		I_{sc}	8.214	A
		V_{oc}	32.9	V
		a	1.3	-
		R_p	415.405	Ω
		R_s	0.221	Ω
		N_c	54	-
		N_s	1	-
		N_p	1	-
	Parameters of the simplified electrical circuit	V_{eq}	51.5970	V
		R_{eq}	3.3242	Ω
	Parameters given at MPP	V_{MPP}	26.3	V
		$V_{out_{MPP}}$	316.34	V
		I_{MPP}	7.61	A
		D_{MPP}	0.91686	-
Parameters of the DC-DC boost converter		L	0.4	mH
		C_1	4700	μF
		C_2	1200	μF
Resistive load		R	500	Ω

The power voltage, i.e. $(P - V)$ characteristic of the $KC200GT$ panel is shown in Figure 7 under variable solar radiation and absolute temperature. The maximum power under STC conditions (i.e., $T = 25$ and $G = 1000W / m^2$) is $P = 200.1\, W$ at $V = 26.3V$. The peak energy decreases when the solar radiation value decreases. The main objective of this study is to design a PID voltage controller, which provides excellent tracking dynamics of MPP under changing climatic conditions.

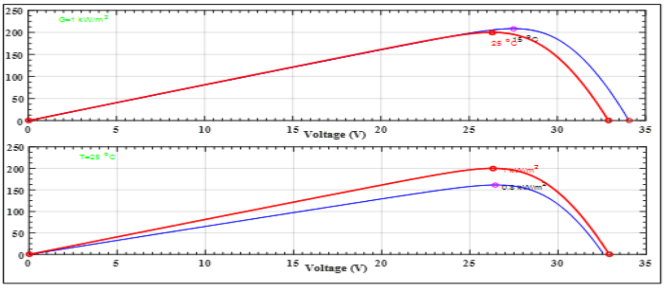

Fig.8. $P - V$ characteristic of $KC200GT$ panel

To verify the controller performances, the preceding two climatic conditions are chosen according the profile given in Fig.9.

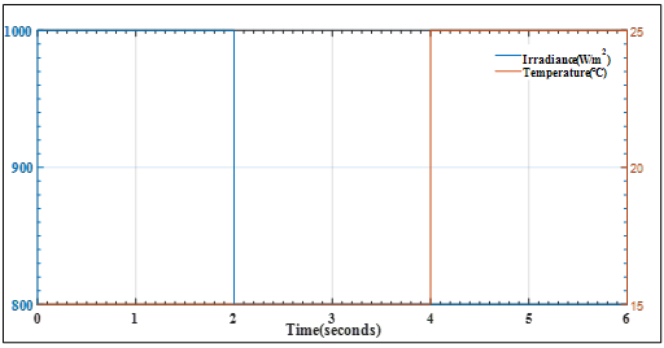

Fig.9.Irradiance and temperature variation

Figure 10 shows the comparison between the two systems $P\&O - MPPT$ and $FLC - MPPT$ with a closed loop, both of which provide excellent tracking dynamics and a fast and accurate MPP response without ripples, but we note from the figure that the dynamics provided by the $P\&O - MPPT$ system are better than those provided by the $FLC - MPPT$ system in terms of speed and accuracy response.

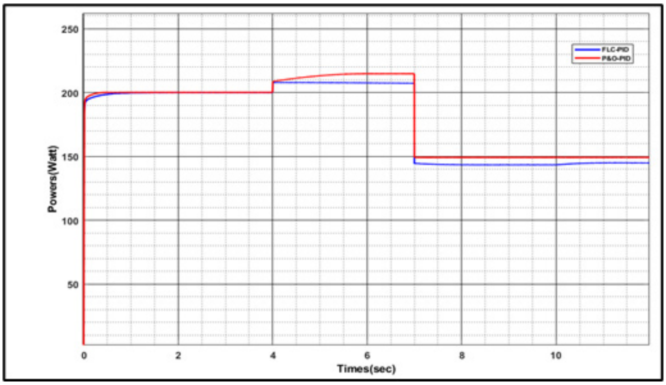

Fig.10. shows the comparison between the two systems $P\&O - MPPT$ and $FLC - MPPT$ with a closed loop

VII. CONCLUSION

The improved control strategy $P\&O - MPPT$ and $FLC - MPPT$ were applied to monitor the solar system based on the $KC200GT$ panel and compared. The comparison results confirmed that the tracking dynamics of the reference voltage provided by the $P\&O - MPPT$ control strategy is superior to the tracking dynamics provided by the $FLC - MPPT$ control strategy, from Where the speed and accuracy of response under sudden changes in weather conditions.

REFERENCES

[1] Femia, N., Petrone, G., Spagnuolo, G., & Vitelli, M. (2005). Optimization of perturb and observe maximum power point tracking method. IEEE transactions on power electronics, 20(4), 963-973.

[2] Ngan, M. S., & Tan, C. W. (2011, April). A study of maximum power point tracking algorithms for stand-alone photovoltaic systems. In 2011 IEEE Applied Power Electronics Colloquium (IAPEC) (pp. 22-27). IEEE.

[3] Algazar, M. M., Abd El-Halim, H., & Salem, M. E. E. K. (2012). Maximum power point tracking using fuzzy logic control. *International Journal of Electrical Power & Energy Systems*, *39*(1), 21-28.

[4] Elgharbaoui, E., Essadki, A., & Nasser, T. (2014, November). MPPT commands for a photovoltaic generator using the Incremental Conductance Method and the fuzzy logic command. In *2014 International Conference on Electrical Sciences and Technologies in Maghreb (CISTEM)* (pp. 1-6). IEEE

[5] Zaghba, L., Borni, A., Bouchakeur, A., & Terki, N. (2014, November). An intelligent approach based on fuzzy logic for improving and optimizing the performance of a photovoltaic system. In *2014 International Conference on Electrical Sciences and Technologies in Maghreb (CISTEM)* (pp. 1-6). IEEE.

[6] Kumar, M., Kapoor, S. R., Nagar, R., & Verma, A. (2015). Comparison between IC and fuzzy logic MPPT algorithm based solar PV system using boost converter. *International Journal of Advanced Research in Electrical, Electronics and Instrumentation Engineering*, *4*(6), 4927-4939

[7] A. Harrag and M. Sabir. "Variable step size modified P&O MPPT algorithm using GA-based hybrid offline/online PID controller." Renewable and Sustainable Energy Reviews 49 (2015): 1247-1260.

[8] Subiyanto, A. M., & Hannan, M. A. (2010). Photovoltaic maximum power point tracking controller using a new high performance boost converter. *International Review of Electrical Engineering*, *5*(6), 2535-2545.

[9] Pattanaik, B., & Bakare, Y. B. (2022). PV System-Based Switched Capacitor DC–DC Converter for High Voltage Gain Using Fuzzy-PID Controller. In *Advances in Micro-Electronics, Embedded Systems and IoT* (pp. 59-65). Springer, Singapore.

[10] Harrag, A., & Messalti, S. (2015). Variable step size modified P&O MPPT algorithm using GA-based hybrid offline/online PID controller. *Renewable and Sustainable Energy Reviews*, 49, 1247-1260.

[11] Paital, S. R., & Ray, P. K. (2021). An optimised Interval type-2 fuzzy PID-based PSS for stability improvement in solar-PV integrated power system considering uncertainties. *International Journal of Ambient Energy*, 1-15.-frequency DC–DC converters. *IEEE Transactions on Power Electronics*, *32*(4), 2508-2520.

[12] Garud, K. S., Jayaraj, S., & Lee, M. Y. (2021). A review on modeling of solar photovoltaic systems using artificial neural networks, fuzzy logic, genetic algorithm and hybrid models. *International Journal of Energy Research*, *45*(1), 6-35.

[13] M. G.Villalva, T. G.De Siqueira&E.Ruppert, (2010). Voltage regulation of photovoltaic arrays: small-signal analysis and control design. *IET Power Electronics*, 3(6), 869-880.

[14] Bechouat, M., Sedraoui, M., Feraga, C. E., Aidoud, M., & Kahla, S. (2019). Modeling and Fuzzy MPPT Controller Design for Photovoltaic Module Equipped with a Closed-Loop Cooling System. *Journal of Electronic Materials*, 1-10.

[15] Olusegun, A. T., Adebukola, A. Z., Denwigwe, I. H., Oluseyi, P. O., & Olubayo, B. M. (2019). Comparative analysis of two direct MPPT methods used for tracking maximum power points in a photovoltaic system. World Scientific News, 131, 123-146.

[16] Owusu-Nyarko, I., Elgenedy, M. A., Abdelsalam, I., & Ahmed, K. H. (2021). Modified variable step-size incremental conductance MPPT technique for photovoltaic systems. Electronics, 10(19), 2331.

[17] Lawan, M., Aboushady, A., & Ahmed, K. H. (2020, September). Photovoltaic MPPT techniques comparative review. In 2020 9th International Conference on Renewable Energy Research and Application (ICRERA) (pp. 344-351). IEEE.

[18] Anuradha, T., Sundari, P. D., Padmanaban, S., Siano, P., & Leonowicz, Z. (2017, June). Comparative analysis of common MPPT techniques for solar PV system with soft switched, interleaved isolated converter. In 2017 IEEE International Conference on Environment and Electrical Engineering and 2017 IEEE Industrial and Commercial Power Systems Europe (EEEIC/I&CPS Europe) (pp. 1-6). IEE

Chapter 8

Microstructure, Mechanical Properties and Fatigue Behavior of 6005 Aluminum Alloy in Different Precipitation Hardening Conditions

DEBIH Ali[1]

1 Mechanical Department, Faculty of Technology, University of M'sila, Algeria, (ali.debih@univ-msila.dz.com)

I. INTRODUCTION

Aluminum alloys became very attractive candidates to replace heavier materials like steel and iron. [1-2], duo to their better physical and mechanical properties as high-strength , toughness and stiffness to density ratio, excellent machining properties , high corrosion resistance in most environment, good formability, recyclability , weldability and reflectivity.

Alloys of the 6XXX series based on the Al–Mg–Si system, Copper and manganese are usually added to the alloys to improve properties [3]. They were placed first in production among all aluminum alloys. They present up more than 90% of the production of extruded aluminum products [4]. They are the most successfully used group of age hardenable aluminum alloys in a wide range of industrial applications as packaging, aeronautic and automotive[5].

Age hardened by precipitation aluminum alloys is one of various technological methods to changing the mechanical properties. It consists to heating and cooling operations. This technic can enhance the fatigue life of structures or machine components, by inhibiting or retarding propagation of fatigue crack according to cutting precipitates by dislocations as a result of the resolved shear stress or looping around the precipitates by the Orowan mechanism, it can also improve the mechanical properties of alloys. The complexity of early stage precipitation reactions in this alloy system, the quenching rate and temperature of age hardening, are also three of the most critical factors to affect the age hardening of Al-Mg-Si alloys. To suppress the decomposition of solid solution, reduce residual stress and distortion and create homogeneous nucleation during artificial aging, the quenching rate of this series should be done as quickly as possible [6]. Alloys with a potential high strength would get low mechanical property if they are cooled too slowly. And during this process, heterogeneous precipitation would appear and have negative effects on the final mechanical properties. The presence of the intermetallic compound "Mg_2Si" in 6000 aluminum matrix is an important responsible of strengthening, the precipitation sequence have reported and accepted as:[α (SSS) $\rightarrow$GP zones$\rightarrow\beta''\rightarrow\beta'\rightarrow\beta(Mg_2Si)$], it consist of annealing, quenching and aging.

Some researchs have been done to improve the mechanical properties of aluminum alloys.

Buha et al. [7] confirmed the improvement of the mechanicals properties and microstructural development of aluminum 6061 treated to interrupted aging conditions, then L. W. Meyer et al. [8] and K. Hockauf et al. [9] reported the positive effect of ultrafine-grained obtained by thermomechanical treatments on the microstructure and mechanical properties of 6000 aluminum alloys. The combined effects of stress ratio and material on the fatigue crack growth in

AA2017 T4 were indicated by L.P. Borrego et al. [10]. K. Strobel et al. [11] presented the strong relation between Quench Sensitivity and microstructure in 6000 Series Aluminum Alloys. In the same context, Hong-ying LI et al. used Time-temperature-property curves to evaluated the quench sensitivity of 6063 aluminum alloy , they confirmed that the quench sensitivity of 6063 alloy is lower than that of 6061 or 6082 alloy.[12]. The effect of the remaining phase $Al_{15}(FeMn)_3Si_2$ after homogenization treatment, on the material performance of an Al−0.66Mg−0.85Si , was discussed by Li-zhen YAN et al [3]. V. M. Monteiro et al. [13] investigated the microstructural changes of different aluminum alloys (1100, 3104 and 8011) under various treatment conditions for different soaking times. Peak values were evaluated by P. Juijerm et al. [2] to static and dynamic properties of AA6061 at peak aged condition compared to non aged, under and over aged conditions.

The focus of the current contribution is to investigate the effect of various heat treatments with tow cooling rate associated to quenching media and the temperature of age hardening, on the mechanical properties, fatigue behavior and microstructural development of AA6005. Microstructure evolution during different heat treatments was studied, and the influence of microstructural morphologies on mechanical properties of AA6005 alloy was analyzed.

II. MATERIALS, SPECIMENS AND HEAT TREATMENTS

A. Level-2 Heading

An aluminium wrought alloy Al-0.69 Mg-0.40 Si-Mn (AA6005) with an Mg-Si ratio of (1.69) was received in the annealed temper and in form of rods bars with diameter about 25 mm.

Level-2 and level-3 headings can be used to detail main headings.

B. Heat treatments

Samples of (Ø25x 90) and (Ø25x 230) were cut from the extruded bars, and then heat treated according the time-temperature sequences described in Fig. 1. All samples have been solution heated at 520°C for 01 hour in a circulating air furnace, and then they were devised in two parts. The first group (half of quantity) was quenched to (25°C Room Temperature "RT") in water immediately (WQ); the second was quenched in controlled cool compressed air (AQ) with a rate of (45°C/min).

The first subgroup (WQ) samples were aged immediately at 180° for 8 hours, which will be designated as T6 Artificial aging. The second subgroup was aged at 40° for 336 hours and quoted T4 Natural aging.

The first subgroup of the second group (AQ) samples was also aged at 180°C for 8hours, designated as T5 Artificial aging. Then the second subgroup was aged at 40°C for 336 hours and named T1 Natural aging

C. Page Numbers, Headers and Footers

Tensile cylindrical specimens with a diameter of 8 mm and a gauge length of 75 mm (Fig .1a) and fatigue specimens with a diameter of 8mm and a length of 145 mm (Fig.1b) were cut from these bars. The loading direction during tensile corresponds to the extrusion direction of the bar. All specimens for tensile and fatigue tests were polished parallel to the specimens axis with abrasive paper grade 1200, in length leading to avoid any machining effects. The specimen surface roughness was about 0.2 µm.

All samples for microstructural analysis, hardness, DSC and DRX tests were cut from the bars then treated according to treatments sequences detailled above. Using standard procedure, Metallographic sections were prepared according metallographics standards, in other words: grounded, polished and etched using Keller's reagent. Detail of the preparation can be found in Ref [14].

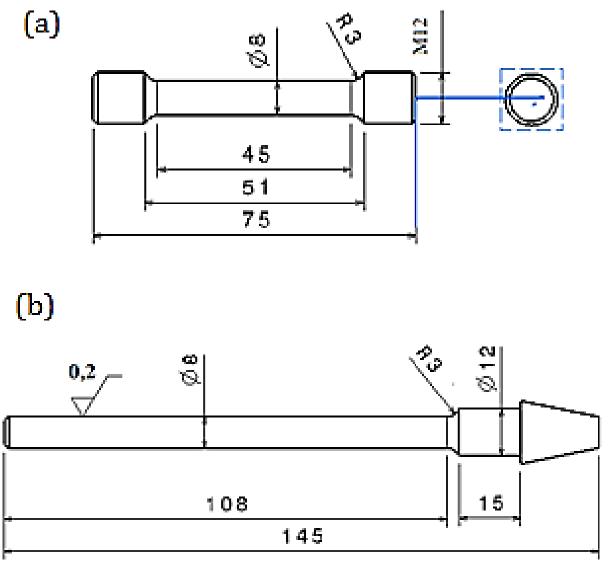

Fig. 1 Specimen for tests; (a) tensile test specimen; (b) fatigue test specimen (all dimensions in mm).

III. EXPERIMENTAL PROCEDURE

According to the [ASTM B557-84], cylindrical specimens (Fig .1a) were tested in tensile strength until fracture at room temperature, using à hydraulic testing machine, at a strain rate of ($d\mathcal{E}/dt=10\text{-}3\ S\text{-}1$). The loading during testing corresponds to the extrusion direction of the bar. Average value of three specimens for each heat treatment condition was taken.

Rotating Bending fatigue tests were conducted with a mechanical testing machine at constant amplitude loading. Stress ratios were maintained at (R= -1), the fatigue specimens with 8 mm diameter and 108 mm gauge length (Fig. 3) were solicited at frequency of 28 Hz, according to [ASTM E 466-82].

The Vickers hardness tests (HV) were measured on cross section, using a microhardness tester type Wolpert Wilson Hardness. The load used for the microhardness test was 0.5N for an indentation time of 15 second with objective (x10) and indenter Vickers. Three points were tested in each specimen to obtain an average value, according to [ASTM E 384].

Metallographic investigations were performed on the samples at as received (AS-R) and treated states. The microstructures were observed and analyzed by (OM) and (SEM) equipped with (EDX) spectrometry.

Phase transformations in precipitation sequences of the investigated alloy were determined with DSC analysis on SETARAM- DSC 92 at a heating rate of 10°C/min from 20 to 550°C. During scanning measurements, the samples were protected with flowing argon.

Spectral characterization of samples was performed using X-ray diffraction analysis. This technique consisted of directing an X-ray beam of wavelength ($\lambda K\alpha 1=1.5418$ A°) on to the samples on cross section. The crystalline phases of matrix and precipitates present were identified and all changes in the microstructure (phase composition, dislocation density, lattice parameter, size of crystallites, residual stresses, full width at half maximum "FWHM" values and microdistortions were determined. The analysis was conducted taking into consideration the following parameters: " voltage 35 kV and a current 20 mA, scanning step 0.05° in the range of 2θ angles from 30° to 90°.

IV. RESULTS AND DISCUSSION

A. X Ray Analysis

Figure 2, Shows the X-Ray diffraction analysis results for the alloy in various conditions of treatments, additional to the peaks of aluminum matrix, peaks relative to Mg_2Si and Mg_5Si_6 precipitates and the complex intermetallic dispersoids are detected. The EDAX spectral analysis confirmed the presence of Al, Mg, Si, Fe and Mn bearing precipitates and intermetallic particles in the alloy.

The FWHM "Full Width at Half Maximum "evaluated in Table 1 varies inversely with crystallite size. as the crystallite size gets smaller, the FWHM gets broader according to The Scherrer Equation:

$$B(2\theta)=[(K.\ \lambda)/\ (L.\ \cos\theta)] \tag{1}$$

where "B" is Peak width and "L" the crystallite size and "K"=1.

Table 1. Parameters for (111) and position of precipitates and dispersoids

Condition	Pos 2θ°	d Spacing	FWHM	Crystallite size	Mg_2Si/ Pos	Mg_5Si_6 /Pos	Microstrain
6005 AS R	37,948	2,369	0,190	562,594	40,74	/	0,21055
6005 T1	38,190	2,355	0,28	313,116	40,97	/	0,37615
6005 T4	37,950	2,369	0,27	352,993	41	/	0,33557
6005 T5	38,292	2,354	0,206	493,519	41,06	46,80	0,23853
6005 T6	38,478	2,337	0,180	600,123	41,28	46,80	0,19476

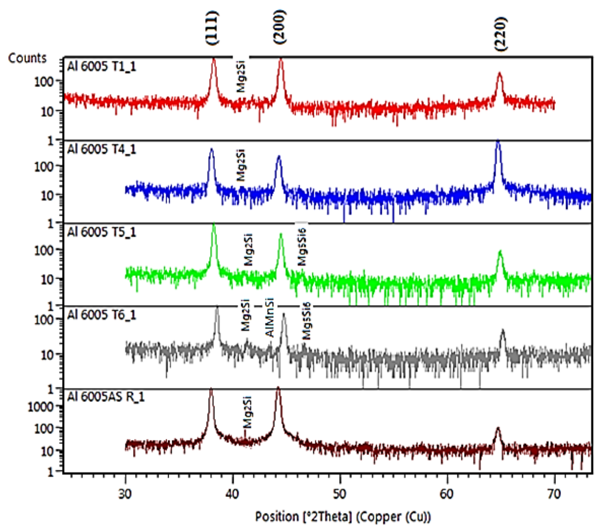

Fig. 2. X-ray diffraction spectra of AA 6005 in various treatments conditions.

B. DSC Analysis

The correlation between the DSC peaks curve of as water quenched sample and precipitation process is as follows: (Fig. 3a). The first exothermic peak appeared at around 85° is caused by the formation of clusters Si and Mg and GP zones. (110-186°C) there is the range temperature of transition to GP zones dissolution; it was presented by endothermic peak. The formation of metastable precipitate β" was responsible for the exothermic peak at 213°C in the range of (190–250°C), the total dissolution of β" was centered in the endothermic peak at 250°C. A melting exothermic in the range of 255-305°C and a sharp peak temperature at 285°C are caused by formation of β' precipitate. The next melting endothermic situated between 340-400°C, with a major peak centered at 380°C corresponds to the dissolution of β', the last exothermic peak situated at 435°C was due to formation of β (Mg_2Si) and the broad endothermic peak on the DSC curve is most likely caused by the dissolution of β.

Some changes in the DSC spectrum were marked for the air quenched sample comparatively to water quenching (Fig .3b). Initial small exothermic peak just at 100 °C in a range of (50-130°C), linked with the formation of clusters and GP Zones, then the endothermic peak appeared at 200°C is due to dissolution of GP zones. Wide temperature range was linked to the formation of β" and β' precipitates with shifting towards a high temperature between (190-310°C), the two precipitates have partially merging into a single peak. The formation of β peak of β situated in the temperature range (410- 465 °C) with an exothermic peak at 435°C.

The DSC curve for the sample under T4 condition (Fig. 3c) showed the absence of the first peak, indicating the total formation of GP zones during natural aging. Wide endothermic range appeared between 170 and 255°C linked with the transition to GP zones dissolution, this zone was characterized by big peak area. The first exothermic peak indicates the formation of β" precipitates and appears as a shoulder of second peak attached to the formation of β' precipitates, the two peaks were arranged between 260 and 350°C. The delay formation of β"and β' was due to preliminary presence of GP zones. The last peak situated at 420°C indicates the formation of β precipitate.

The DSC Curve obtained for the samples under T1 condition (Fig. 3d), shows a complete absence of the first exothermic peak attached to the formation of zones GP, on other hand there is an appearance of a less intense endothermic peak in the interval between (195 to 265°C) and also the presence of two exothermic peaks shoulders in the interval between (275 to 365°C) linked to the formation of the two metastable precipitates β" and β'. In the domain (390 and 465°C) temperature, the curve shows the dissolution of the metastable precipitates and the formation of β precipitate.

Due to the lower cooling rate the DSC curve for T1 condition present a small shift of the peaks towards the higher temperatures comparatively toT4 condition.

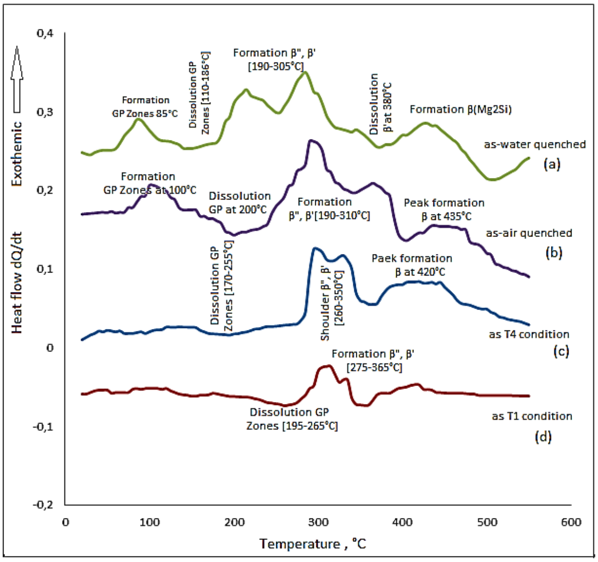

Fig. 3. DSC curves comparison performed at a scan rate of 10 °C/min after solution treatment and quenching at RT (a) water quenching, (b) air quenching, (c) T4 Condition, (d) T1Condition.

C. Tensile tests

The static Mechanical properties as the strengths (Ultimate Tensile Stress "UTS" and Yield Stress "YS"), elongation (A%), the strain hardening exponent (n), the strength coefficient (K) of 6005 alloy in As-R and after solutionizing and aging at various state treatments were determined from tensile test. The Values of (n) and (K) are determined according to Hollomon's law, $S= K. \varepsilon^n$.
The results of these tests are shown in Table 2 and Figure 4.

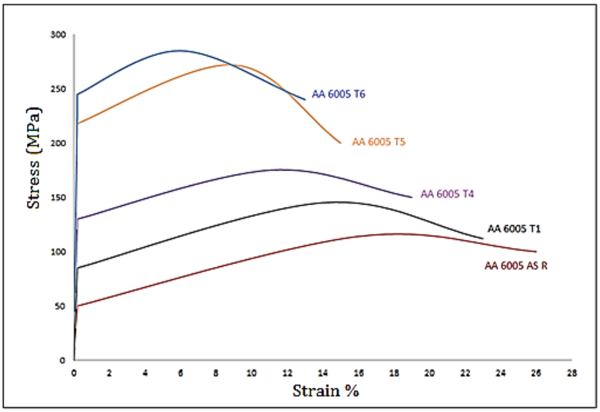

Fig. 4 Engineering stress–strain curves of AA6005 in different aging treatments.

As it is shown in Table 2 and Figure 4, it is noticed that there is a big divergence between different work conditions, specimens of AS-R condition had the lower properties (UTS and YS and higher elongation (Ɛ %) value as compared to treated conditions. The reason for that was the larger grain sizes (d=41.3 µm) in AS-R condition, figure 5.

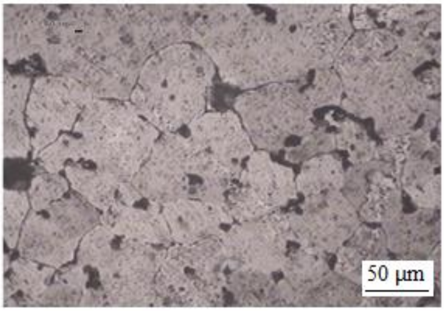

Fig. 5. Optical Microstructure of AA6005-AS-R, grain size (d ≈ 41.3µm).

AA6005 alloy exhibits (UTS) and (YS) in T6 higher than that in T5 condition. This difference is due to the grain size justified by Hall –Petch relation, figure 6 and metastable precipitates density, depending on cooling rate called quench sensitivity. The size of grain for T6 condition was (d=27µm), then for T5 condition was (d=39 µm). These results are at total according to the work of O. Kessler and M. Reich on Al-0.6Mg-0.7Si [6] and K. Strobel et al. [11] on AA 6000.

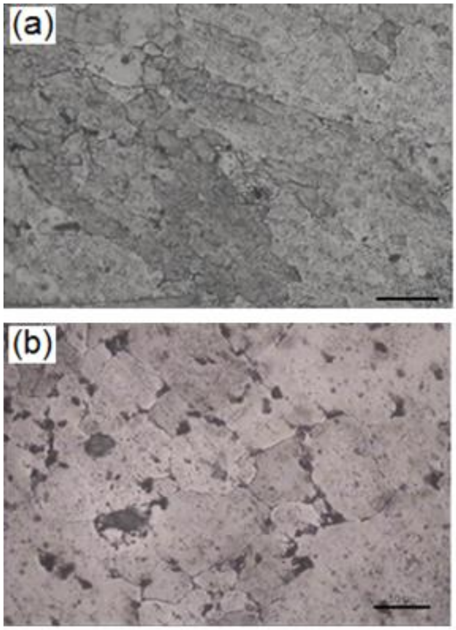

Fig. 6. Optical Microstructure of AA6005; (a) T6 condition with grain size (d≈27 μm); (b) T5 condition with grain size (d≈39 μm).

Table 2. Tensile properties of AA6005 at different aging treatments.

Condition	Quenching Media	Aging parameters	UTS (MPa)	YS (MPa)	ε %	SHC (UTS-YS)	n	K(MPa)
6005As-R	/	/	114	50	26	64	0.16	150
6005 T6	Water	180°C-8h	285	245	13	40	0.06	340
6005 T5	Cooled air	180°C-8h	272	218	15	46	0.09	335
6005 T4	Water	40°C - 336 h	175	130	19	55	0.11	225
6005 T1	Cooled air	40°C - 336 h	145	85	23	60	0.14	190

The reasons of lower UTS and YS of T1 as compared to T4 condition were the larger grain sizes (d= 39.6 μm for T1 condition), then d is around 29 μm for T4 condition, (figure. 7), because of the low cooling rate of quenching in the first state and the high number of vacancies assisted with diffusion mechanism formation of high volume fraction of (GP) zones in the second state, justified by the big air under curve for GP dissolution at [170-225°C], (Fig. 3c and d).

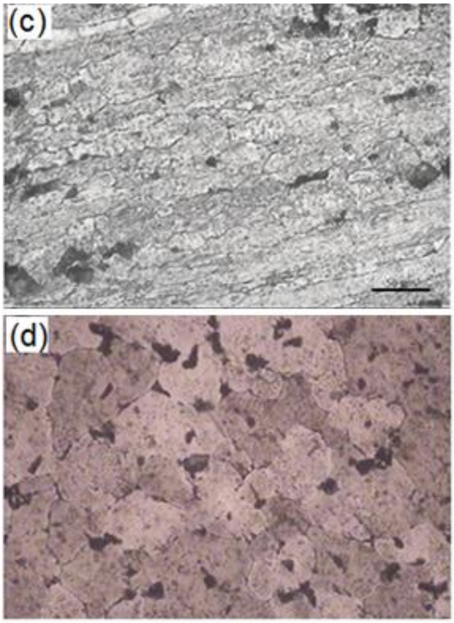

Fig. 7. Optical Microstructure of AA6005; (c) T4 condition with grain size (d≈29 μm); (d) T1 condition with grain size (d≈39.6 μm).

The SHC (Strain Hardening Capacity) of As-R, T1 and T4 conditions show the highest and moderate values (64, 60 and 55 MPa respectively) which give an indication to the cyclic hardening behavior under fatigue. Although the small values of HSC, (46 and 40 MPa) for the T5 and T6 conditions respectively, give an indication to the cyclic softening behavior under fatigue.

As-R, T1 and T4 conditions have the highest n values more than 0.1(0.16, 0.14 and 0.11 respectively) and small K values less than 300 MPa (150, 190 and 225) because of the absence of precipitates in As-R condition or presence of small size precipitates and less grain boundaries due to greater grain in T1 and T4 conditions which facilitates crack propagation.

The T5 and T6 conditions have n values smaller than 0.1 and K values greater than 300 MPa because of the presence of adequate size precipitates and more grain boundaries to prevent crack propagation.

D. Hardness tests

The hardness values summarized in Table 3 follow a similar trend to that of the ultimate and yield strengths of 6005 alloy, when they increase after various aging treatments.

Table.3 Hardness Values of AA6005 in different aging treatments.

Condition	As-R	T6	T5	T4	T1
Hv	62.05	88.15	85.65	82.85	72.6

Two factors are dominant to evaluating the hardness of As-R and aged specimens, the first is the quench rate and the second is the precipitates and dispersoids density related to the diffusion kinetics as function of temperature, consequently the artificially aged specimens showed an increase in hardness compared to the natural aging. The second factor was confirmed by K. Strobel et al **[11]** for same 6000 alloys.

The As-Received condition had the lower hardness value justified by the reduced amount of vacancies due to the much slowly quench rates (subsaturation) after extrusion and the non-aged condition after quenching.

The hardness of T1 condition increase as well as As-R by moderate increasing of vacancies amount as function of quenching rate and natural aging characterized by slowest diffusion kinetics and limited solubility at low temperatures.

In T4 condition. The high supersaturating of vacancies retained by rapid quenching causes the formation of (GP) zones at low temperature by diffusion kinetics of small precipitates which can improve the hardness as well as As-R and T1 conditions.

The formation and evolution in size of the metastable precipitates β'' and β' due to the rapid diffusion kinetics at high temperature (180°C) within a reduced amount of vacancies produced by the low cooling rate led to an increase in the hardness up to 85,65 Hv for T5 condition (Fig. 8).

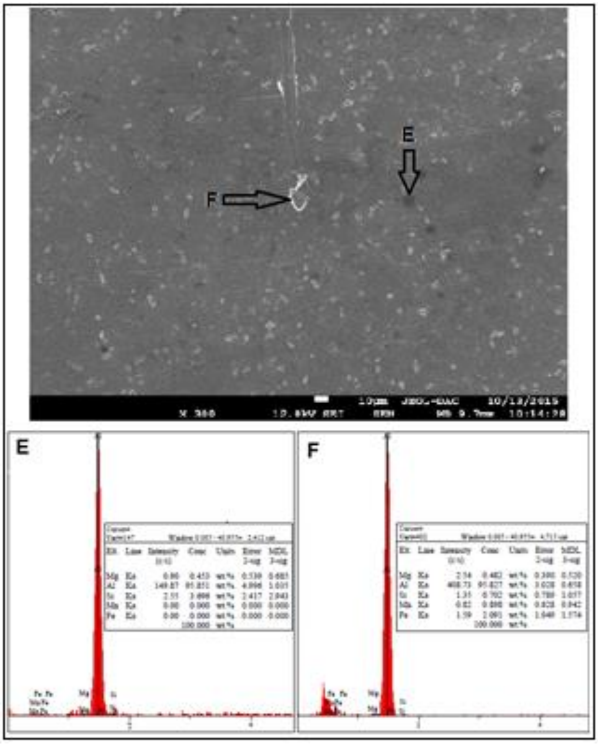

Fig. 8. Microstructures of AA6005-T5 base material by SEM, (E and F) EDS spectrum analysis obtained on two of the particles.

The peak value "88.15 Hv" was recorded to T6 condition, The basic reason for that would be the adequate size of metastable precipitates β" and β' due to the rapid diffusion kinetics at high temperature and the higher amount of vacancies produced by the rapid quenching, (Fig. 9). This result is in agreement with the work of B. Milkereit et al.[15].

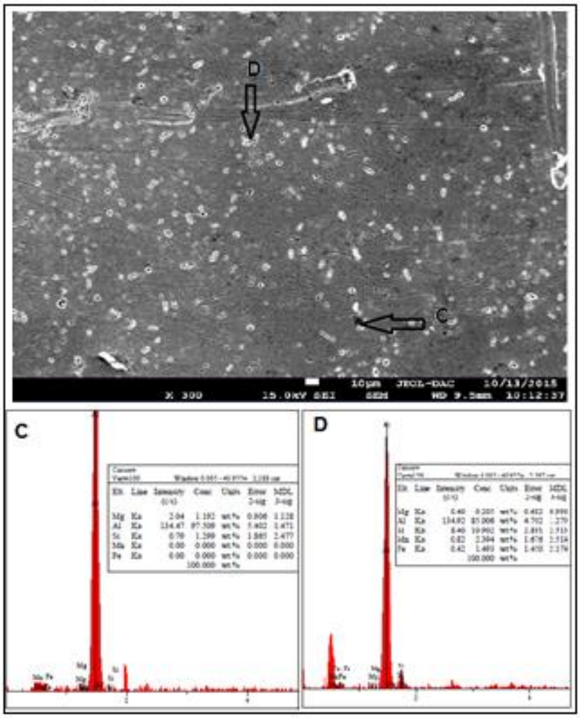

Fig. 9. Microstructures of AA6005-T6 base material by SEM, (C and D) EDS spectrum analysis obtained on two of the particles.

E. Fatigue behavior of AA6005 alloy

The results of fatigue tests at room temperature of prepared AA6005 in as received and different ageing treatments are shown as S/N-curves, where the number of cycles to failure (Nf) is measured as a function of cyclic stress amplitude, Fig. 10.

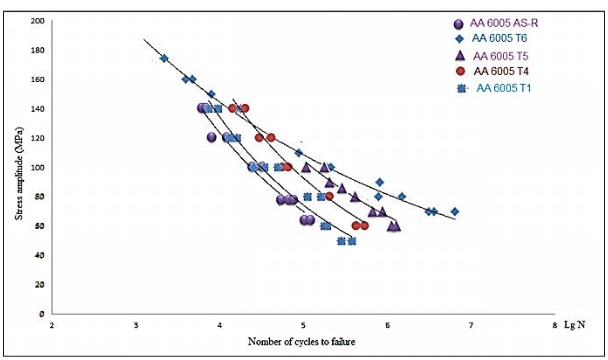

Fig. 10. Non statistically evaluated S/N curves of an AA6005 in as received and different aging treatments.

The peak fatigue strength was marked for T6 condition, this increase is due to the adaptation of initial microstrain to the cyclic softening during fatigue, more grain boundaries figure 6a, high number of non-shearable precipitates β" and β' figure 10, and the adequately crystallites size (table 1) which can increase the dislocation density then the precipitates–dislocations and dislocations-dislocations interactions. Fatigue crack growth in Al–Mg–Si alloys can be highly influenced by the contents of dispersoid due to the presence of manganese (Fig. 2), this is in agreement with [11].

The moderate amount of obstacles formed by non shearable precipitates prevents crack propagation (Fig. 8 and 3b), increases in crystallite (Table 1), the less grain boundaries are the reasons to reduce the fatigue strength of T5 as well as T6 condition.

Due to the small size of clusters and GP Zones (Shearable precipitates) formed by lower diffusion kinetic at low temperature (Fig. 3c), the initial high microstrain in addition to cyclic hardening during fatigue and the small size of crystallites (Table 1), the T4 condition had a lower fatigue strength as well as T6 condition.

The T1 condition presents low fatigue strength as compared to the T5 condition, this can be explained by the limited number of shearable precipitates "GP" (Fig. 3d), higher microstrain (Table 1), cyclic hardening during fatigue and less grain boundaries (Fig. 7d).

V. CONCLUSION

The main conclusions of the study should be summarized in a short Conclusions section.

1. The Fatigue behavior of AA6005 under different treatment conditions can be predicted from (HSC) and strain hardening exponent (n).
2. The investigated alloy AA6005 shows cyclic hardening in T4, T1 and AS-R conditions whereas the T6 and T5 conditions show cyclic softening in stress-controlled fatigue tests at room temperature.
3. As rate quenching increased, the recrystallized grain size became smaller, and enhancing the strength and hardness.
4. The microscopic analysis proved the presence of two types of precipitates, Mg_2Si and (Si, Mn, Fe) Al.
5. The cooling rate is a determinant factor for the amount of precipitation vacancies.
6. The precondition presence of precipitates GP can delay the formation of the metastable precipitates β"and β'.

ACKNOWLEDGMENT

The heading of the Acknowledgment section and the References section must not be numbered.

.

REFERENCES

[1] Adnan N. Abood1, Ali H. Saleh2 & Zainab W. Abdullah. "Effect of Heat Treatment on Strain Life of Aluminum Alloy AA 6061". *Journal of Materials Science Research*, vol. 2, No. 2. 2013. DOI:10.5539/jmsr.v2n2p51

[2] P. Juijerm, I. Altenberger, B. Scholtes. "Fatigue and residual stress relaxation of deep rolled differently aged aluminium alloy AA6110". *Materials Science and Engineering: A,* vol. 426, Issues 1–2. p. 4. 2006, https://doi.org/10.1016/j.msea.2005.11.064

[3] Li-zhen YAN, Yong-an ZHANG, Xi-wu LI, Zhi-hui LI, Feng WANG, Hong-wei LIU, Bai-qing XIONG. " Microstructural evolution of Al–0.66Mg–0.85Si alloy during homogenization". *Trans. Nonferrous Met. Soc. China*, vol. 24. p. 939. 2014. https://doi.org/10.1016/S1003-6326(14)63146-0

[4] P. Yu Bryantsev. “Continuous cooling transformation diagrams for 6XXXaluminium alloys”. *IOP Conf. Series: Materials Science and Engineering,* 5 012010. 2009. doi:10.1088/1757-899X/5/1/012010

[5] Stefan Pogatscher, Helmut Antrekowitsch, Thomas Ebner and Peter J. Uggowitzer “The Role of Co-Clusters in the Artificial Aging of AA6061 and AA6060”. *Light Metals.* p.415. 2012. DOI: 10.1007/978-3-319-48179-1_70

[6] O. Kessler, M. Reich. “Mechanical properties of an undercooled aluminum alloy Al-0.6 Mg-0.7 Si”. *IOP Publishing, Journal of Physics: Conference Series 240 012093*. 2010 doi:10.1088/1742-6596/240/1/012093

[7] J. Buha, R. Lumley, A. Crosky. " Microstructural development and mechanical properties of interrupted aged Al-Mg-Si-Cu alloy". *Metallurgical and Materials Transaction A; vol.37A.* p.3119 2006. DOI:10.1007/S11661-006-0192-X

[8] L. W. Meyer , R. Schönherr , M. Hockauf. " Increasing strength, ductility and impact toughness of ultrafine-grained 6063 aluminium alloy by combining ECAP and a high-temperature short-time aging". IOP *Publishing. Journal of Physics: Conference Series 240 012123.* 2010. doi:10.1088/1742-6596/240/1/012123

[9] K. Hockauf, T. Niendorf , S. Wagner , T. Halle."Cyclic behavior and microstructural stability of ultrafine grained AA6060 under strain-controlled fatigue". *Procedia Engineering;* vol. 2. P.2199. 2010. http://dx.doi.org/10.1016/j.proeng.2010.03.236

[10] L.P. Borrego, J.M. Costa , F.V. Antunes , J.M. Ferreira." Fatigue crack growth in heat-treated aluminum alloys". *Engineering Failure Analysis xxx (2009) xxx–xxx*. Article in Press. doi:10.1016/j.engfailanal.2008.11.007

[11] Katharina Strobel, Mark A. Easton, Lisa Sweet, Malcolm J. Couper, Jian-Feng Nie. " Relating Quench Sensitivity to Microstructure in 6000 Series Aluminium". *Materials Transactions, Vol. 52, No. 5 p. 914.* 2011. https://doi.org/10.2320/matertrans.L-MZ201111

[12] Hong-ying LI, Cui-ting ZENG, Mao-sheng HAN, Jiao-jiao LIU, Xiao-chao LU." *Trans. Nonferrous Met. Soc. China.* Vol. 23. p.38. 2013.

[13] Valmir Martins Monteiro, Saulo Brinco Diniz, Bruna Godoi Meirelles, Luis Celso da Silva, Andersan dos Santos." Microstructural and mechanical study of Aluminium alloys submitted to distinct soaking times during solution heat treatment*". Tecnol. Metal. Mater. Miner., São Paulo*, vol. 11,No. 4, p.332. 2014. http://dx.doi.org/10.4322/tmm.2014.047

[14] ASM Metal Hand book, Chemical and electrolytic polishing metallography and structures ,Vol 09 ASM international, OHIO (2004) , p. 281-293.

[15] Benjamin Milkereita, Nelia Wanderka, Christoph Schick, Olaf Kessler. " Continuous cooling precipitation diagrams of Al–Mg–Si alloys" *Materials Science and Engineering A*. vol. 550. 2012 p.87. dx.doi.org/10.1016/j.msea.2012.04.033.

[16] S. M. Metev and V. P. Veiko, *Laser Assisted Microtechnology*, 2nd ed., R. M. Osgood, Jr., Ed. Berlin, Germany: Springer-Verlag, 1998.

[17] J. Breckling, Ed., *The Analysis of Directional Time Series: Applications to Wind Speed and Direction*, ser. Lecture Notes in Statistics. Berlin, Germany: Springer, 1989, vol. 61.

[18] S. Zhang, C. Zhu, J. K. O. Sin, and P. K. T. Mok, “A novel ultrathin elevated channel low-temperature poly-Si TFT,” *IEEE Electron Device Lett.*, vol. 20, pp. 569–571, Nov. 1999.

[19] M. Wegmuller, J. P. von der Weid, P. Oberson, and N. Gisin, “High resolution fiber distributed measurements with coherent OFDR,” in *Proc. ECOC’00*, 2000, paper 11.3.4, p. 109.

[20] R. E. Sorace, V. S. Reinhardt, and S. A. Vaughn, “High-speed digital-to-RF converter,” U.S. Patent 5 668 842, Sept. 16, 1997.

[21] (2002) The IEEE website. [Online]. Available: http://www.ieee.org/

[22] M. Shell. (2002) IEEEtran homepage on CTAN. [Online]. Available: http://www.ctan.org/tex-archive/macros/latex/contrib/supported/IEEEtran/

[23] *FLEXChip Signal Processor (MC68175/D)*, Motorola, 1996.
[24] "PDCA12-70 data sheet," Opto Speed SA, Mezzovico, Switzerland.
[25] A. Karnik, "Performance of TCP congestion control with rate feedback: TCP/ABR and rate adaptive TCP/IP," M. Eng. thesis, Indian Institute of Science, Bangalore, India, Jan. 1999.
[26] J. Padhye, V. Firoiu, and D. Towsley, "A stochastic model of TCP Reno congestion avoidance and control," Univ. of Massachusetts, Amherst, MA, CMPSCI Tech. Rep. 99-02, 1999.
[27] *Wireless LAN Medium Access Control (MAC) and Physical Layer (PHY) Specification*, IEEE Std. 802.11, 1997.

Chapter 9

Low-Cost Seismic Station Design: A Case of Study Armutlu Network (Arnet)*

Deniz Çaka[1]

Emrah BUDAKOĞLU[2]

* This study was funded by The Scientific and Technical Research Council of Turkey (TÜBİTAK) (project number: 117Y184).

[1] Arş. Gör. Dr. Department of Geophysical Engineering, Faculty of Engineering, Kocaeli University, Umuttepe 41001, Türkiye; caka@kocaeli.edu.tr; ORCID: 0000-0003-2125-6489

[2] Dr. Öğr. Üyesi Department of Geophysical Engineering, Faculty of Engineering, Sakarya University, Serdivan 54050, Türkiye; ebudakoglu@sakarya.edu.tr; ORCID: 0000-0002-9897-2435

1. INTRODUCTION

Seismic monitoring allows the analysis of many tremors, such as earthquakes, explosions, and human activities. For an excellent seismic observation, appropriately arrayed seismic stations that provide quality data are needed. Locations of seismic events can be determined more reliably, and sensitive data can be provided. Thus, the data required for many seismological studies are assembled.

Active tectonism in Turkey is controlled by the right-lateral North Anatolian Fault (NAF) and the left-lateral East Anatolian Fault (EAF), which are formed as a result of the westward movement of the Anatolian Block (average 20-30 mm/year) (Barka et al. 1988; Reilinger et al. 1997; McClusky et al. 2000). This regions, where devastating earthquakes have occurred in the historical process, needs detailed examination for seismic hazard and various seismological studies. For this purpose, Armutlu Network (ARNET) was established in September 2005 in the Marmara region, which hosts Turkey's most economically and socially important cities (Figure 1). Founded in collaboration with Kocaeli University Earth and Space Sciences Research Center (ESSRC) and the German Geosciences Research Center GeoForschungsZentrum (GFZ) in Potsdam, ARNET aims to understand the seismicity, hydrothermal activity, and tectonism in the region (Tunç et al. 2011).

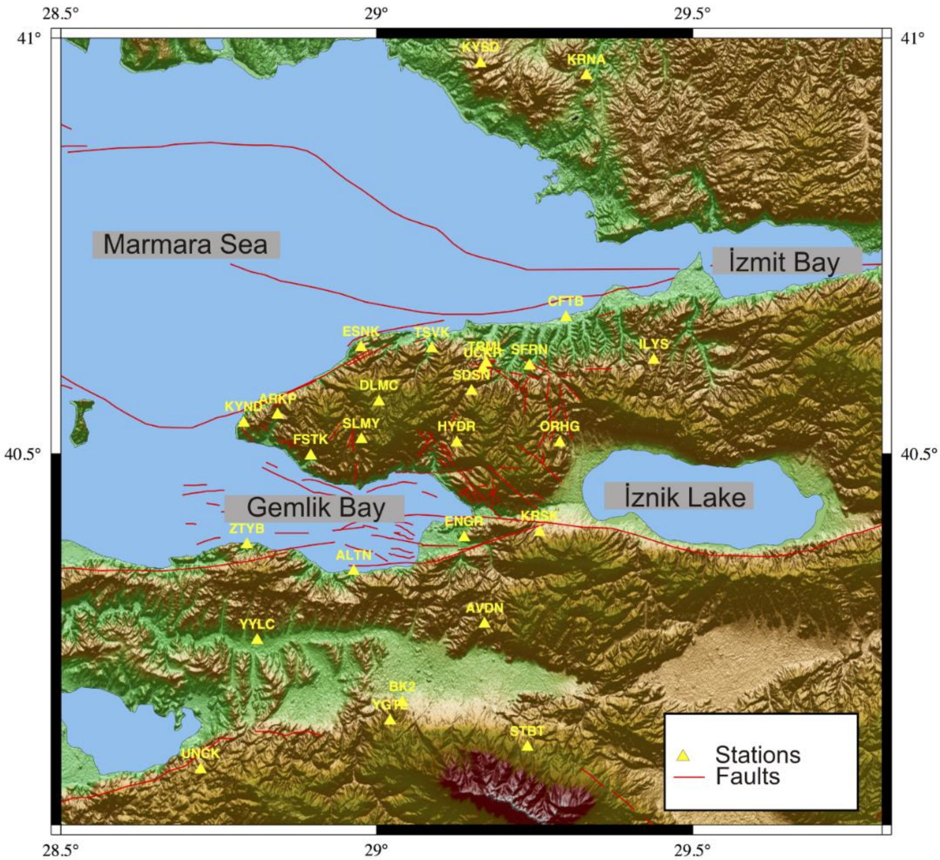

Figure1. Distribution of stations in the ARNET seismic network. Faults were taken from Emre et al. (2018)

The instruments that measure and record seismic events are called seismographs. Seismograph; it is a device used to record ground shaking caused by earthquakes, explosions, or other seismic events, and generally records the movement of the pendulum and the ground relative to each other. In general, seismographs and home seismometers are used synonymously. The first known seismoscope was invented in 132 AD by the Chinese philosopher Chang Heng (Figure 2a) (Agnew et al. 2002; Yan, 2007; Batlló, 2014). However, this mechanism did not record the earthquakes but only showed that there was an earthquake. The first seismograph to actually record earthquakes was developed in 1890. Many types of seismometers are available for different purposes (SYY, 2023). Seismometers can be broadly classified as Broadband (BB), Short Period (SP), Long Period (LP), and Strong Motion accelerometers according to their intended use. The most widely used type of seismometer is broadband seismometer (Figure 2b). Due to the wide frequency range, the application area is quite broad. Seismometers are called horizontal and vertical components according to the type of motion they record. Vertical component seismometers record movements of ground motion in the vertical (Z) direction. Horizontal components measure horizontal ground motion (North-South (NS) and East-West (EW)). Seismometers can record three components simultaneously. Accelerometers (strong motion) are a type of seismometer used frequently in recent years. They are specifically designed to record large amplitude vibrations in major earthquakes. Accelerometers offer the most excellent solution for earthquake early warning, seismic damage detection, and civil engineering applications.

Seismic stations provide data transmission to each other through communication systems such as satellite, telephone, and internet lines. In this way, information is instantly transferred to seismological centre when seismic activity occurs anywhere in the world. Ground vibrations are detected by a real-time seismometer, recorded, and then transmitted via one of the transmission systems. The record of ground motion is called a seismogram. Seismograms of the previous period are expressed in analogy. Today, recordings are made digitally. This way, data analysis can be done faster, and storage capacity limits increase considerably.

Seismologic centres carry out continuous monitoring of ground movements by incorporating a large number of seismometers. One of the most important digital networks in the world is the Global Seismographic Network (GSN). It serves worldwide with numerous stations in the network. Turkey has many universities, municipalities, and scientific research centers with seismic networks. However, two major institutions are observing seismic activity in Turkey. The Kandilli Observatory and Earthquake Research Institute-Regional Earthquake and Tsunami Monitoring Centre (KOERI-RETMC) and the Disaster and Emergency Management Authority (AFAD). They study seismic activity in detail with the widespread station network and types of seismometers serving different purposes.

Figure 2. The oldest and newest seismometers **a)** The oldest known seismoscope manufactured by Chang Heng (Yan, 2007) **b)** The most preferred GURALP-3ESPC Feedback Broadband seismometer for new generation and seismological monitoring networks (SYY, 2023)

Seismometers are highly sensitive and costly instruments. Affording this cost alone is not enough. Also, seismometers must operate safely in a safely designed cabin or reinforced concrete structure (Figure 3). In this way, quality and nonstop data acquisition are achieved. However, cabins or reinforced concrete structures increase costs and take time to build. Therefore, a new and low-cost cabinet design has been developed to at least avoid costs other than the seismometer as much as possible. This design will be detailed in the next section.

Figure 3. Different types of built seismic stations a) reinforced concrete structure (SAÜ Emarc, 2023) b) Cabin (KOERI, 2023)

2. SITE SELECTION OF SEISMIC STATIONS

Many factors should be considered during the selection of seismic station locations (Trnkoczy et al. 2012). First of all, possible locations are determined by considering the azimuthal distribution on the map in the office environment. Then, observations are made by going personally to more determined possible places. In this process, known as field studies, many parameters are taken into account. These can be listed as the ease of access to the selected location on the map, the suitability of geological conditions, the availability of electricity or data transmission resources, and the current situation of seismic noise sources (such as traffic noise, wind, location of high voltage lines, etc.).

In this study, measurements were taken for seismic noise detection within the scope of field studies by going to the points determined on the map. These measurements taken are given as noise spectra. These measurements provide important information about the possible location of the seismic station and the noise sources around it. Güralp Systems 40T model 30-second seismometer was used for measurement. By evaluating the data in the frequency domain, it was investigated whether these points are in the range of NHNM (New High Noise Model), NLNM (New Low Noise Model), Peterson (1993), and the presence of invisible noises in the time domain.

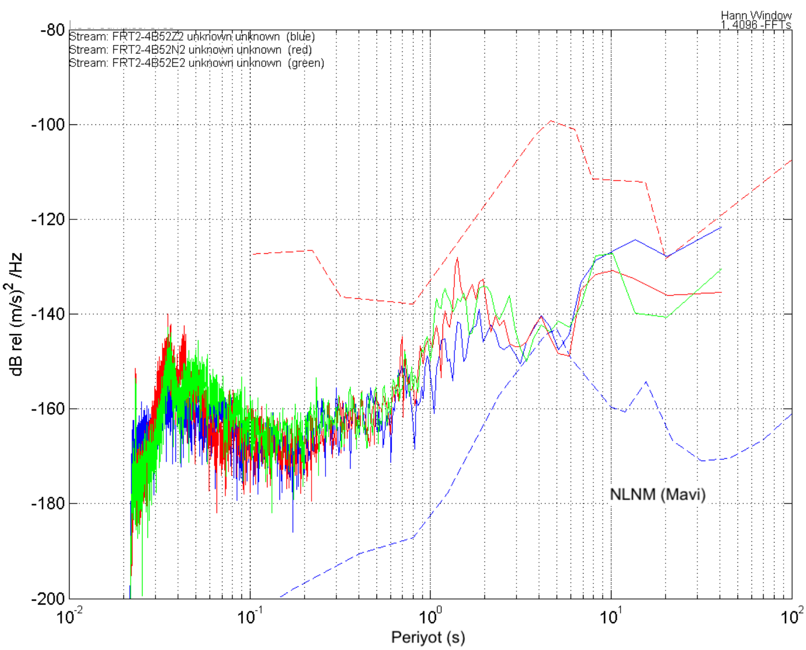

Figure 4. The power density spectrum of the measurement made to determine the station location suitability

When the power density spectrum in Figure 4 is examined, it is seen that the noise spectra of the measured points are within the given ranges (NLNM and NHNM). There is no dominant data in any period/frequency in the power density spectrum. For this reason, if this point also provides other selection parameters, it has been determined that it is suitable for station installation.

3. DESIGN OF STATION CABINS

The devices to be placed inside the seismic stations must be designed to protect them from seasonal conditions, theft, and similar external interventions. In addition, the stations to be established should be able to produce and store the electrical energy they need. For this, the station cabin must be sufficient to accommodate recording devices, batteries, and solar panels. For this purpose, cabins with a front view in Figure 5 and a perspective view in Figure 6 have been designed. Later, these cabins were specially manufactured.

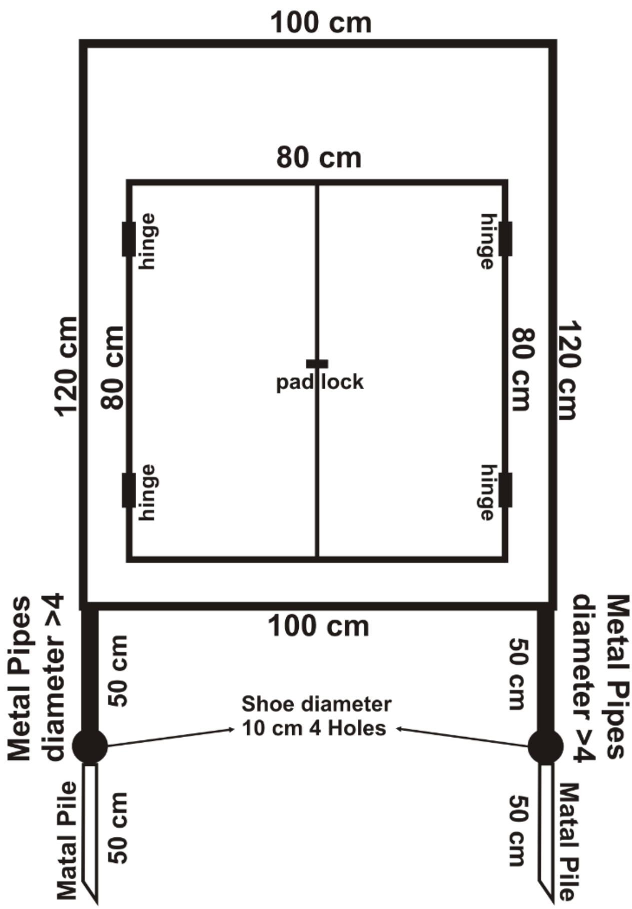

Figure 5. Schematic front view of the designed seismic station cabin

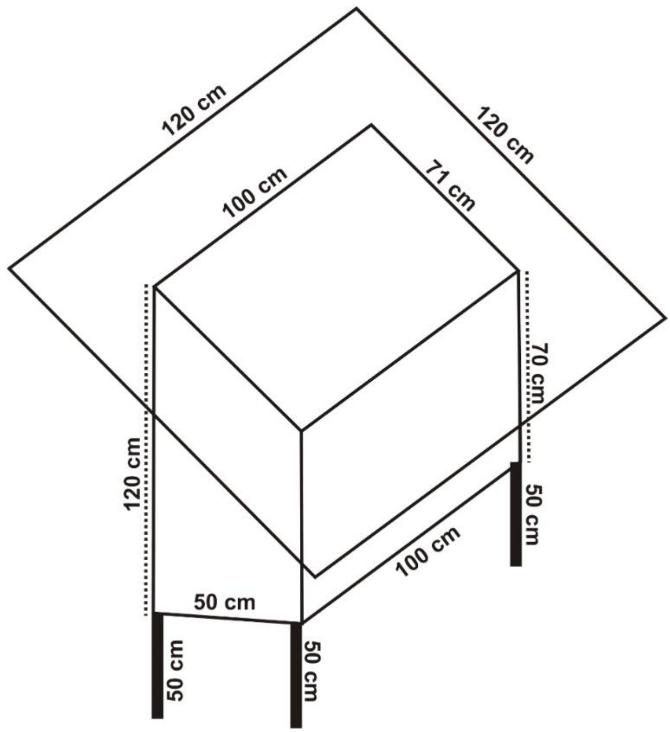

Figure 6. Schematic perspective view of the designed seismic station cabin

To obtain the highest efficiency in data quality from the stations planned to be established within ARNET is the main aim of a seismology study. Our purpose in establishing a station in the target area is to record the micro earthquakes with a good station distribution and to determine the locations of the earthquakes with high reliability. All the studies have been done to record the earthquakes that will occur in the best way with the least noise. One thing that needs to be done for this is to place the earthquake sensors underground in a way that will be least affected by external factors. For this purpose, a pit of 80 x 80 cm and a depth of 1 m was dug outside, where the station cabin will be installed to install sensors (Figure 7a). The 40 x 40 x 20 cm (width x length x height) mold placed at the bottom of the pit is filled with cement. In order to maximize the highest contact of the cement with the ground, 4 pieces of 50 cm long iron rods were driven into the ground, and these rods were connected to each other with iron rods in the mold. Thus, the concrete floor's interaction with the environment increased, and the concrete was more durable (Figure 7b).

The prepared mold is completely filled with cement. Thus, a suitable environment was provided for the seismometer installation underground.

Although earthquake recorders are produced as water-proof, they must be used with the best possible protection since they are high-tech and costly devices. For this reason, the best possible protection has been provided for the devices to be placed in the ground. For this, the water-proof plastic drum with the bottom cut off was placed on the cement floor before the prepared cement dries (Figure 7c). Although the drying of the cement on the drum created an impermeable environment, the interior of the drum-cement cross-section has been improved by completely covering it with silicone. For the cables of the seismometer placed in the drum to reach the cabin, the drum was drilled from a suitable position at a sufficient size.

The underground installation was completed with the installation of the cables passed through the throat pipe placed here and between the hollow leg of the cabin to the sensor (Figure 7d). Since the seismometer will remain airtight in the drum and the cement is still damp, silica gel packages that absorb the humidity of the environment are left, and the lid is closed so that the seismometer connectors and cables are not damaged. In some cases, it is necessary to dry the water on the ground due to the very rainy seasonal conditions and the station location conditions. A drainage system was built to eliminate this situation, preventing the installation of seismometers healthily, and the water on the ground was discharged (Figure 7e). Gravel was laid around the prepared concrete floor, and the drainage pipe turned around was taken out of the area where the drum was located, inclined to the outside. To prevent the holes of the pipe from being blocked, the pipe was covered with a permeable material, and the drainage process was completed by covering it with gravel again.

Figure 7. Stages of station setup **a)** The holes dug for the installation of the station **b)** The mold and iron prepared for the concrete table where the sensor will be placed **c)** The construction phase of the environment in which the earthquake sensor will be placed **d)** The connections prepared for the installation of the earthquake sensor **e)** Drainage process

After the necessary procedures were completed, all the pits opened were closed. The installation of the station was completed with the lining of the cabin and the connections of the devices (Figure 8a). One of the stations established within the scope of the project is shown from different sides in Figures 8b and 8c as an example.

Figure 8. Final images of the designed seismic station **a)** Earthquake recording station interior view **b)** Earthquake recording station back view **c)** Earthquake recording station front view

4. RESULTS

Monitoring seismic activities (earthquakes, various explosions, nuclear tests, etc.) in a region is important. This way, tectonism, and seismic risk areas can be detailed, forensic events can be shed light on, and many benefits can be provided.

Setting up a seismic network is a costly and intensive procedure. This study presents a low-cost cabin design in which seismic stations are located, which constitutes a significant part of the seismic network cost. The design of the cabin is presented in all details with drawings. At the same time, station location selection and points to be considered are mentioned. With this and similar studies, it aims to contribute to developing seismic networks, which benefit many important issues at affordable costs.

5. REFERENCES

1. Agnew, D. C., Lee, W. H. K., Kanamori, H., Jennings, P. C., & Kisslinger, C. (2002). History of seismology. International handbook of earthquake and engineering seismology, 81(A), 3-11.
2. Barka, A. A., and Kadinsky-Cade, K. (1988). Strike-slip fault geometry in Turkey and its influence on earthquake activity. Tectonics, 7(3), 663-684. https://doi.org/10.1029/TC007i003p00663
3. Batlló, J. (2014). Historical seismometer. Encyclopedia of Earthquake Engineering, Springer Verlag, Heidelberg. https://doi. org/10.1007/978-3-642-36197-5_171-1.
4. Emre, Ö., Duman, T. Y., Özalp, S., Şaroğlu, F., Olgun, Ş., Elmacı, H., & Çan, T. (2018). Active fault database of Turkey. Bulletin of Earthquake Engineering, 16(8), 3229-3275.
5. KOERI (2023). The Kandilli Observatory and Earthquake Research Institute-Regional Earthquake and Tsunami Monitoring Center (KOERI-RETMC), http://www.koeri.boun.edu.tr/sismo/2/sismik-ag/sismik-ag-listeleri/istasyon-kurulus-raporlari, Access Date: 22/02/2023
6. Mcclusky, S., Balassanian, S., Barka, A., Demir, C., Ergintav, S., Georgiev, I., ... & Veis, G. (2000). Global Positioning System constraints on plate kinematics and dynamics in the eastern Mediterranean and Caucasus. Journal of Geophysical Research: Solid Earth, 105(B3), 5695-5719. https://doi.org/10.1029/1999JB900351
7. Peterson, J. (1993). Observations and modeling of seismic background noise (Vol. 93, pp. 1-95). Reston, VA, USA: US Geological Survey.
8. Reilinger, R. E., McClusky, S. C., Oral, M. B., King, R. W., Toksoz, M. N., Barka, A. A., ... & Sanli, I. (1997). Global Positioning System measurements of present-day crustal movements in the Arabia-Africa-Eurasia plate collision zone. Journal of Geophysical Research: Solid Earth, 102(B5), 9983-9999. https://doi.org/10.1029/96JB03736
9. SAÜ Emarc (2023). Earthquake Monitoring and Research Center, Emarc (Divam), https://jfm.sakarya.edu.tr/en/icerik/7625/8408/divam, Access Date: 30/01/2023
10. SYY (2023). Sentez Yer ve Yapı Mühendisliği, https://syy.com.tr/sismoloji, Access Date: 15/02/2023
11. Trnkoczy, A., Bormann, P., Hanka, W., Holcomb, L. G., Nigbor, R. L., Shinohara, M., ... & Suyehiro, K. (2012). Site selection, preparation and installation of seismic stations. In New Manual of Seismological Observatory Practice 2 (NMSOP-2) (pp. 1-139). Deutsches GeoForschungsZentrum GFZ.

12. Tunc, B., Caka, D., Irmak, T. S., Woith, H., Tunc, S., Baris, S., ... & Zschau, J. (2011). The Armutlu Network: an investigation into the seismotectonic setting of Armutlu–Yalova–Gemlik and the surrounding regions. Annals of Geophysics, 54(1), 35-45. https://10.4401/ag-4877
13. Wang, Z. D. (1936). Conjecture of Zheng Heng’s Seismoscope. Yenching University Journal of Chinese Studies (in Chinese), Beijing, 20, 577-586.
14. Yan, H. S. (2007). Zhang Heng's seismoscope. In History of Mechanism and Machine Science (pp. 119-161). Springer Netherland. https://doi.org/10.1007/978-1-4020-6460-9_5

Chapter 10

Metal Phosphides for Supercapacitors

Mohamed ABD-ASSALAM ALI EBRAIGI[1]
Fatma MEYDANERİ TEZEL[2]

1 Ph.D. Student, Karabük University, Faculty of Engineering, Department of Metallurgy and Materials Engineering, 78050, Karabük, Turkey,
E-mail: mohamedabd832@gmail.com
2 Prof. Dr., Karabük University, Faculty of Engineering, Department of Metallurgy and Materials Engineering, 78050, Karabük, Turkey,
E-mail: fatmameydaneri@karabuk.edu.tr, meydaneri@yahoo.com, ORCID ID: 0000-0003-1546-875X

1. INTRODUCTION

The first super capacitor was invented by General Electric in 1957 and its foundation was a double-layer methodology. It had a high capacitance value and presumed that energy was preserved in carbon cavities [1]. The first super capacitor device was created by Cleveland (SOHIO) Company, in 1966 utilizing the same double-layer energy storage system [2]. Since then, the development of supercapacitors has been rapidly progressed, and they are becoming more and more common in vehicle industries, particularly, for prototype automobiles and as extra fuel storage for battery-powered electronics.

The growing need for energy around the world, driven by economic growth, has led to two major problems: petroleum fuels' diminishing supply reserves and ecologic deterioration. One of major challenges facing society today is finding cost-efficient and eco-friendly power reserve solutions [3]. Super capacitors are also called ultra capacitors; they are attracting significant attention as a possible solution, because they have a long lifespan, a high fast response, and a comparatively high energy density. Supercapacitors are a promising power reserve devices in light of their large power density, excellent cycle stability, and quick charging and discharging. Nevertheless, its density of energy compared to traditional batteries is still less. These characteristics may take up the slack between batteries and traditional capacitors [4,5]. In order to address the issue, scientists have been developing new materials for the electrodes of supercapacitors, with a focus on modern metal- compounds, for instance, phosphides and sulfides. These materials have the potential to store extra vigor than carbon materials, because of the faradaic exactions reaction that occur during the electrochemical process. This approach is being heavily investigated as a technique to get around the restrictions of current super capacitor technology and improve their practical applications. As shown in Figure 1, super capacitors exhibit a much higher power density compared to rechargeable batteries, while the latter has a higher energy density. Thus, researchers are looking on super capacitors for deeming in high power uses, including electronic tools, systems that capture energy and electric and vehicles based on hybrid system [6] (as seen in Figure 2).

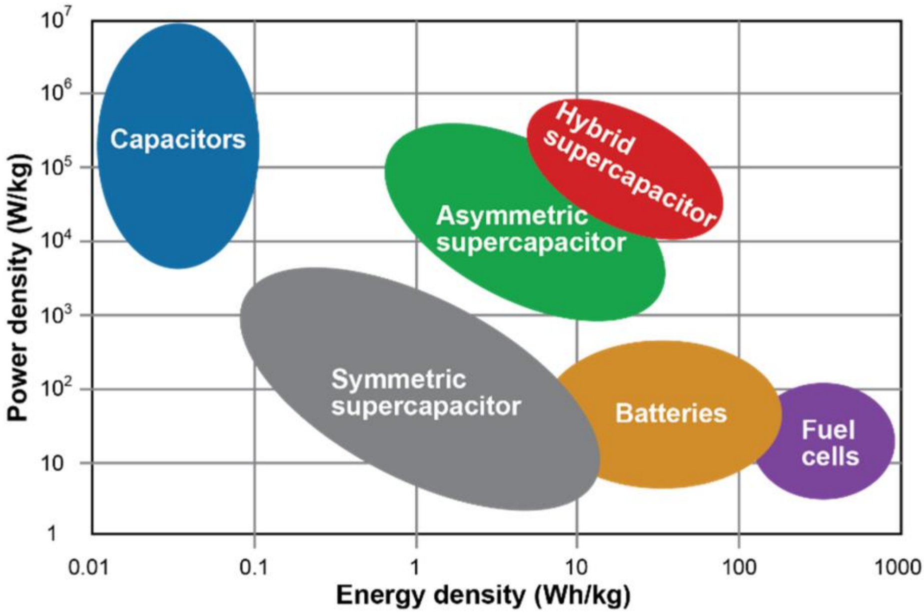

Figure 1. Plot comparing supercapacitors to different energy storage technologies [6].

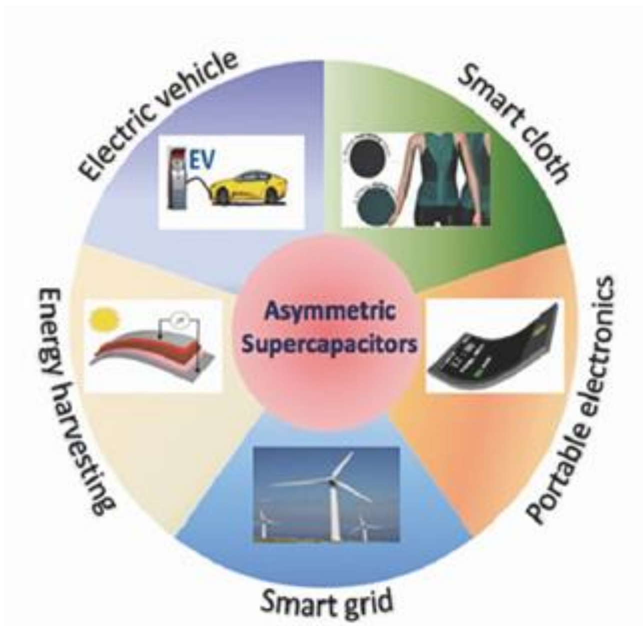

Figure 2. Show application examples of super capacitors [6].

It is widely known that the chemical reactions involved inside of batteries can significantly harm them; therefore, the lifespan of batteries might be shortened by charging and discharging them [7]. Super capacitors, on the other hand, use recombinant redox processes through electron charge transfer on the electrode surface and electrostatic power storage in the interfacial layer as its technique. It is anticipated that super capacitors will quicker charge-discharge times and longer lifetimes than batteries due to the few chemical processes that are involved [8].

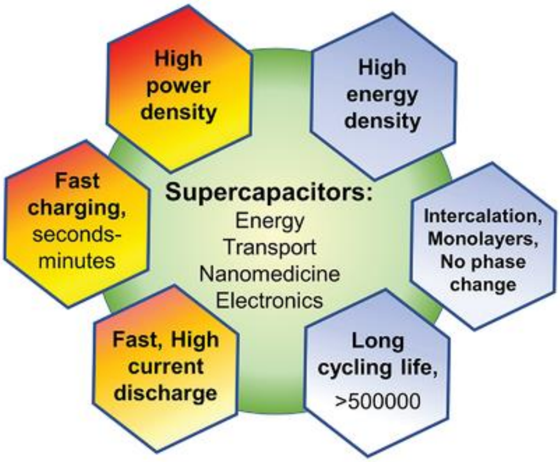

(a)

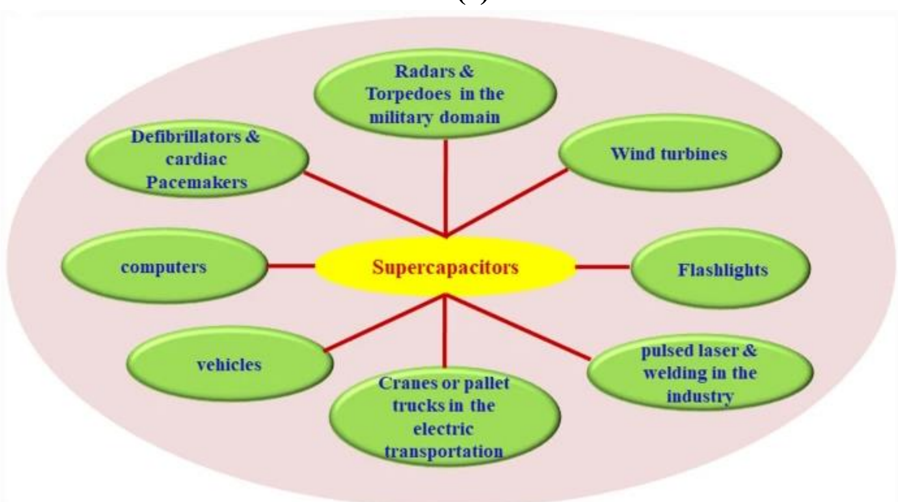

(b)

Figure 3. Shows **(a)** advantages and **(b)** usage areas of super capacitors [9,10].

Despite the many advantages of super capacitors, they still have some drawbacks like as high manufacturing costs and reduced power density [11]. The development of super capacitor innovation must overcome these significant obstacles. One way is to develop new materials for super capacitor's electrodes that may solve low density of energy. Sulfides and phosphides compounds materials have been identified as potential materials for next-generation super capacitors [12].

2. Classification of Supercapacitor

Supercapacitors operate on similar principles as typical capacitors, but to achieve greater capacitances, use electrodes with a larger surface area and narrower dielectrics. This makes super capacitors an appealing power option for a spectrum of uses, enabling power density larger than those of ordinary capacitors and power densities greater than those of battery packs. The electrode, electrolyte, separator, and collector are a super capacitor's primary parts. At the electrode-electrolyte boundary, ions react with the electrode material and are stored in the active species of the electrode, which acts as a storage location for electricity. Porosity, area, and conduction are three crucial electrode features that govern energy density. Strong super capacitors may be created by enhancing such properties that use in electronic devices such as laptops and mobile phones. A super capacitor electrode's surface area and the amount of energy it can store are inversely related. Therefore, studies are being conducted worldwide to find materials with high surface areas for energy storage devices. A larger density is achieved by forming a Helmholtz double layer, where the quantity of ions stored at the electrode grows with surface area. Due to its high capacitance in both aqueous and organic electrolytes, activated carbon is frequently used as an electrode material [13].

Pseudo capacitors, hybrid capacitors, and electrochemical double layer capacitors (EDLCs) are the essential categories that may be used to classify super capacitors.

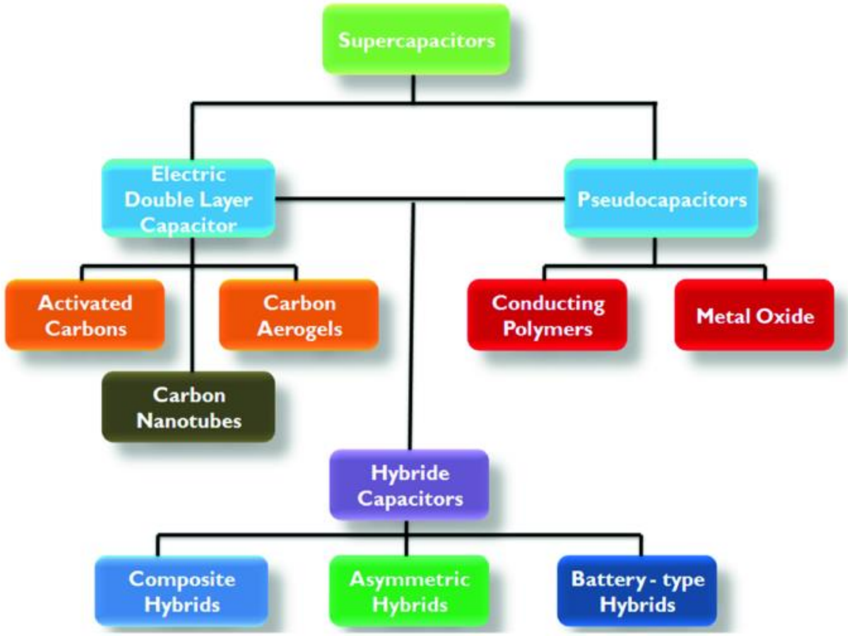

Figure 4. Shows of supercapacitor types and classification [14].

EDLCs, also known as electrostatic capacitors, store energy through the physisorption of electrode structure's pores contain electrolyte molecules. These materials must have high surface area to allow for effective ion absorption, and common examples include carbon-based materials [15]. Pseudocapacitors store energy quickly via the electrolyte ions and the activated sites on the electrode molecule's pores, transient faradic reactions occur in between electrolyte ions. Transition metal compounds are frequently studied as electrode materials, such as NiO/hydroxide, CoO/hydroxides, MnO_2, and RuO_2 [16,17]. Hybrid Capacitors combine the benefits of both battery-type electrodes, made from metal hydroxides, oxides, sulfides, and metal phosphides, and capacitor-type electrodes to offer great power and energy intensity [18]. All of the aforementioned types include two highly conductive electrodes separated by an electrolyte containing mobile ionic species as a universal structural element [19].

There is widespread usage of energy storage technologies including batteries, fuel cells, and capacitors. Thin layers of dielectric material and metal plates serve as the end points of capacitors, which store energy via charge separation. Super capacitors are a particular type of capacitor that employs metal oxide as the active material in the electrodes. They are also known as electrochemical capacitors. Both double-layer capacitance and pseudo capacitance are used as their primary storing techniques. The charge separation in a double layer at the interface of a conducting electrode's surface and an aqueous solution allows for electrostatic storage, which produces the double-layer capacitance mechanism. The use of pseudo capacitance, on the other hand, to electrochemically store electrical charges involves recombinant oxidation reaction on the surface of appropriate electrode materials [20]. A extremely quick series of reversible redox, electrosorption or intercalation reactions results in pseudo capacitance, which is associated with an electron charge transfer between an adsorbed and desolvated ion in between electrolyte and the electrode [21]. It is obvious that the specific capacitance and power density of transition metal-based super capacitors are larger than carbon materials and conducting polymer materials [22].

3. Phosphides for Supercapacitors

Materials produced recently in terms of the variety of compositions and controllability of structure can be considered as a candidate for porous materials. However, only large metal phosphides (MPs) will be responsible for producing metalorganic frameworks (MOFs) derived from phosphide materials in the conventional manner. In the last few years, many methods have been developed to synthesize derived- MOFs from nanostructured transition metal phosphides. As for synthesis methods, the available strategies that are currently underway fall into several categories. There are other methods such as solvothermal method, pyrolytic production, hydrothermal production, template strategy and microwave assisted method, electrochemical method and sonochemical method (Figure 5). Moreover, derived-MOFs from phosphide nanomaterials exhibit excellent electrochemical performance in most common applications. The synergistic effects and surface oxidation of intrinsic TMPs are responsible for the high reaction performance [23].

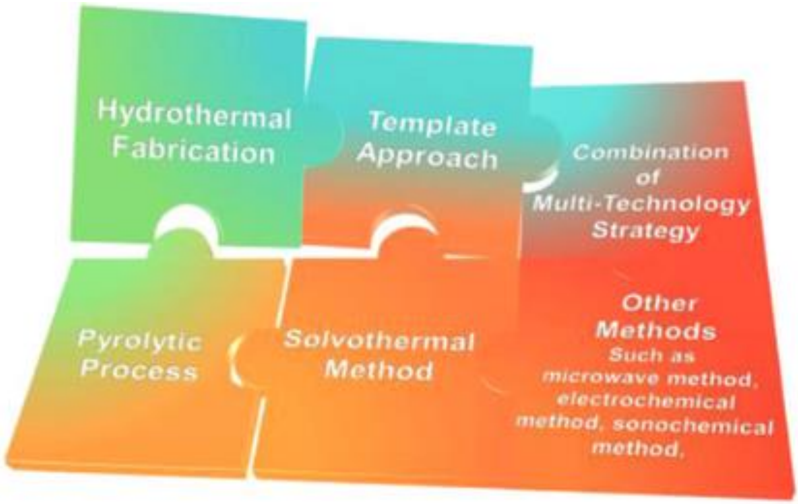

Figure 5. The synthesis method's summary of phosphide-derived nanomaterials [24].

The solvothermal and hydrothermal technique supports the reaction and provides the driving force to the crystallization step, and hand-held MOF structures generally have high thermal stability [24].

Template tip: The use of template tip to synthesize nanostructured MOF structures is a good choice for effective control of morphology. [24].

Pyrolytic process: It is the most widely used technique for the fabrication of monotonous dimensional MOF-derived materials. Successful MOF-derived structures have the advantage of high porosity [24].

Microwave-assisted method: This method facilitates the production of ultra-small hollow nanoparticles with good dispersion and high phase purity from MOF materials [24].

Electrochemical method: This method can be classified into anodic synthesis, cathodic synthesis, indirect bipolar electrodepositon, electroplating displacement, and electrophoretic deposition (EPD), allowing rapid generation of MOF structures with excellent porosity and controllable morphology [24].

Sonochemical method: Helps form homogeneous MOF materials and requires less time to crystallize [24].

According to their exceptional capacity to retain electrochemical energy, strong conductivity, and capacity to be produced in a variety of topologies, phosphides, specially, cobalt-based phosphides, are regarded as attractive candidate materials for transition metal-based supercapacitors. However, when they are not made correctly, they frequently display a fairly low specific capacitance. As result of their high conductivity and exceptional electrochemical reactions, transition metal phosphides (TMPs) electrode show excellent electrochemical features such as high capacity, capability, and stability of cycling in comparison to hydroxide, oxide, or sulfide counterparts. For instance, TMPs with compositions such as Ni_xP_y, Zn-Ni-P, Ni-Fe-P and $Ni_xCo_{3-x}P_y$. The many valent forms of the transition metal cations and the changeable coordination number are to blame for the diversity in the formulas and crystals structures of TMPs [25]. In light of this, it is possible to manipulate the compositions and structures of TMPs to achieve desired physicochemical features [26]. As shown in Fig.6, (M_xP_y) include MoP with hexagonal WC-type structure, MnP, FeP, CoP, and NiP [27], within orthorhombic structure, and Fe_2P-type structure including Ni_2P, Fe_2P and Mn_2P. These structures make TMPs desirable as electrode materials for super capacitors because they have a multitude of metal-metal and metal-phosphorus bonds [28]. Depending on the stoichiometry and content of the elements, M_xP_y may have ionic, covalent or metallic bonds. P frameworks illustrate high flexibility, due to the wide range of various stoichiometries and crystal forms are possible because to the phosphorus-phosphorus interaction angles [29].

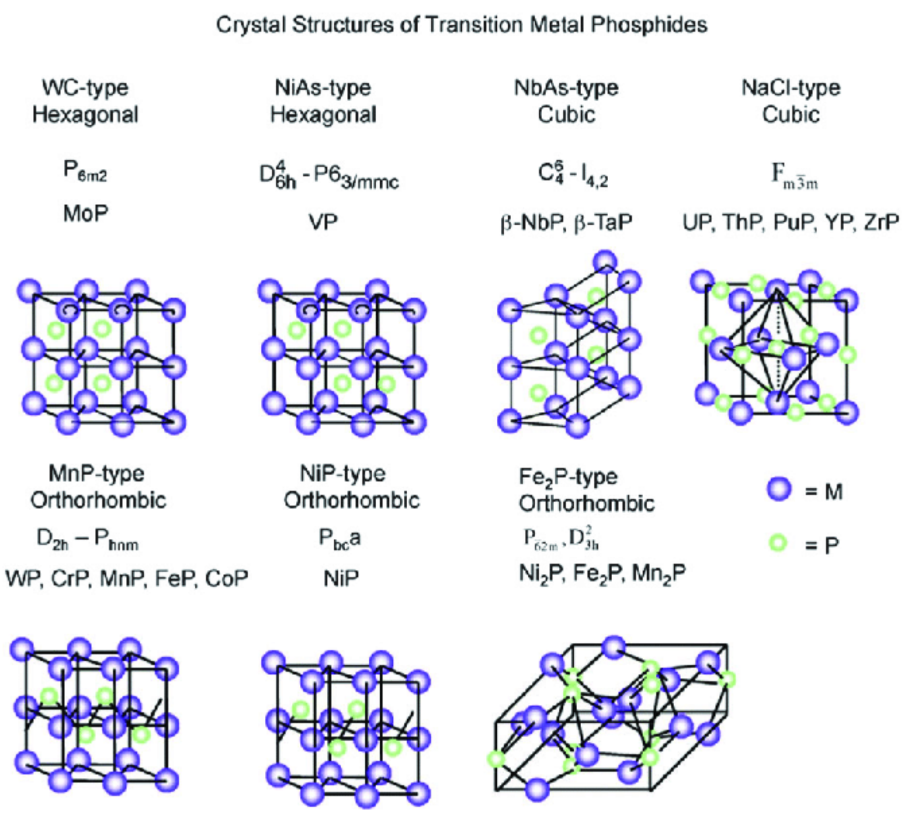

Figure 6. Show structures of metal phosphides' crystal [30].

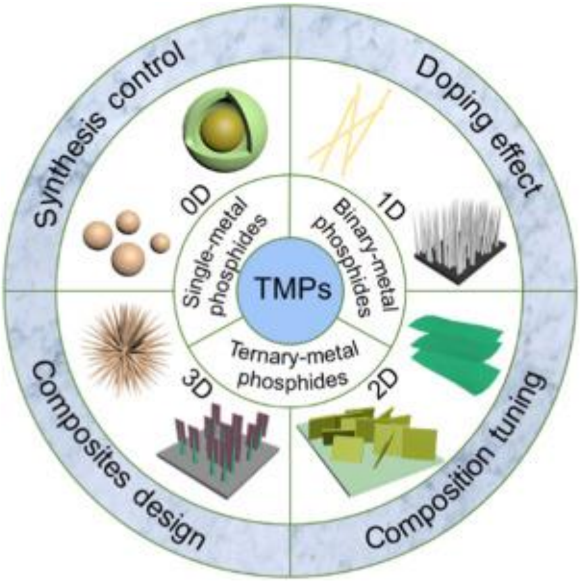

Figure 7. Show structures and advantages of transition metal phosphides [31].

3.1. Monometallic phosphides

Monometallic phosphines containing Ni, Co, Mo and W, bulk phases and structures with different components draw attention as catalysis to a great extent due to their performance. Because their performance is close to that of metals, they have good thermal chemical resistance, high thermal stability and good thermal conductivity [32-36]. Until now, the most common and effective production method for derived-MOF structures from monometallic phosphides with appropriate scale and morphology under reaction time, temperature, environmental control and more conditions are pyrolytic and template approaches [37]. At the same time, some typical strategies for production continue to be developed [24].

3.2. Bimetallic Phosphides

Compared to monometallic phosphides, it provides a more surface active state as it improves the catalytic efficiency and stability of the catalysis, and the synergistic role of two different metal ions can play an important role in changing the electronic structure of the electrical catalyst. Exploring synthesis methods to investigate the derivation and properties of bimetallic phosphides has been the breaking point. Compared with the production methods of monometallic phosphides, the production methods of bimetallic phosphides are more diverse: pyrolytic process, hydrothermal method, solvothermal method, template strategy and solid-phase temperature pres [24].

Using a prospective method, Liang et al. revealed creating metal phosphide electrodes. They generated arrays of Ni-Co hydroxides by a hydrothermal process. The Ni_2P and CoP nanosheets were then produced by thermal phosphidization applying PH_3 plasma at 250 °C for 15 min. by PECVD. The Ni_2P delivers a high specific capacity of 166 mAh g^{-1} at 1 A g^{-1}, CoP exhibits a relatively low specific capacity of 108 mAh g^{-1} at 1 A g^{-1} (Fig. 8-a). The CoP also shows better stability than Ni_2P. The capacity retention is as high as 89% after 5000 cycles even at a high discharge current density of 10 A g^{-1} (Fig. 8-b) [38].

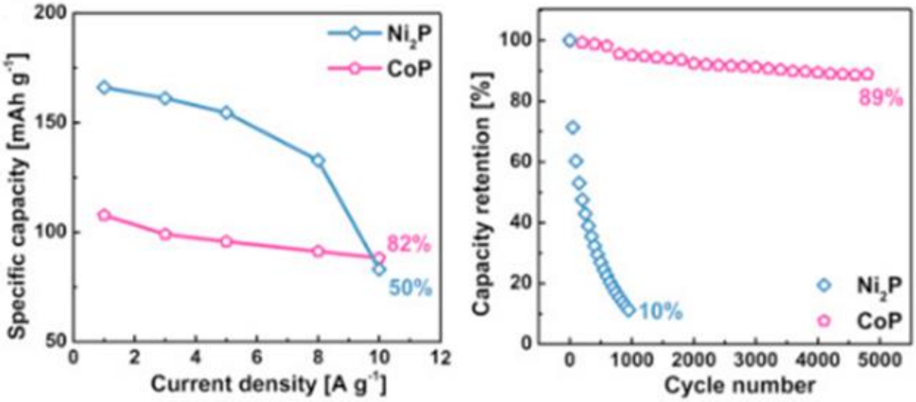

(a) **(b)**

Figure 8. (a) The specific capacity's analogy of the Ni_2P and CoP. **(b)** Cycling stability's analogy of the Ni_2P and CoP [38].

3.3. Trimetallic phosphides

Thermal phosphorization of the triple PBA precursor induces carbon mixing and results in displacement of surface defects onto the NCs. Concise methods exist to describe transition metal-based bifunctional electrocatalysis devices useful for ambient water splitting. The doped materials, especially the trimetallic phosphide materials, show both remarkable stability and electrocatalytic activity for HER and OER. Although the catalytic activity is significantly improved, the enhancement of their catalytic activity does not only make a significant contribution to the synergy of the active states. The specific contribution of active states to synergistic effects is not clear. Doping of many metal elements, from monometallic to trimetallic phosphides, improves not only the properties of materials, but also their electrochemical properties. Although the catalytic activity is clearly enhanced, the specific role of active states in the synergistic effect is not clear. Therefore, trimetallic phosphides have not been studied in depth and production approaches are more limited. Although the pyrolytic process [39-42] is more dominant, the hydrothermal method [43], solvothermal production and electrospinning methods have been widely used [24].

Using a prospective method, Liang et al. revealed creating metal phosphide electrodes. They generated arrays of Ni-Co hydroxide nanosheets on carbon fabric by a hydrothermal process. The required NiCoP nanosheets were then produced by thermal phosphidization applying PH_3 plasma at 250 °C for 15 min. by PECVD a NiCoP carbon cloth electrode, a maximum capacity of 194 mAh/g at 1 A/g was produced. During the density was raised to 10 A/g, the capacitance is kept at 169 mAh/g. It is noteworthy that after 5000 charging and discharging cycles at 10 A/g, 81% of the starting capacity was still present, as shown in Figure 9 (a-d). The asymmetric capacitor of graphene films and NiCoP nanostructures tend to possess high energy density of 32.9 Wh/kg and high power of 8.509 kW/kg along with superior charging performance (83% capacity preserved beyond 5000 cycles at 20 A/g) [38].

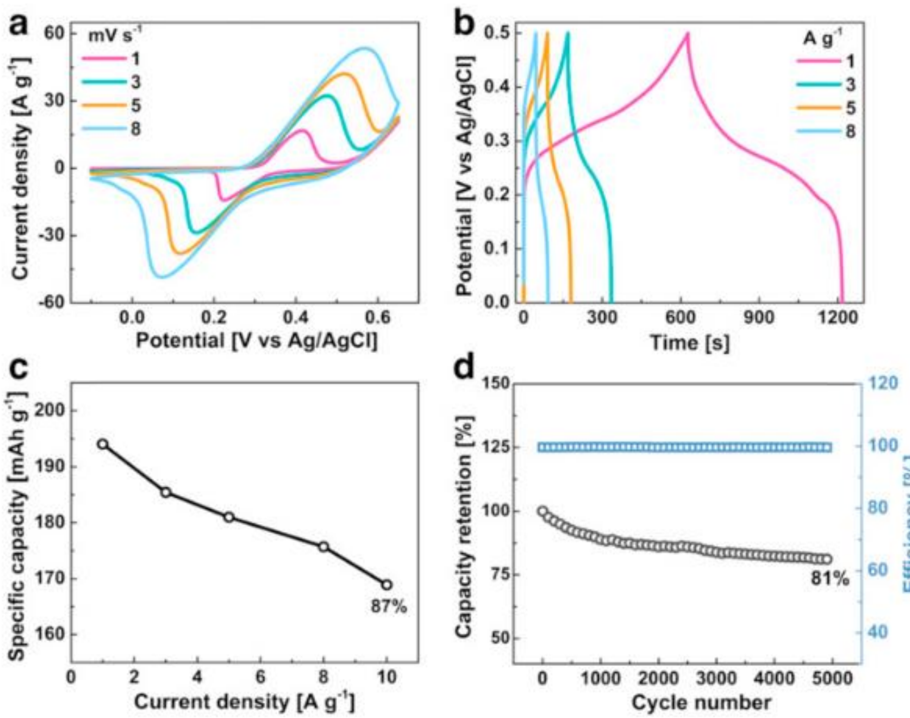

Figure 9. Electrochemical performance of NiCoP for supercapacitors. **(a)** CV curves at different scan rates. **(b)** GCD profiles at different current densities. **(c)** Specific capacity. **(d)** Cycling performance at a constant current density of 10 A g^{-1}[38].

Currently, the invention of Co, Ni-based bimetallic phosphates has received some interest. As a result of their large electrochemical activities, the mesoporous ($NiCo_2(PO_4)_2$, $Ni_2Co(PO_4)_2$, and $Co_3(PO_4)_2$), which had the relatively high surface area when used as electrode materials in supercapacitors. This could offer the material better electrochemical characteristics by increasing the electro active regions and the pathways for electrolyte ion transport [44].

Kong and coworkers have developed self-supported ternary NiCoP nanosheet arrays on Ni foam using post-thermal phosphidization of Ni-Co hydroxides [45]. NiCoP/NF was topotactically converted from $NiCo(OH)_xF$/NF [46]. When compared to Ni-Co hydroxide alone, the NiCoP/NF electrode achieved a higher areal capacitance (9.2 F/cm^2 at 2 mA/cm^2) at 50 mA/cm^2. It had a 5.97 F/cm^2 areal capacitance; achieved sixty-seven percent of the start capacitance that was preserved over 2 thousand cycles at 50 mA/cm^2 at density of 1.6 mW/cm^2, the hybrid capacitor employing active carbon as the anode and NiCoP/NF as the cathode produced a high energy density of 1.16 mWh/cm^2. Additionally, it has excellent rate capability, with 72% of its original capacitance being reached after 2000 cycles around fifty mA/cm^2.

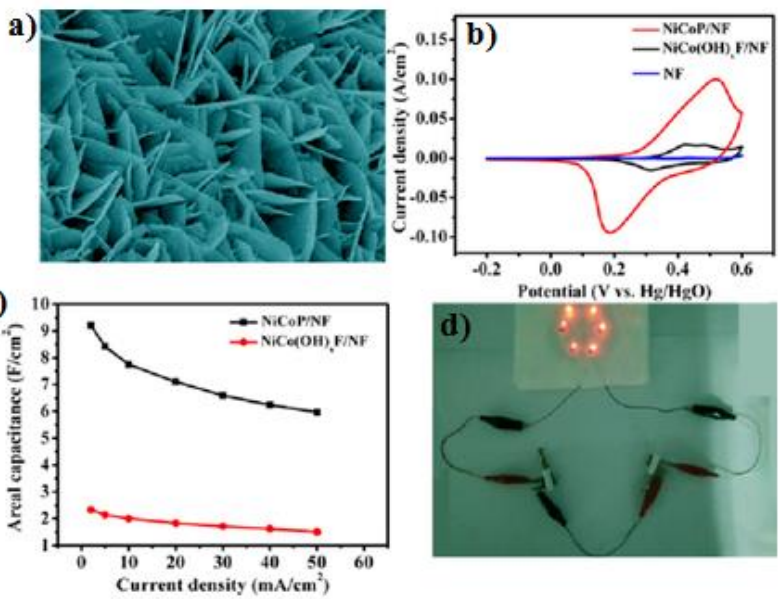

Figure 10. (a) SEM images of NiCoP. **(b)** CV curves at scan rate of 5 mV s^{-1} in 2 M KOH. **(c)** Areal capacitances in different current densities. **(d)** Asymmetric supercapacitor (ASC) devices in series perform effectively to light six LED indicators [45].

3.4. Carbon and Ni-doped with MPs

Carbon materials with metal phosphide have utility as compounds and may exhibit fundamentally unexpected properties [47-50]. Recently, several new approaches have been applied to produce metal phosphide carbon materials.

Due to its low cost and reliability, nitrogen has been a suitable additive for phosphide materials, and the nitrogen additive accelerates the success rate physically and chemically. Recently, new materials have been further developed with nitrogen-doped metal phosphides to strengthen some specific properties of phosphides, and several approaches have been registered for plastics applications [24].

The synergistic interaction of bimetallic oxide and phosphide might enhance the electrochemical activity of bimetallic phosphide. As an illustration, 3D hierarchical $Ni_xCo_{1-x}O/Ni_yCo_{2-y}P@C$ (NiCoOP@C). Thermal phosphidization of $Ni_xCo_{1-x}O@C$, as illustrated in Figure 11-a, was used to create the structures, which had two distinct morphologies: one dimension in the core and two dimensions in the shell. The ion diffusion and electron corridors are improved by 3D structures. As a result, at 1 A/g, the corresponding electrode displayed a specific capacity of 2638 F/g, and at 20 A/g, it remained constant at 1144 F/g. After 3000 continuous charge-discharge cycles at 10 A/g, 84% of the initial capacitance was still present, indicating that NiCoOP@C displays higher ionic conductivity than individual $Ni_xCo_{1-x}O@C$, $Ni_yCo_{2-y}P$, and NiCo nanowire arrays electrodes (see Figure 11 (b and c). Even though, transition phosphides have relatively high capacitance and strong electric conductivity, there is still a lot that may be done to boost the electrochemical performance of electrode materials that are actually produced. For instance, phosphorous can be replaced with sulfur or nitrogen, and a unique protective layer that stabilizes metal phosphide in an alkaline electrolyte can result in a significant enhancement [51].

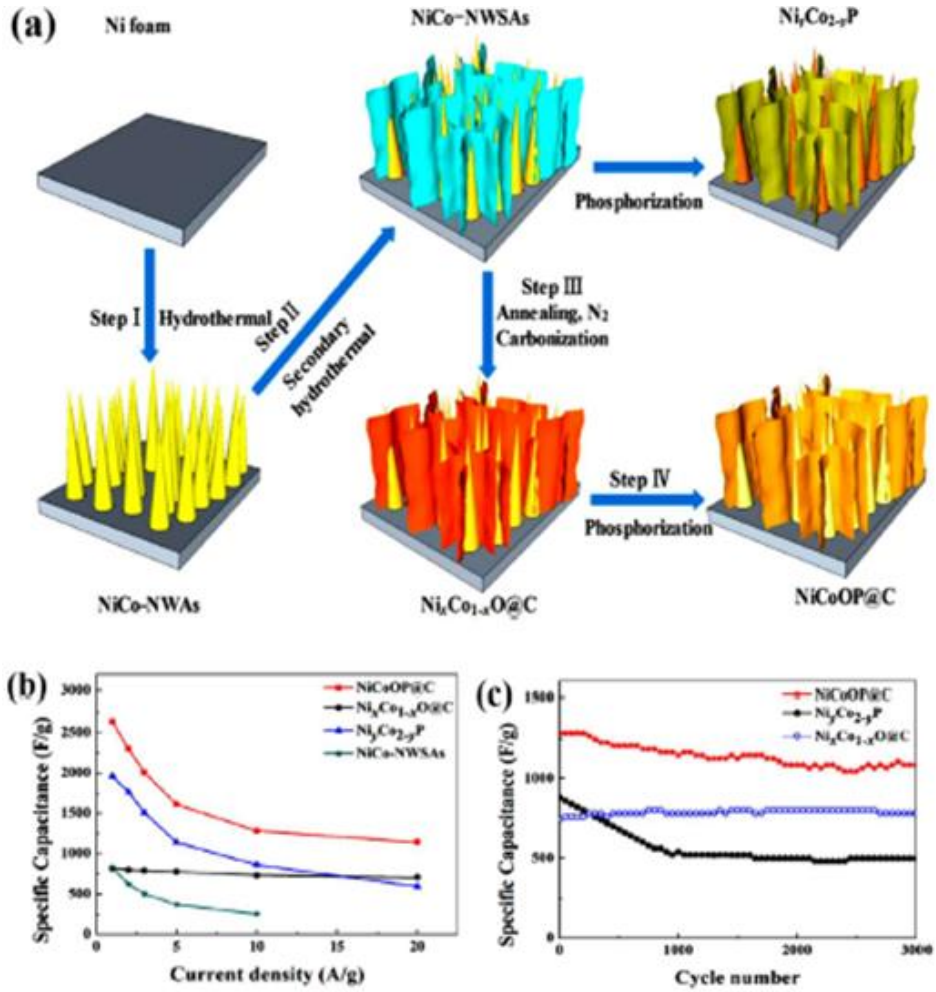

Figure 11. Shows **(a)** scheme of the synthesis process for the 3D hierarchical NiCoOP@C, **(b)** SEM image of NiCoOP@C, **(c)** particular capacitance evaluated at various current densities, and **(d)** cycling performance at 10 A/g of the NiCo nanowire arrays, $Ni_yCo_{2-y}P$, $Ni_xCo_{1-x}O@C$, and NiCoOP@C [51].

3.5. Advantages and Applications of Phosphides

Metal phosphides are still under development, but may have several applications for supercapacitors in different industry fields as following [50].

1. In transmission lines for energy.

2. SC UPS: To treat critical loads problem, which need ride-through of few second, SC system without any batteries are useful.

3. Hybrid SC-Battery UPS: Together, SC and battery may overcome each other's weaknesses, reducing battery cycling and extending battery life.

4. To rectified the system frequency as well as stability control.

5. Micro grid and micro-generation, SC can be utilized as a source of power storage in a micro source system connected to a network.

6. In order to protect sensitive equipment from voltage sag, super capacitors are produced as an energy storage solution.

7. In a wind turbine system, SC can offer a straight forward, extremely dependable solution.

8. In order to ensure extremely dependable operation in communications, "hot stand by system" is frequently supported by redundant DC-DC converters, parallel type UPSs, and batteries. In the standby unit, there is some power usage. Due to the importance of electricity conservation, it becomes a severe issue. As a result, they need a cold standby device, such as a fuel cell or diesel generator set. However, they take a while to respond. Utilizing SC, which starts working faster as soon as a system disruption happens, is the answer.

9. Igniting a diesel engine in cold weather under conditions as low as -40 °C, it is more challenging to start diesel-fuelled engines. When starting engines, lead acid batteries have been employed. The high resistance a battery offers at low temperatures has an effect on the necessary high current discharge of a battery in the situation. The internal resistance increases further when the battery ages once again, and the capacity for current discharge significantly decreases. Battery and SC bank can be utilized to provide the engine the necessary cranking current.

10. Hybrid electric vehicle that is powered only by a battery system using a motor and inverter. When utilized in tandem with transient demand, or the need for a pulse of current when accelerating, is fulfilled by the SC of a battery that has a high energy density and a high power density, and the energy is returned to the SC upon deceleration or breakdown. Consequently, a sizable percentage of the energy spent during acceleration may be recovered.

4. Summary and Outlook

Super capacitors perform well in a variety of crucial applications that call for a combination of high power, quick charging, excellent cycle stability, and long shelf life. Good performance for super capacitor applications is provided by composites made of transition noble metal phosphides and their composites. Own to their high-calculated capacity, cheap cost, and there reactivity, transition metal-based compounds are recommended as more creative possibilities for industrial application than conventional materials. However, meeting the need for high-energy storage for industrial applications still present’s enormous problems. Hence, the best way to develop materials of the coming generation that will increase the density of SC material systems is to have a solid grasp of the working process.

REFERENCES

[1] US patent 2800616, "Low voltage electrolytic capacitor", granted 1957-07-23.

[2] US patent 3288641, "Electrical energy storage apparatus", granted 1966-11-29.

[3] Arico, A. S., Bruce, P., Scrosati, B., Tarascon, J. M., & Van Schalkwijk, W. (2005). Nanostructured materials for advanced energy conversion and storage devices. Nature materials, 4(5), 366-377.

[4] Kandalkar, S. G., Dhawale, D. S., Kim, C. K., & Lokhande, C. D. (2010). Chemical synthesis of cobalt oxide thin film electrode for supercapacitor application. Synthetic Metals, 160(11-12), 1299-1302.

[5] Zhang, L. L., & Zhao, X. S. (2009). Carbon-based materials as supercapacitor electrodes. Chemical Society Reviews, 38(9), 2520-2531.

[6] Zhong, X., Jiang, Y., Chen, X., Wang, L., Zhuang, G., Li, X., & Wang, J. G. (2016). Integrating cobalt phosphide and cobalt nitride-embedded nitrogen-rich nanocarbons: high-performance bifunctional electrocatalysts for oxygen reduction and evolution. Journal of Materials Chemistry A, 4(27), 10575-10584.

[7] Padhi, A. K., Nanjundaswamy, K. S., & Goodenough, J. B. (1997). Phospho-olivines as positive-electrode materials for rechargeable lithium batteries. Journal of the electrochemical society, 144(4), 1188.

[8] Kötz, R., & Carlen, M. J. E. A. (2000). Principles and applications of electrochemical capacitors. Electrochimica acta, 45(15-16), 2483-2498.

[9] Hepel, M. (2022). Advances in micro-supercapacitors (MSCs) with high energy density and fast charge-discharge capabilities for flexible bioelectronic devices-A review. Electrochemical Science Advances, e2100222.

[10] Dhilip Kumar, R., Nagarani, S., Sethuraman, V., Andra, S., & Dhinakaran, V. (2022). Investigations of conducting polymers, carbon materials, oxide and sulfide materials for supercapacitor applications: A review. Chemical Papers, 76(6), 3371-3385.

[11] Zhang, S. W., & Chen, G. Z. (2008). Manganese oxide based materials for supercapacitors. Energy Materials, 3(3), 186-200.

[12] Babakhani, B., & Ivey, D. G. (2010). Improved capacitive behavior of electrochemically synthesized Mn oxide/PEDOT electrodes utilized as electrochemical capacitors. Electrochimica Acta, 55(12), 4014-4024.

[13] Pan, H., Li, J., & Feng, Y. (2010). Carbon nanotubes for supercapacitor. Nanoscale research letters, 5(3), 654-668.

[14] Balaji, T. E., Tanaya Das, H., & Maiyalagan, T. (2021). Recent trends in bimetallic oxides and their composites as electrode materials for supercapacitor applications. ChemElectroChem, 8(10), 1723-1746.
[15] Zou, Y., Cai, C., Xiang, C., Huang, P., Chu, H., She, Z., ... & Kraatz, H. B. (2018). Simple synthesis of core-shell structure of Co-Co_3O_4@ carbon-nanotube-incorporated nitrogen-doped carbon for high-performance supercapacitor. Electrochimica Acta, 261, 537-547.
[16] Haldorai, Y., Choe, S. R., Huh, Y. S., & Han, Y. K. (2018). Metal-organic framework derived nanoporous carbon/Co_3O_4 composite electrode as a sensing platform for the determination of glucose and high-performance supercapacitor. Carbon, 127, 366-373.
[17] Guan, C., Liu, X., Ren, W., Li, X., Cheng, C., & Wang, J. (2017). Rational design of metal-organic framework derived hollow $NiCo_2O_4$ arrays for flexible supercapacitor and electrocatalysis. Advanced Energy Materials, 7(12), 1602391.
[18] Yang, S., Wu, C., Cai, J., Zhu, Y., Zhang, H., Lu, Y., & Zhang, K. (2017). Seed-assisted smart construction of high mass loading Ni–Co–Mn hydroxide nanoflakes for supercapacitor applications. Journal of Materials Chemistry A, 5(32), 16776-16785.
[19] Salanne, M., Rotenberg, B., Naoi, K., Kaneko, K., Taberna, P. L., Grey, C. P., ... & Simon, P. (2016). Efficient storage mechanisms for building better supercapacitors. Nature Energy, 1(6), 1-10.
[20] Huang, M., Li, F., Dong, F., Zhang, Y. X., & Zhang, L. L. (2015). MnO_2-based nanostructures for high-performance supercapacitors. Journal of Materials Chemistry A, 3(43), 21380-21423.
[21] Burke, A. (2000). Ultracapacitors: why, how, and where is the technology. Journal of power sources, 91(1), 37-50.
[22] Conway, B. E., & Conway, B. E. (1999). Electrochemical capacitors based on pseudocapacitance. Electrochemical supercapacitors: scientific fundamentals and technological applications, 221-257.
[23] Shi, Y., Li, M., Yu, Y., & Zhang, B. (2020). Recent advances in nanostructured transition metal phosphides: synthesis and energy-related applications. Energy & Environmental Science, 13(12), 4564-4582.
[24] Wang, X., Zhang, G., Yin, W., Zheng, S., Kong, Q., Tian, J., & Pang, H. (2022). Metal–organic framework-derived phosphide nanomaterials for electrochemical applications. Carbon Energy, 4(2), 246-281.
[25] Gao, Y., Chen, S., Cao, D., Wang, G., & Yin, J. (2010). Electrochemical capacitance of Co_3O_4 nanowire arrays supported on nickel foam. Journal of Power Sources, 195(6), 1757-1760.

[26] Chen, H., Hu, L., Chen, M., Yan, Y., & Wu, L. (2014). Nickel–cobalt layered double hydroxide nanosheets for high-performance supercapacitor electrode materials. Advanced Functional Materials, 24(7), 934-942.
[27] Dinh, K. N., Liang, Q., Du, C. F., Zhao, J., Tok, A. I. Y., Mao, H., & Yan, Q. (2019). Nanostructured metallic transition metal carbides, nitrides, phosphides, and borides for energy storage and conversion. Nano Today, 25, 99-121.
[28] Huang, B., Wang, H., Liang, S., Qin, H., Li, Y., Luo, Z., ... & Chen, L. (2020). Two-dimensional porous cobalt–nickel tungstate thin sheets for high performance supercapattery. Energy Storage Materials, 32, 105-114.
[29] Carenco, S., Portehault, D., Boissiere, C., Mezailles, N., & Sanchez, C. (2013). Nanoscaled metal borides and phosphides: recent developments and perspectives. Chemical reviews, 113(10), 7981-8065.
[30] Oyama, S. T., Gott, T., Zhao, H., & Lee, Y. K. (2009). Transition metal phosphide hydroprocessing catalysts: A review. Catalysis Today, 143(1-2), 94-107.
[31] Zong, Q., Liu, C., Yang, H., Zhang, Q., & Cao, G. (2021). Tailoring nanostructured transition metal phosphides for high-performance hybrid supercapacitors. Nano Today, 38, 101201.
[32] Jiao, L., Zhou, Y. X., & Jiang, H. L. (2016). Metal–organic framework-based CoP/reduced graphene oxide: high-performance bifunctional electrocatalyst for overall water splitting. Chemical Science, 7(3), 1690-1695.
[33] Jiang, P., Liu, Q., Liang, Y., Tian, J., Asiri, A. M., & Sun, X. (2014). A cost-effective 3D hydrogen evolution cathode with high catalytic activity: FeP nanowire array as the active phase. Angewandte Chemie, 126(47), 13069-13073.
[34] Chung, D. Y., Jun, S. W., Yoon, G., Kim, H., Yoo, J. M., Lee, K. S., ... & Sung, Y. E. (2017). Large-scale synthesis of carbon-shell-coated FeP nanoparticles for robust hydrogen evolution reaction electrocatalyst. Journal of the American Chemical Society, 139(19), 6669-6674.
[35] Chaudhari, N. K., Yu, P., Kim, B., Lee, K., & Li, J. (2018). Ferric phosphide carbon nanocomposites emerging as highly active electrocatalysts for the hydrogen evolution reaction. Dalton Transactions, 47(45), 16011-16018.
[36] Callejas, J. F., McEnaney, J. M., Read, C. G., Crompton, J. C., Biacchi, A. J., Popczun, E. J., ... & Schaak, R. E. (2014). Electrocatalytic and

photocatalytic hydrogen production from acidic and neutral-pH aqueous solutions using iron phosphide nanoparticles. ACS nano, 8(11), 11101-11107.
[37] Bai, Y., Liu, C., Shan, Y., Chen, T., Zhao, Y., Yu, C., & Pang, H. (2022). Metal-organic frameworks nanocomposites with different dimensionalities for energy conversion and storage. Advanced Energy Materials, 12(4), 2100346.
[38] Liang, H., Xia, C., Jiang, Q., Gandi, A. N., Schwingenschlögl, U., & Alshareef, H. N. (2017). Low temperature synthesis of ternary metal phosphides using plasma for asymmetric supercapacitors. Nano Energy, 35, 331-340.
[39] Gao, W. K., Yang, M., Chi, J. Q., Zhang, X. Y., Xie, J. Y., Guo, B. Y., ... & Dong, B. (2019). In situ construction of surface defects of carbon-doped ternary cobalt-nickel-iron phosphide nanocubes for efficient overall water splitting. Science China Materials, 9(62), 1285-1296.
[40] Zhang, X., Wu, Y., Sun, Y., Liu, Q., Tang, L., & Guo, J. (2019). CoFeP hollow cube as advanced electrocatalyst for water oxidation. Inorganic Chemistry Frontiers, 6(2), 604-611.
[41] Zhang, G., Li, Y., Xiao, X., Shan, Y., Bai, Y., Xue, H. G., ... & Xu, Q. (2021). In situ anchoring polymetallic phosphide nanoparticles within porous prussian blue analogue nanocages for boosting oxygen evolution catalysis. Nano Letters, 21(7), 3016-3025.
[42] Xu, J., Li, J., Xiong, D., Zhang, B., Liu, Y., Wu, K. H., ... & Liu, L. (2018). Trends in activity for the oxygen evolution reaction on transition metal (M= Fe, Co, Ni) phosphide pre-catalysts. Chemical science, 9(14), 3470-3476.
[43] Wei, X., Zhang, Y., He, H., Peng, L., Xiao, S., Yao, S., & Xiao, P. (2019). Carbon-incorporated porous honeycomb NiCoFe phosphide nanospheres derived from a MOF precursor for overall water splitting. Chemical Communications, 55(73), 10896-10899.
[44] Zhang, J., Yang, Y., Zhang, Z., Xu, X., & Wang, X. (2014). Rapid synthesis of mesoporous $Ni_xCo_{3-x}(PO_4)_2$ hollow shells showing enhanced electrocatalytic and supercapacitor performance. Journal of Materials Chemistry A, 2(47), 20182-20188.
[45] Kong, M., Wang, Z., Wang, W., Ma, M., Liu, D., Hao, S., ... & Sun, X. (2017). NiCoP nanoarray: a superior pseudocapacitor electrode with high areal capacitance. Chemistry–A European Journal, 23(18), 4435-4441.
[46] Tian, J., Liu, Q., Asiri, A. M., & Sun, X. (2014). Self-supported nanoporous cobalt phosphide nanowire arrays: an efficient 3D hydrogen-

evolving cathode over the wide range of pH 0–14. Journal of the American Chemical Society, 136(21), 7587-7590.
[47] Breuer, O., & Sundararaj, U. (2004). Big returns from small fibers: a review of polymer/carbon nanotube composites. Polymer composites, 25(6), 630-645.
[48] Zhang, C., Dong, H., & Zhao, Y. S. (2018). Rational design, controlled fabrication, and photonic applications of organic composite nanomaterials. Advanced Optical Materials, 6(21), 1701193.
[49] Akgöl, S., Ulucan-Karnak, F., Kuru, C. I., & Kuşat, K. (2021). The usage of composite nanomaterials in biomedical engineering applications. Biotechnology and Bioengineering, 118(8), 2906-2922.
[50] Prasad, G. G., Shetty, N., Thakur, S., & Bommegowda, K. B. (2019, October). Supercapacitor technology and its applications: a review. In IOP Conference Series: Materials Science and Engineering (Vol. 561, No. 1, p. 012105). IOP Publishing.
[51] Shao, Y., Zhao, Y., Li, H., & Xu, C. (2016). Three-dimensional hierarchical $Ni_xCo_{1-x}O/Ni_yCo_{2-y}P@C$ hybrids on nickel foam for excellent supercapacitors. ACS applied materials & interfaces, 8(51), 35368-35376.

Chapter 11

Variables in Paython

Musa Genemo[1]

1 Doktor Öğretim Üyesi Gumushane Üniversitesi İktisadi İdari Bilimler Fakültesi Yonetim bilisim System Bölümü. Musa.ju2002@gmail.com ORCID No: 0000-0001-9991-3050

Chapter's Objective

- Will have knowledge about values and variables in Python programming language,
- Recognize data types in python and
- You will be able to write a program that uses different variables.

Variable Declaration

A Variable is a name given to a memory location. In python, there is no need to specify the datatype of the variable. Python automatically gets variable datatype depending upon the values assigned to the variable. Python does not provide an explicit way to declare a variable. It uses implicit variable declaration. For instance, in language like Java, you must declare a variable before you can assign it a value. In Python, the variable declaration is done automatically when a variable is assigned a value using the assignment operator (=). The examples below show variable assignment (with implicit declaration).

Variables are not storage containers in python. Memory has values at defined memory locations, and each memory location has a memory address.

10	2	20
x	y	z

When you get statement y =2, the variable rank will be created as a label pointing to the memory location where value 2 is stored. Each memory location has a memory address. When you give y = 5, the label y will not have the same location as earlier. It will now refer to value 5, which is at a different location.

```
# Assignment and implicit data type declaration in Python
index = 10            # An integer data type
distance = 500.05     # A floating point data type
firstname = "Kindson"   # A string data
scores = [67,87,98,54,82] # A list data type
print(index)
print(distance)
print(firstname)
```

```
a = 10
b = 'Hello"
c = 2.4
d = None
```

Value Assignment for Variable

Variables are used to retain values. These values can be in different formats such as numbers, strings, or objects.

Example:

- x=   3, -----. number declaration
- name = “Ali” -----string declaration
- emp = employe() ------object declaration

statement (x =3)is an assignment line. Assignment maps a value to a variable. The most important part of this expression detail is the assignment (=) symbol. With this expression, the value 3 is assigned to the variable x. At this point, x the type of the variable is integer because the value assigned is an integer value. multiple times to a variable assignment can be made. If a different type of value is assigned at this time, the type of the variable also changes. Here, the meaning of the assignment (=) symbol is different from the way it is used in mathematics.

In mathematics, this symbol provides equality, so the expressions on the right and left of this symbol means they are equal. In Python, on the left side of the assignment (=) symbol.

```
x = 3
print(x)
x = 2
print(x)
x = 30
print(x)
```

Out put

First print returns 3

Second prints return 2

As you can see, although the print function is the same on every line, a different value is printed each time. This program shows us that we do not always predict behavior in variable-dependent situations. Some functions may act dependent on one or more variables.

```
a = 3
print ("a = " + str(a))
a = 10
print("a = " + str(a))
a = 20
print("a = " + str(a))
```

Python Statement

Any Instructions that a Python interpreter can execute are called statements. For example, a = 1 is an assignment statement. If statement, for statement, while statement, etc. are other kinds of statements which will be discussed later in upcoming chapters.Let's look at the following example written in python language:

```
sum = 0
x = 3
y = 1
sum = x + y
print(sum)
```

In Python, the end of a statement is marked by a newline character. But we can make a statement extend over multiple lines with the line continuation character (\).

For example:

```
a = 1 + 2+ 3+ \
    4 + 5 + 6 + \
    7+ 8+ 9
Print(a)
```

This is an explicit line continuation. In Python, line continuation is implied inside parentheses ( ), brackets [ ], and braces { }. For instance, we can implement the above multi-line statement as:

```
b = (1 + 2 + 3 +
    4 + 5 + 6 + 6
    7 + 8 + 9)
Print(b)
```

Multiple Assignment

- Assigning the same values to multiple variables.

```
a = 2; b = 3; c = 4
```

- Assigning multiple values to multiple variable

```
x, y = 3,4
```

- Swapping values

```
x, y = y, x
```

Dynamic typing

The data type of a variable depends/changes upon the values assigned to a variable on each next statement.Now at this point, we should be aware that y = x/3 will generate an error. The string cannot be divided.

```
x = 10. X has integer type
x = "hello" The type of x is changed to string type.
```

2.2. More on Python Standard Data Types

The Python Programming Language provided inbuilt data types which a have standard memory size associated with them. The 5 Python standard data types we are going to consider includes:

- Numbers
- String
- Lists
- Tuples
- Dictionary

Numbers in python

Numbers are data types used to store numeric values. The above code creates two number variables, score and total and assigns them values.

```
score = 89.4
total = 200.
```

The four different number types provided by Python are:

int – signed or unsigned integer values. in python Integers typically requires 4 bytes of memory space and ranges from 147483648 to 2147483647.

long – long integers

float – floating-point values. Floating Point data type is used for storing single precision floating point values or decimal values. Float variables typically requires 4 byte of memory space.

complex – complex numbers having real and imaginary parts.

Table 1: The table below gives a summary of different number types provided by Python

Int	long	Float	complex
300	8976576L	0.45	5.56j
55	-0x29656L	45.20	63.j
-524	055L	-52.8	5.087e-24j

Calculation on number

```
a = 4
b =   a * 2
print(b)
```

In this code, the first line (a = 4) creates a new variable a and assign it the value 4.In the second line (b = 4) multiply a by 4 and store the result in b. The third line prints the result of calculation.

```
a = 5
print(b)
```

To change the value of variable a, you just assign a new value to it. The value of b needs to be updated to get correct result.

Python Strings

In Python, strings are identified as a set of characters enclosed in quotes, which may be either single or double quotes. Substrings of a particular string can be formed using the slice operator [] and [:]. A substring is specified with an index starting from 0 for the first character of the string. An index of -1 is also used to indicate the last character on the string. Two strings can be joined together using the concatenation operator (+). Strings can be repeated or multiplied using the repetition operator (*). Let's take some examples: Printing same words several Times using String manipulation:

```
print ("Hello World! ")
print ("Hello World! ")
print ("Hello World! ")
```

In python we can print the same words listed above in different way using single line using backslash and n. Here we go.

```
print ("Hello World! \n Hello World! \n Hello world!")
```

Or we can print the statements number of times as follow:

```
print ("\n Hello World! "* 3)
```

Note: Unless you want to put space no need of giving any gap between \n and follow character.

String Concatenation

In python String Concatenation is done with the "+" sign.Here is example:

```
print (" Hello" + " Python")
```

There is no space between "Hello" and "Python" when printing, it just prints as "Hello Python". If you want to give space between two words you can give space using:

- By Addin space after "Hello"
- Add space before the word "python"
- Add space by adding empty quotation mark " "

In python String concatenation are just merging the two strings together without any space.

```
string = "Hello Python"
print (string)      # Prints out the entire string
print (string [0])      # Prints the first character in the string
print (string [2:4])      # Print the 3rd to the 5th character
print (string [3:]      # Prints the 4th to the last character
print (string + " we love python")   # Attaches “we love python”  to the end of the string
print (string * 3)      # Prints the string 3 times
```

Combining Strings

Variables become useful when you combine them to make new variables. If you add two strings together, you can store the combination in a new variable.

Example:

```
greeting = “Hello”
place = “World”
 sentence = greeting + place
print(sentence)
```

The + symbol combine string.

String Length

In python we use len () function to count the number of characters in a string.

```
greeting = “Hello”
len (greeting)
```

The number of characters counted is 5

Python Lists

Lists are part of Python collection data types. A list in Python contains different values separated by comma and enclosed in square braces []. Items in a list could be of the same or of different data types. Just like in strings, individual elements of a list can be accessed using the slice operator []. Starting from the first element of the list, the index is 0. Starting from the last element, the index is -1. The concatenation operator (+) and the repetition operator (*) applies in list just like in strings. The program code below illustrates the use of lists in Python.

Put a list in a variable

```
Student_name = [“Ali”, “Gamachu”,”Numan”]
```

The lust must separate by comma.

Getting Items from Lists

Once your data is in a list, it’s easy to work with.

```
student_name[0]
student_name[3]
```

In the first line it returns “Ali”
In the second line it returns “Numan”

Example:

```
list1= [ 'python', 3, “Java”, 2.4, 2]
list2 = [“Ali”, 1,4]
print(list1)        # Prints whole list
print(list1[0])   # Prints first item in of the list
print(list1[1:4])   # Prints elements beginning from 2nd till 5th
 print(list1[2:])     # Prints elements beginning from 3rd element
 print (list2 * 2)      # Prints list twice
print (list1 + list2)  # Combines both list1 and list2
```

Python Tuples

Tuples in Python are like lists with the following two difference: Tuples are specified using rounded brackets (). Not square braces! Tuples are immutable –

this means that items in a tuple cannot be modified. Let's take some examples. Every other operation that applies to a list applies to a tuple. But take not that the operations below would succeed in a list but would generate an error in a tuple.

```
tuple1= ('Python', 1, 10.5)
tuple2= (3,4,'x','y')
```

```
list1[0] = 'xyz'      # Would succeed because lists a mutable
tuple1[0] = 'xyz'     # They would fail because tuples are immutable
```

Python Dictionary are used to store key value pairs just like in a hash table. Each entry in a dictionary has a key and a value. Keys and values in a dictionary can be of any type. A typical example of a dictionary in Python is the days of the week where each weekday is assigned a number each corresponding to the day name. This is shown below.

```
weekdays = {1: "Monday",2: "Tuesday",3: "Wednesday",4: "Thursday",5: "Friday",6: "Saturday",7: "Sunday"}
```

The following operations are all valid for a dictionary in Python:

```
print (weekdays [1])       # Prints Monday
print(weekdays)      # Prints the complete dictionary
print (weekdays. keys ())   # Prints all the keys, 1, 2, 3,4,5,6,7
print (weekdays. values()) # Prints all the values: Monday, . . , Sunday
```

REFERENCES

Robert Dondero Introduction to Programming in Python: An Interdisciplinary Approach, Robert Sedgewick, Kevin Wayne, and, Pearson, 2015.

Dil referansı: https://docs.python.org/3.5/reference/index.html

Programlama stil rehberi: https://pycodestyle.readthedocs.io/en/latest/

Chapter 12

Object Oriented Programming In Java

Musa Genemo[1]

1 Doktor Öğretim Üyesi Gumushane Üniversitesi İktisadi İdari Bilimler Fakültesi Yonetim bilisim System Bölümü. Musa.ju2002@gmail.com ORCID No: 0000-0001-9991-3050

Chapter's Objective

- Will have knowledge about basics of OOP in java programming language,
- You will be abele run java using Command promot.
- You will be able to write a simple java program.
- You will map over all of OOP in programming language

What is object Oriented Programming?

Object Oriented Programming is a paradigm that provides many concepts such as inheritance, Encapsulation, Abstraction and, and polymorphism. In real world everything is object. For example, a book, a car, a chair, table etc. Java facilitates to program this real-world program using classes and objects. It simplifies the software development and maintenance.

Java Editors:

To write java code, you can use many editors like note pad, note pad++, sublime text and edit++. Those editors are advisable for java beginners. If you are working real project Integrated Development Environment (IDE) like, eclipse, NetBeans ID, visual studio and, MyEclipse.

How to Run java code

- Step 1: Download the software: -

Download the software based on your operating system& processor because the software is. different from operating system to operating system & processor to processor. Open the Google site type the jdk8 download as shown below.

- Step 2: Install the java software.

Install the java software just like media players in your machine. After installing the software, the installation java folder is available in the fallowing location by default. (But it possible to change the location at the time of installation).

Local Disk c: --->program Files--->java

Jdk : java development kit

Jre: java runtime environment

- Step 3: set the path.

In C language we can run the application only form turbo-C folder but in java it is possible to run the files in any local disk (D: , E: , F: …etc.)when we set the path. Right click on mycomputer --->properties----->Advanced system setting--->Environment Variables --User variables--->new----> variable name : path Variable value : C:\programfiles\java\jdk1.8.0_11\bin;

Java Features

- Simple
- Object Oriented
- Robust
- Architectural Neutral
- Platform Independent
- Portable
- Secure
- Dynamic
- Distributed
- Multithreaded
- High Performance
- Interpreted

How to run java

To run java application, follow the following procedure.
Step 1: write the Application.
step 2: save the Application by using. Java

- If the application has public class save it by public class name
- If there is no public class in source file then we can save by any name

Note: Inside the source file it is possible to declare only one public class

Step 3: Compilation process: java compiler
check syntax.
syntax: javac file_name
example: javac Test.java

- compiler checks syntax error: if any error compiler generates error message
- If there is no error in source file then compiler translate .java----.class file.
-

.java file: contain high level language

.class file contains byte code (intermediate code): it is a platform independent code.

Note: The compiler generates .class files based on number of classes present in source file.

Example: Car.class Student.class Employee.class

Step 4: execution process: JVM

Syntax: java class-name

Example: java Test

Translate byte code to machine code.

- JVM loads .class file byte code into memory (Translation of byte code to machine code)
- After loading the class file JVM calls main method to start the executions.

Java coding conventions

In java class, interfaces, enum, and annotation starts with uppercase. Methods, package, keyword, constant, and packages.

Java Packages

we have two default packages in java.

- String
- System

In java importing these two default packages are not mandatory. java contains 14-predefined packages.

1. Java.io
2. Java.nio
3. Java.time
4. Java.sql

5. Java.util
6. Java.security
7. Java.swing
8. Java.applet
9. Java.rmi
10. Java.beans
11. Java.math
12. Java.net
13. Java.text
14. Java.lang
15.

Case 2: compilation: we can compile multiple files at a time.

X.java
Y.java
Z.java

- javac X.java 1 file is compiled.
- javac Y.java Y.java 2 files compiled.
- javac *.java all files are compiled.
- javac Emp*.java The files start with EMP compiled.
- javac *Students The files ends with student compiled(DStudent.java, IStudent.java)

we can execute only one .class file at a time.

Case 3: user defined class and Predefined class

- user defined class can start by lower case.
- but predefined class must start with upper case.

Note: Coding conventions is optional for user defined class & mandatory for predefined class.

Case 4: The class which contains main method is called main class.

```
class Test2{
        public static void main(String[] arg){
                System.out.println("Test class..");
        }}
class A{
 public static void main(String[] arg){
                System.out.println("Test class..");
        }}

class B
{
        public static void main(String[] arg){
                System.out.println("Test class..");
        }
}
```

The source files allow to declare multiple main classes.
Note:

- the source file is allows to declare multiple classes.
- the source files allows to declare only one public class.
- the source files is allows to declare multiple main method.

Case 5: print () vs println()
print (): control stay on same line.
println(): control goes to next line

Case 6: escape sequence characters used to represent data with back slash.

- System.out.print("hi" Musa"sir"); : invalid
- System.out.println("hi\"Musa\"Sir");
- System.out.println("hi\\Musa\\Sir");
- System.out.println("hi\'Musa\'Sir");
- System.out.println("hi\t\ratan\t\t\sir");

Case 7: you can give multiple space between tokens.

```
System.
out.
println("Hi");
```

Case 8: java is platform independent language it supports all operating systems.

JVM is platform dependent. Because it comes along with JDK software, the software is changed to OS to OS.

Data types

Data types: to represent your data.

Data types

1.	byte	1
2.	short	2
3.	int	4
4.	long	8
5.	float	4
6.	double	8
7.	char	2
8.	Boolean	none

- **Numeric data**: byte, short, int, long: 10 20 30 40
- Decimal data: float double: 10.5, 20.5
- Char data: char : 'a'
- Boolean data: true, false

Range: range is the minimam and maximum value of primitive data types in java

- **byte**: 1-byte
  range: -128 to 127
  formula to calculate range: -2^n to 2^n-1 where n= number of bits n=8
  1-bit sign: 0=+ve 1 =-ve
  7-bit range:
  Range: 2^7 to 2^7-1

- **short**:
  2-byte
  bit range 16
  range: 2^{15} to $2^{15}-1$

- **char size**:
  2-byte

range: 2^{16} to 2^{16}-1
note: we have no sign bits in char.
int num =10.
System.out.println(num);//10
int num;
System.out.println(0);//defualt value
Char : space
boolean : false

```
class Emp
{
int eid=111;
String ename="Musa";
double esal=1000.45;
}
```

Note: String is not a data type, it is a class present in java.lang packages to represent a group of characters enclosed in double quotes.
String str1 ="Musa";
System.out.println(str1);//Musa
String str2;
System.out.println(str2);//null

Note: any class type the default value is null value.

```
class Test
{
        public static void main(String[] arg){
                float f = 10.5;  // error the decimal data is double by default
                  //use f constant
                System.out.println(f);
                double d = 20.5;
                System.out.println(d);
        }
}
```

ex-1: In java the decimal value is by default double value, so to represent float value use f or F constant

ex-2: in java numeric number by default is integer.

- Use l or L constant.
- Long card = 8767209510947820L.

Ex-3: To make numeric data more readable we can put underscores in numeric literals from java seventh versions. Underscores ignored during compilations itself.

- 8767_2095_1094_7820L

Underscores rules:

- It is possible to give multiple consecutive underscores,
  int num = 34_45__64
- It is not possible to give underscore starting and ending of the number.
  int num = _2345
  int num =4324_
  int num = _34245_
- It is not possible to give underscores before and after the decimal points.
  double d = 4534_.3545
  int num = 4534. _3545
  int num = 4534_. _.3545
- It is not possible to give underscore before and after the constant.
  float f = 10.5_f.
  float f = 10.5f_
  float f = 10.5_f_

Binary data representation is: 0B.
Hexadecimal Representation: 0X

- byte b = 0B1010.
- int c = 0Xaf1.

It is not possible to use the underscores before and after the representations.

Number system

- Binary numbers: 0,1 0B
- Octal numbers: 0-7 start with 0
- Decimals numbers: 0-9 by default
- Hexadecimal number: 0-9 a-f 0x 0X

0 = disable

1 = enable

Binary number system Example:

```
class Test2
{
        public static void main(String[] arg){
                int a = 0b1100;

                System.out.println(a);//12
                int b = 0133;
                System.out.println(b);//91
int c = 0xAB;
                System.out.println(c);//171
        }
}
```

int d = 15; //Decimal

System.out.println(Integer.toBinaryString(d));//1111

Java identifiers: any name in java like method name, class-name, variable-name is called identifier.

Rules:

1.the identifier contains a-z, A-z,0-9, $, _ but should not start with number & does not allows special characters.

- class Test123: valid
- class 123Test: invalid
- class Test*123: invalid
- class Test_123: valid
- class _Test: valid

2. The identifier must be unique.

- Class A{}
- Class A{}

  In valid

3. the identifiers are case sensitive:

- int A =10;
- int a = 20;// is not same

4. There is no length limit for identifiers.

5. keywords are not allowed us identifiers

- int try = 10; :invalid
- int new =20; :invalid
- int this = 10; : invalid

6. it is possible to take predefined class names and interface names as identifiers, but it is not recommended.

  - int Serializable = 200;
  - int String = 100;

Comments in java:

- Comments are used to write the description about the applications logic to understand the logic easily.
- The min objective of the comments the project maintenance will become easy.
- Comments are none executable code. These are ignored by compiler.

Types of comments in java:

- Single line comment: Single line description. only one line //
- Multi line comment: we can write description more than one line. /*…….*/
- Documentation comment: SRS or manual of the project

API: Application programming interface

- It contains detailed description about the product.
- It is a interface between end user product.

REFERENCE

Altuğ B. Altıntaş, Java Programlama Dili ve Yazılım Tasarımı, Papatya Yayıncılık, İstanbul, 2012. Tevfik Kızılören, Java ve Java Teknolojileri, Kodlab Yayın, 2011.

Internet & World Wide Web How to Program, 4/e, Harvey M. Deitel and Paul J. Deitel, Prentice Hall, 2007

http://www.w3shools.com